THE INTERNATIONAL

SUMMER CONFERENCE ON THEORETICAL PHYSICS

17-21 June 2024
St. Petersburg

Conference Proceedings

Quadratic Zeeman effect in boronlike ions

V. A. Agababaev[1,2], D. A. Glazov[1], A. V. Malyshev[3,4],
E. A. Prokhorchuk[3], V. M. Shabaev[3,4], A. V. Volotka[1]

[1]ITMO University, Kronverksky pr. 49, 197101 St. Petersburg, Russia

[2]St. Petersburg Electrotechnical University "LETI",
Professor Popov st. 5, 197376 St. Petersburg, Russia

[3]Department of Physics, St. Petersburg State University,
Universitetskaya nab. 7/9, 199034 St. Petersburg, Russia

[4]Petersburg Nuclear Physics Institute named by B. P. Konstantinov of
National Research Centre "Kurchatov Institute", Gatchina, Russia

[1]v.agababaev@yandex.ru

Abstract

Theoretical evaluation of the quadratic Zeeman effect is implemented for the wide range of Z. The one-photon-exchange correction is evaluated within standard QED. In order to take into account the higher orders in $1/Z$ various screening potentials are used. The self-energy correction is calculated using the rigorous QED approach. The electric-loop contribution to the vacuum-polarization correction is calculated employing the Uehling potential.

Key words: highly charged ions, bound-state quantum electrodynamics, relativistic atomic theory, Zeeman effect

The significant progress was achieved in the last two decades in the field of g factor of highly charged ions as a result of both experimental and theoretical work [1, 2]. The substantial accuracy improvement of the electron mass determination has been reached in these studies [3]. It's expected that high-precision g-factor measurements in hydrogen-, lithium- and boronlike ions will provide an independent determination of the fine structure constant α [4, 5]. The ALPHATRAP project is aimed at the g-factor measurements in the ground state for wide range of highly charged ions including boronlike ones [11]. In the framework of this project the g factor of boronlike argon $^{40}Ar^{13+}$ was measured [10]. The ARTEMIS experiment to measure the Zeeman splitting in middle-Z boronlike ions is also carried out [12, 13]. In particular, the first of the investigated ions was also boronlike argon $^{40}Ar^{13+}$. At present, the g factor has been well investigated theoretically including the QED, interelectronic-interaction and nuclear effects (see e.g. [14]). The leading order of the quadratic Zeeman effect, the

one-loop QED correction, and the one-photon-exchange correction for boronlike argon have been calculated in Ref. [7]. The leading order of the cubic Zeeman effect has been evaluated in Ref. [8].

The studies of the quadratic Zeeman effect have about of 80-years history and run since 1930s starting from the discovery by Jenkins and Segré and its quantum mechanical explanation by Shiff and Snyder [15, 16]. Close attention of the scientific society have been attracted by the magnetars and other objects with high and extra-high (up to 10^{11} T) magnetic induction where the quadratic effect becomes principal [17, 18, 19]. Researches of the quadratic Zeeman effect in solid states and also in Bose-Einstein condensates have separately developed [20, 21]. A numerous studies of the quadratic effect have also been undertaken in molecules, atoms and exotic systems such as positronium [22, 23, 24, 25]. However, the studies of the quadratic Zeeman effect in highly-charged ions are only at the beginning of their journey.

We present *ab initio* QED calculation of the quadratic Zeeman effect for the ground and first excited states of boronlike ions in the wide range of Z including the first-order corrections: one-photon exchange, self-energy and vacuum polarization. We employ the perturbation theory in the presence of external magnetic field, the fully relativistic approach, i.e., exact to all orders in αZ.

References

1. S. Sturm *et al.*, Ann. Phys. (Berlin) **525**, 620 (2013).
2. V. M. Shabaev *et al.*, J. Phys. Chem. Ref. Data **44**, 031205 (2015).
3. S. Sturm *et al.*, Nature **506**, 467 (2014).
4. V. M. Shabaev *et al.*, Phys. Rev. Lett. **96**, 253002 (2006).
5. V. A. Yerokhin *et al.*, Phys. Rev. Lett. **116**, 100801 (2016).
6. D. von Lindenfels *et al.*, Phys. Rev. A **87**, 023412 (2013).
7. V. A. Agababaev *et al.*, Nucl. Instr. Methods Phys. Res. B **408**, 70 (2017).
8. A. S. Varentsova *et al.*, Nucl. Instr. Methods Phys. Res. B **408**, 80 (2017).
9. A. S. Varentsova *et al.*, Phys. Rev. A **97**, 043402 (2018).
10. I. Arapoglou *et al.*, Phys. Rev. Lett. **122**, 253001 (2019).
11. S. Sturm *et al.*, Phys. Rev. Lett. **122**, 253001 (2019).
12. D. von Lindenfels *et al.*, Phys. Rev. A **87**, 023412 (2013).
13. M. Vogel *et al.*, Annalen der Physik p. 1800211 (2018).
14. V.A. Agababaev *et al.*, X-Ray Spectrometry. **49**, 143 (2020).
15. F. A. Jenkins and E. Segr'e, Phys. Rev. **55**, 52 (1939).
16. L. I. Schiff and H. Snyder, Phys. Rev. **55**, 59 (1939).
17. G. W. Preston, Astrophys. J. **160**, L143 (1970).
18. S. B. Kemic, Astrophysics and Space Science **36**, 459 (1975).
19. C. Moran *et al.*, Mont. Not. of the R. A. S. **299**, 218 (1998).
20. J. Stenger *et al.*, Nature **396**, 345 (1998).

21. A. Thilderkvist *et al.*, Phys. rev. B **49**, 14270 (1994).
22. W. R. S. Garton and F. S. Tomkins, Astrophys J **158**, 839 (1969).
23. G. Feinberg *et al.*, Phys. Rev. A **41**, 3478 (1990).
24. M. Raoult *et al.*, JPB: Atomic, Mol. and Opt. Phys. **38**, S171 (2005).
25. K. Numazaki *et al.*, Phys. Rev. A **81**, 032124 (2010).

The International Summer Conference on Theoretical Physics 2024
Faculty of Physics of ITMO University
Abrikosov Center for Theoretical Physics

Synchronization transition in system of superconducting grains on weighted undirected graph

Artem Alexandrov[1,2]

[1]Institute for Information Transmission Problems, Moscow, 127994, Russia

[2]Moscow Institute of Physics and Technology

[1]aleksandrov.aa@phystech.edu

Abstract

We discuss an appearance of superconducting phase in the array of superconducting grains placed on weighted undirected graph. That system can be realized by placing the superconducting grains on a surface of graphene/metal. We treat such system in terms of Kuramoto model with inertia and noise and apply the Penrose method to investigate the transition between non-synchronized (non-superconducting) and synchronized (superconducting) phase.

Key words: Synchronization, Josephson junctions, superconducting grains, phase transition

Systems of superconducting (SC) grains (islands) were discussed in the pioneering paper by Efetov [1], where each grain is characterized by its own gap and phase of gap. Next, this topic has drawn a lot of attention by different researchers [2, 3]. The crucial feature of such systems is that even at zero temperature superconducting state may not appear. The underlying mechanism of this phenomenon is a concurrence between Josephson energy (which described tunneling effects between grains and it corresponds to the interaction energy) and charge energy of grains. Roughly speaking, the onset of superconducting state is possible if the Josephson energy is greater than the charge energy. This treatment implies that the superconducting phase matches the synchronized state of grains phases, whereas the non-superconducting fits the non-synchronized state. One more important fact is that dissipation effects play a substantial role in the study of phase transition between these two phases [4]. Next, in papers [5, 6] the authors have considered SC grains on graphene & metal surface and have shown that in this set up the Hamiltonian is very similar to XY-model with long-range interactions and additional dissipation term.

Considering all the above, we treat the system of SC grains on weighted undirected graph in terms of Kuramoto model with inertia and noise [7]. The equation of motion

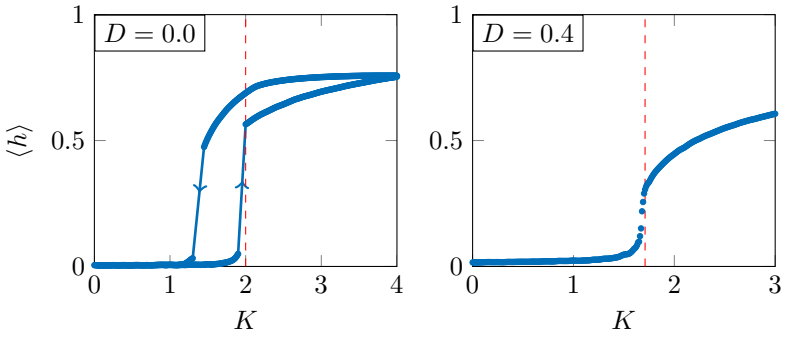

Figure 1: Synchronization transition in Kuramoto model with inertia and noise with $m = 1$. Dashed line corresponds to analytical expression for K_c, $\langle h \rangle$ is the order parameter (phase synchronization measure)

for this model are given by

$$m\ddot{\varphi}_i + \dot{\varphi}_i = \omega_i + \frac{2K}{N}\sum_{j=1}^{N} W_{ij}\sin\left(\varphi_j - \varphi_i\right) + \eta_i, \tag{1}$$

where m described mass (inertia); K is the coupling constant, which directly maps onto the Josephson energy; ω_i plays role of external current applied to grains and η_i is the white noise that mimics thermal or shot noise. In the large-N limit, this model has the well-defined continuum limit, which is governed by certain Fokker-Planck equation. In terms of Kuramoto model, the onset of superconductivity coincides with appearance of synchronized state. We investigate this problem by the linear stability analysis of Fokker-Planck equation and show that this analysis coincides with the eigenvalue problem of certain functional operator. Using the Penrose method, we analyze the spectrum of this operator and find analytically the critical coupling K_c for the synchronization transition. In case of complete graph, $W_{ij} \equiv 1$, the explicit expression of K_c is

$$K_c^{-1} = D\int_{-\infty}^{+\infty} \frac{d\omega\, g(\omega)}{D^2 + \omega^2} - m\left(1 + mD\right)\int_{-\infty}^{+\infty} \frac{d\omega\, g(\omega)}{(1+mD)^2 + m^2\omega^2}, \tag{2}$$

where $g(\omega)$ is the distributin of ω_i and D is the amplitude of noise. Having determined K_c, we analyze the exotic chimera-like states (when the sizeable fraction of phases is not synchronized but the total synchronization is not zero) and cluster states. We describe such states by the so-called critical Penrose curves. The obtained results can be interesting for realization with help of SC grains on graphene [8].

References

1. KB Efetov. Phase transition in granulated superconductors. *Sov. Phys.-JETP (Engl. Transl.);(United States)*, 51(5), 1980.

2. E Šimánek. Reentrant phase diagram for granular superconductors. *Physical Review B*, 32(1):500, 1985.

3. Patrik Fazekas. Reentrant phase transition in granular superconductors. *Zeitschrift für Physik B Condensed Matter*, 45(3):215–221, 1982.

4. E Šimánek and R Brown. Effect of dissipation on the phase transition in granular superconductors. *Physical Review B*, 34(5):3495, 1986.

5. Mikhail Viktorovich Feigel'man, Aleksandr Ivanovich Larkin, and Mikhail Andreevich Skvortsov. Quantum superconductor–metal transition in a proximity array. *Physics-Uspekhi*, 44(10S):99, 2001.

6. Mikhail Viktorovich Feigel'man, Mikhail Andreevich Skvortsov, and Konstantin Sergeyevich Tikhonov. Proximity-induced superconductivity in graphene. *JETP letters*, 88:747–751, 2008.

7. Artem Alexandrov and Alexander Gorsky. Penrose method for kuramoto model with inertia and noise. *Chaos, Solitons & Fractals*, 183:114938, 2024.

8. Zheng Han, Adrien Allain, Hadi Arjmandi-Tash, Konstantin Tikhonov, Mikhail Feigel'Man, Benjamin Sacépé, and Vincent Bouchiat. Collapse of superconductivity in a hybrid tin–graphene josephson junction array. *Nature Physics*, 10(5):380–386, 2014.

One-electron matter-antimatter quasimolecules within the finite-basis-set method for the two-center Dirac equation

A. Anikin[1,2], A. Danilov[1], D. Glazov[1,3], A. Kotov[1], D. Solovyev[1,4]

[1] Department of Physics, St. Petersburg State University, St. Petersburg, Russia

[2] D.I. Mendeleev Institute for Metrology, St. Petersburg, Russia

[3] School of Physics and Engineering, ITMO University, St. Petersburg, Russia

[4] Petersburg Nuclear Physics Institute named by B.P. Konstantinov of National Research Centre 'Kurchatov Institut', Gatchina, St. Petersburg, Russia

Precision molecular spectroscopy embraces a broad range of problems in modern physics. It is used as a tool to determine the values of fundamental physical constants, such as, for example, the proton-electron mass ratio or the proton charge radius [1], to construct optical clocks, and to test fundamental interactions [2].

Over the last decades, accurate studies of molecular systems containing an antiproton have been successfully carried out [3]. The study of antiparticle systems is of special importance because of the possibility of a direct check of CPT invariance by comparing the spectra of matter and antimatter [4]. Experimental successes in two-photon spectroscopy of antiproton helium [5] have encouraged theoretical calculations of exceptionally small effects, which enables accurate determination of transition frequencies [6]. The continued development of experimental techniques for the antihydrogen atom synthesis [7] enables the precise experimental determination of the energies of Lyman$-\alpha$, hyperfine, etc. transitions in antiatoms [8].

Being a many-body problem, the theoretical description of one-electron quasimolecules is carried out using numerical methods. Among the most widely used is the solution of the nonrelativistic two-center problem and the use of nonrelativistic quantum electrodynamics (NRQED) to obtain relativistic corrections [6]. A different approach to resolve the one-electron problem for a binuclear quasimolecule is to solve the Dirac equation with a two-center Coulomb potential. Within this approach, different wave function decompositions are used, for example, partial wave and Dirac-Sturm decomposition [9]. In this work, the decomposition over a finite basis set of B-splines generalized to axisymmetric systems (A-DKB) [10] is employed. Using this method, the energy spectra of different antiprotonic one-electron ions are obtained.

Funding The work is supported by the Russian Science Foundation grant no. 23-22-00250.

References

[1] Karr J.P. et al. (2016). Phys. Rev. A, 94:050501.
[2] Schiller S. et al. (2014). Phys. Rev. Lett., 113:023004.
[3] Doser M. (2022). Progress in Particle and Nuclear Physics, 103964.
[4] Myers E.G. et al. (2018). Phys. Rev. A, 98:010101.
[5] Hori M. et al. (2011). Nature, 475, 7357:484.
[6] Korobov V.I. et al. (2008). Phys. Rev. A, 77:042506.
[7] Baur G. et al. (1996). Phys. Lett. B, 368:251.
[8] Ahmadi M. et al. (2017). Nature, 548:66.
[9] Tupitsyn I.I. et al. (2010). Phys. Rev. A, 82:042701.
[10] Rozenbaum E.B. et al. (2014). Phys. Rev. A, 89:012514.

The International Summer Conference on Theoretical Physics 2024
Faculty of Physics of ITMO University
Abrikosov Center for Theoretical Physics

Vavilov-Cherenkov radiation and equivalent photon emission with vortex electrons

A. D. Chaikovskaia [1]

[1]School of Physics and Engineering, ITMO University, 197101
St. Petersburg, Russia

[1]adkatanaeva@itmo.ru

Abstract

We present a theoretical investigation of the Vavilov-Cherenkov (VC) radiation by plane-wave and vortex electrons. Special emphasis is put on the question whether and at what conditions the emitted VC photons can be twisted. It is shown that if one uses a detector sensitive to the twisted electron (photon) with the definite projection of the total angular momentum (TAM), then the final photon (electron) also will be in the twisted state with a definite TAM projection. We investigate the polarization properties of the emitted twisted photon and explore a similar process of the equivalent photon emission in the Weizsacker-Williams method.

Key words: vortex particles, orbital angular momentum, Cherenkov radiation, *ep*-scattering, quantum entanglement

Vavilov-Cherenkov radiation

In any quantum process the detection scheme plays a crucial role in the measurement of the final quantum state characteristics. In the previous studies of Vavilov-Cherenkov (VC) radiation, e.g. [1], the calculations are performed for the final states detected in the form of plane waves both for the electron and the photon. Another approach was recently put forward in [2, 3]. It is based on the so-called generalized measurements, focuses on the entanglement between a pair of the final particles and implies a post-selection protocol for the final electron, in which the momentum is potentially measured with some uncertainty (necessary for the detection of vortex states). In this approach, the *evolved* state of the emitted photon appears.

We perform an analysis of VC process, $e \to e' + \gamma$, in the lowest order of the perturbation theory in QED for the case of an ordinary plane-wave initial electron and derive the evolved wave function of the quantum system in the coordinate and momentum representations that corresponds to the entangled state of an emitted photon and an outgoing electron. It is remarkable that a symmetrical and relatively simple wave function could be obtained. Further, we generalize the calculation for the case of the initial twisted electron represented as a proper superposition of the plane waves comprising a Bessel wave state.

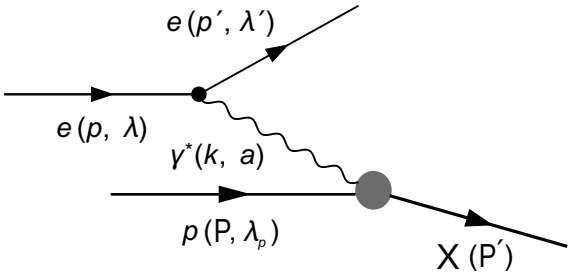

Figure 1: Feynman diagram for the virtual process describing emission and absorption of an equivalent photon of momentum k and polarization a.

Weizsäcker-Williams approximation in ep-scattering

The exploited method can also be applied to the problem of characterizing the final wave function in the process of radiation of an equivalent photon (EP) by high-energy charged particle. Let us consider the process of inelastic high-energy ep-scattering (Fig. 1), $e(p)+p(P) \to e(p')+X(P')$, where X is the final hadronic state with the total momentum P'. This process may be seen as a two steps reaction, the first one being the emission of an EP γ^* with momentum $k = p-p'$ and virtuality $k^2 < 0$ by the initial electron. The general cross-section of the inelastic ep scattering with the unpolarized electrons, $d\sigma_{ep} = dn_T\,\sigma_T + dn_S\,\sigma_S$, could be simplified in the Weizsäcker-Williams (or equivalent photon) approximation. In the region of small virtuality of EP, we can neglect the contribution of the scalar EP and replace the cross section σ_T by its value on the mass-shell $\sigma_T(kP, k^2) \to \sigma_\gamma(kP)$, when $k^2 \to 0$. Emission of T photons in the approximation has a close similarity with the VC radiation, the distinction related to kinematics being taken into account. We obtain the wave function of the final evolved state in the process of EP emission and analyze the total angular momentum transfer to the final hadron state X after a head-on collision of EP with a plane-wave proton.

References

1. I.P. Ivanov, V.G. Serbo, V.A. Zaytsev, *Phys. Rev. A* **93**, 053825 (2016)

2. D. V. Karlovets, S. S. Baturin, G. Geloni, G. K. Sizykh and V. G. Serbo, Eur. Phys. J. C **82** (2022) no.11, 1008.

3. D. V. Karlovets, S. S. Baturin, G. Geloni, G. K. Sizykh and V. G. Serbo, Eur. Phys. J. C **83** (2023) no.5, 372.

The effect of axion exchange on the energy of lithium-like ions

R.R. Abdullin

ITMO University

Axions arise in the context of solving the strong CP - problem [1-2] in the Peccei-Quinn (PQ) theory, where an additional global U(1) symmetry is introduced in the SM QCD Lagrangian and is spontaneously broken, leading to the appearance of a pseudoscalar pseudo-Nambu-Goldstone boson known as the axion [3-4]. The dark matter problem is another important challenge in modern physics [5-7], and its composition remains uncertain. Axions stand out among several potential candidates for cold dark matter. The role of the axion in solving the strong CP problem and its connection to dark matter make it an interesting object of study

This study examines the contribution of axion interaction to the energy transitions of lithium-like ions. Precision atomic spectroscopy methods have proven exceptionally effective for testing the Standard Model and detecting deviations from its various modifications. Axion exchange can cause shifts in energy levels in the compounds under consideration. This study involves measuring these energy shifts. The data obtained will help establish constraints on the axion interaction constant.

In our work, a universal expression for the axion reduced matrix element has been obtained. This matrix element is similar to the Breit part of the photon matrix element, which leads to the investigation of systems where the Breit contribution is prominently expressed. Such systems typically involve heavy charged ions, meaning that the probability of detecting axion contributions is high. The plan for future research includes searching for specific systems in which the Breit contribution is well-expressed.

References

[1] Peccei, R.D. and Quinn, H.R. "Constraints imposed by CP conservation in the presence of pseudoparticles." *Phys. Rev. D*, vol. 16, no. 6, pp. 1791-1797, 1977.

[2] Peccei, R.D. and Quinn, H.R. "CP Conservation in the Presence of Pseudoparticles." *Phys. Rev. Lett.*, vol. 38, no. 25, pp. 1440-1443, 1977.

[3] Weinberg, S. "A New Light Boson?" *Phys. Rev. Lett.*, vol. 40, no. 4, pp. 223-226, 1978.

[4] Wilczek, F. "Problem of Strong P and T Invariance in the Presence of Instantons." *Phys. Rev. Lett.*, vol. 40, no. 5, pp. 279-282, 1978.

[5] Bertone, G., Hooper, D., and Silk, J. "Particle Dark Matter: Evidence, Candidates and Constraints." *Phys. Rep.*, vol. 405, pp. 279-390, 2005.

[6] Steffen, F.D. "Dark-matter candidates: Axions, neutralinos, gravitinos, and axinos." *The European Physical Journal C*, vol. 59, pp. 557-588, 2005.

The International Summer Conference on Theoretical Physics 2024
Faculty of Physics of ITMO University
Abrikosov Center for Theoretical Physics

Time-optimal quantum state transfer in a topological qubit array

K. Chernova[1], A. Stepanenko[2,1], M. Gorlach[1]

[1]School of Physics and Engineering, ITMO University, Saint Petersburg 197101, Russia

[2]London Institute for Mathematical Sciences, Royal Institution, 21 Albemarle St, London W1S 4BS, UK

[1]kseniya.chernova@metalab.ifmo.ru, [2]andrey.stepanenko@metalab.ifmo.ru, [3]m.gorlach@metalab.ifmo.ru

Abstract

We investigate a problem of the high-fidelity quantum state transfer in a finite qubit array. Considering the quantum variational problem, we derive the analytical form of the time-optimal control of the system parameters. Specifically, we study the time evolution of the single excitation in the one-dimensional chain of superconducting qubits, described by the tight-binding model with fixed network geometry. The obtained solution enables an optimally fast ideal state transfer, gaining time for executing quantum algorithms.

Key words: Topological photonics, Quantum brachistochrone, Qubits

Introduction

Superconducting circuits are known to be a promising candidate to realize quantum computing [1], which has gained significant attention in recent years. One of the major challenges is the realization of efficient quantum information routing within qubit networks. There are several known ways for high-fidelity quantum state transfer by changing the couplings between qubits. They include perfect transport [2] and stepwise switching when couplings between two adjoining qubits are included in stages. While these methods are used in practice, they are non-optimal in terms of their temporal duration. Here we present the time-optimal control of quantum state transfer in finite qubit chains.

Main text

We consider a chain of superconducting qubits (two-level systems) shown in Fig. 1(a), described by the tight-binding Hamiltonian $\hat{H} = \sum_m (J_1(t)\hat{a}^\dagger_{2m-1}\hat{a}_{2m} + J_2(t)\hat{a}^\dagger_{2m}\hat{a}_{2m+1} + \text{h.c.})$ with restriction $J_1^2(t) + J_2^2(t) = J_0^2$.

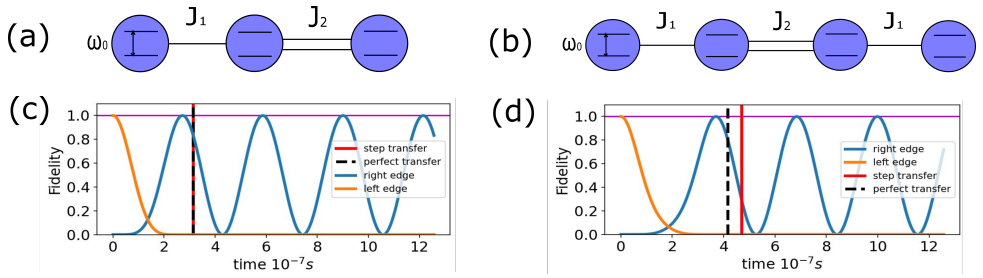

Figure 1: The scheme of the system of the (a) three and (b) four qubits chains. The instantaneous fidelity with the initial (orange) and final (blue) state in time for the chain of (c) three and (d) four qubits. (c) Time of both perfect (dashed black) and stepwise switching (red) transfer equals π/J_0. (d) Time of perfect transport (dashed black) $\sqrt{7}\pi/(2J_0)$ is less the time of stepwise switching transfer (red) $3\pi/(2J_0)$ but not optimal.

To find optimal control, we solve the quantum brachistochrone problem with the Lagrangian [3]

$$L = \sqrt{\frac{\langle\dot{\psi}|(1-P)|\dot{\psi}\rangle}{\langle\psi|\hat{H}^2|\psi\rangle - \langle\psi|\hat{H}|\psi\rangle^2}} + (i\langle\dot{\varphi}|\psi\rangle + \langle\varphi|\hat{H}|\psi\rangle + \text{h.c.}) + \lambda\left(\text{Tr}\,\hat{H}^2 - \omega^2\right) . \quad (1)$$

The Lagrangian variation over unknown coupling coefficients yields time-optimal equations on them. Search for analytical solutions to these equations appears to be a non-trivial task even for small systems. Here, we present optimal controls for the chain of three qubits shown in Fig.1(c):

$$J_1 = J_0\cos(\Omega t + \varphi), \quad J_2 = J_0\sin(\Omega t + \varphi), \quad (2)$$

where J_0, Ω, φ are constants given by the initial conditions and the minimal transfer time is $\tau = \pi/(2\Omega) = \sqrt{3}\pi/(2J_0)$. Analogously, for the four-qubit chain (Fig. 1(b)) we obtained an analytical solution allowing ideal quantum state transfer in time $\tau \approx 3.7$. However, it is hard to find time-optimal control. Having the choice of constants we can find a solution that is faster than both perfect transport and stepwise switching (Fig. 1(d)).

References

1. M. Kjaergaard, M.E. Schwartz, J. Braumüller, P. Krantz, J. I.-J. Wang, S. Gustavsson, and W.D. Oliver, 2020, Superconducting Qubits: Current State of Play, *Annual Review of Condensed Matter Physics*, Vol. **11**, pp. 369-395.

2. M. Christandl, N. Datta, A. Ekert, and A. J. Landahl, 2004, Perfect State Transfer in Quantum Spin Networks, *Physical Review Letters*, Vol. **92** 187902

3. A. Carlini, A. Hosoya, T. Koike, Y. Okudaira, 2007, Time-optimal unitary operations, *Physical Review A*, Vol. **75** 042308

The International Summer Conference on Theoretical Physics 2024
Faculty of Physics of ITMO University
Abrikosov Center for Theoretical Physics

Transit-time effects toward the search for the T, P-odd interactions

D. Chubukov

ITMO University

dmitry.chubukov@metalab.ifmo.ru

Abstract

The investigation of the process of photon absorption by a two-level system briefly interacting with a laser beam is presented.The experimental prospects of searching for the T, P-odd interactions are discussed in detail.

Key words: transit-time effects, laser field, two-level system, absorption, emission, T, P-odd Faraday effect, ultrashort pulses

We investigate the process of photon absorption by atoms or molecules shortly interacting with a laser beam in the dipole approximation [1]. Assuming that the interaction time τ is much smaller than the lifetime of the corresponding excited state, we examine the absorption probability as a function of τ. Besides, we incorporate Doppler broadening due to nonzero temperature of the atoms (molecules). It is demonstrated that in the case of a zero detuning and without Doppler broadening, the absorption probability is quadratic in τ. Once Doppler broadening is taken into account or the laser beam is off from the resonant frequency, the absorption probability becomes linear in τ. Our findings are expected to be important for experimental studies in optical cells or cavities where atoms or molecules traverse continuous laser beams. A principle scheme of the proposed experimental setup is depicted in Fig. 1. An atomic (molecular) beam crosses a high-finesse optical cavity between two mirrors in a transverse direction. Within the cavity, the particles interact with an a linearly polarized laser beam. The overlap of these two beams is located in a background electric field directed along the laser beam axis. The detection of optical rotation (either using simple polarimetry, or phase-sensitive techniques) happens at the output of the cavity. The experimental prospects of searching for the electric dipole moment (EDM) of the electron are discussed in detail.

Also we consider the process of transition of a two-level system to the excited state with subsequent photon emission in the presence of a laser pulse with a high degree of unipolarity [2]. Within the framework of quantum electrodynamics, we obtain analytical expressions for the differential probability of the process depending on the temporal scales of the problem: laser pulse duration, excited-state lifetime, inverse transition frequency, and inverse frequency of the photon emitted. Besides, we calculate the total absorption probability by integrating over the three-dimensional

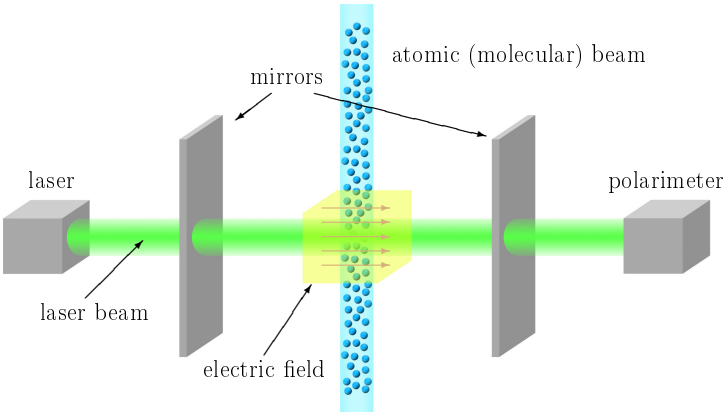

Figure 1: Principle scheme of the experimental setup for measuring the $\mathcal{P}$, $\mathcal{T}$-odd Faraday rotation. A beam of atoms or molecules (blue) traverses a high-finesse optical cavity between two mirrors and interacts with a linearly polarized laser beam (green). The interaction region is located in a background electric field (yellow) directed along the laser beam axis. The laser radiation transmitted through the mirrors is detected by means of a polarimeter.

photon momentum and summing over polarizations. We compare the results obtained for unipolar and bipolar (many-cycle) pulses.

References

1. D.V. Chubukov, I.A. Aleksandrov, L.V. Skripnikov, and A.N. Petrov, Progress toward the P, T-odd Faraday effect: Light absorption by atoms briefly interacting with a laser beam // Phyical. Review A 108, 053103 (2023).

2. I.A. Aleksandrov, D.V. Chubukov, N.N. Rosanov, Probability of absorption and emission by an atom interacting with ultrashort laser pulses // Opt. and Spectr. 131, 1582 (2023).

The model description of the transit time problem for the fast particles crossing the laser beam

In the present communication the model description of the spectral line broadening for atoms crossing the laser beams is presented: the combined effect of the transit time broadening, natural broadening and transverse Doppler broadening is considered. This is done by introducing one-parametric adiabatic damping of atom-laser interaction wherefore the particles interact with laser during the finite time interval. The simplest rectangle distribution of the light intensity inside the laser beam is employed. The dependence of absorption probability on the transit time for different detunings is calculated and compared with earlier results. The limits for using the Lorentz line profile, which is widely employed throughout atomic physics, for describing the interaction of the fast particles with laser beams are established. This becomes especially important when the natural broadening (natural width Γ_N) is negligible, and transit broadening (transit width Γ_T) begins to determine Lorentz profile of resonant spectroscopic line, taking place of Γ_N in the Lorentz denominator. To justify this replacement is the main goal of the present communication. In this model both broadenings, Γ_N and Γ_T, arrive in the energy denominators as a result of evaluation of interaction between atomic electron and the classical potential, presenting the laser field.

Adiabatic potential curves of $H - p$ and $He^+ - p$ ions: relativistic treatment

A. Danilov[1*], A. Anikin[1,2], D. Glazov[1,3], E. Korzinin[2], A. Kotov[1†], D. Solovyev[1,4]

[1] Department of Physics, St. Petersburg State University, Peterhof, Oulianovskaya 1, 198504, St. Petersburg, Russia

[2] D. I. Mendeleev Institute for Metrology, St. Petersburg, 190005, Russia

[3] School of Physics and Engineering, ITMO University, Kronverkskiy pr. 49, 197101 St. Petersburg, Russia

[4] Petersburg Nuclear Physics Institute named by B.P. Konstantinov of National Research Centre "Kurchatov Institut", St. Petersburg, Gatchina, 188300, Russia

[*]st063038@student.spbu.ru

Abstract

In the present paper, a completely relativistic approach is used to obtain adiabatic potential curves for molecular terms within the A-DKB method. Solving the two-center Dirac equation, two compounds are described: one-electron homonuclear $H - p$ and one-electron heteronuclear $He^+ - p$ (quasi-)molecular ions. In the framework of the Born-Oppenheimer approximation, the electron binding energies (ground and several first excited states) in a wide range of inter-nuclear distances have been obtained. Using the relativistic approach, energy splittings, crossings, and identification of energy terms are discussed. The results are compared with those characterized within the nonrelativistic approach, widely covered in the literature.

Key words: Theoretical physics, Dirac equation, potential curves, quasimolecular ions, A-DKB method

Introduction

Two-atomic molecules have been the subject of study since the advent of the quantum mechanics (QM) theory. The one of widely used method consists in application of nonrelativistic approach. To accurately calculate the binding energy of an electron, the Schrödinger equation is solved and then various relativistic and radiative corrections evaluated within the framework of nonrelativistic quantum electrodynamics theory

(NRQED). An alternative approach corresponds to a solution of the Dirac equation involving also a two-center potential. In this case, the most commonly used approach is the decomposition of Dirac wave functions into partial waves. On this basis, the energies of low-lying states in the molecular ion H_2^+ have been calculated with an accuracy of the order of $10^{-14} - 10^{-13}$ [1].

In the present work, another completely relativistic approach (A-DKB method) is used to study hydrogen-proton ($H - p$) and singly ionized helium-proton ($He^+ - p$) compounds. This method is described in detail in [2]. The development of the A-DKB method has provided a theoretical description of heavy one-electron quasi-molecular compounds [3]. Here we apply the A-DKB approach to obtain the ground and several excited quasi-molecular terms in the ions mentioned above.

Main text

The molecular energy state of an electron is characterized by the projection of the total angular momentum onto the axis of the molecule. Being a conserved quantity for the systems with axial symmetry, such a description leads to a degeneracy defined by the opposite sign of m_j. For homonuclear systems, the two nuclei are identical, there is an additional quantum number g (gerate) and u (ungerade) for even and odd states, respectively, expressing symmetry with respect to reflection in the plane perpendicular to the axis of the molecule. In addition, the specific energy state of an electron can be considered in the limit of zero internuclear distance, "joined" atom. Then the "joined" nuclear charge is determined by the sum of Z_1 and Z_2, and the ordinary atomic notations of the energy state can be used: nl_j, where n is the principal quantum number, l is the orbital momentum and j is the total angular momentum of the electron. Thus, the electron molecular term can be determined by the formula $nl_j\lambda_p m_j$ [4], where λ is the projection of the electron orbital moment onto the molecular axis and (only for homonuclear systems) p reflects the parity of the state when the nuclei are permuted. Similar designations can be introduced by considering the limit of the infinite inter-nuclear distance, when the electron is entirely located only on one of the nuclei. In this study, we follow the notations corresponding to the "joined" atom.

Thus, as a result of the calculation, we get the picture presented in FIG. 1. All terms are shown here without taking into account intersections with different projections m_j. After this, we highlight the areas where our terms presumably intersect. Then, following the continuity of the wave function and its derivative, we numerically calculate its derivative (reducing the mesh if necessary). The presence of a jump in the derivative indicates the intersection of terms. Such an analysis is carried out for all nearby terms, which allows for their complete identification within the framework of the relativistic approach, described above.

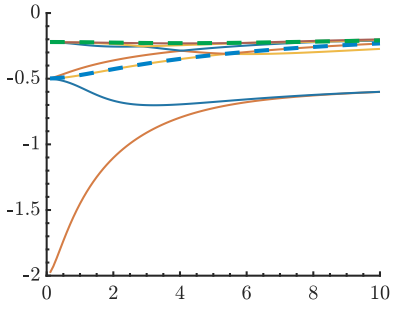

FIG.1. The adiabatic potentials found through the A-DKB method for the first seven states with $m_j = -1/2$ (solid lines) and the first two states with $m_j = -3/2$ (dashed line) of the $H - p$ quasi-molecular ion. All values are in a.u.

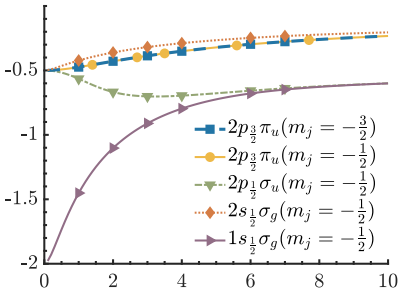

FIG.2. The adiabatic potential curves of the ground and first four excited states of the quasi-molecular ion $H - p$. All values are given in a.u.

As a result, for the case in FIG. 2 we have the following behavior of the first five terms. A similar analysis was carried out for a heteronuclear system using the example of $He^+ - p$ with a separate consideration of the region of small internuclear distances.

Acknowledgements

This work was supported by RSF grant №23-22-00250.

References

1. I. Tupitsyn and D. Mironova, "Relativistic calculations of ground states of single-electron diatomic molecular ions," *Optics and Spectroscopy*, vol. 117, pp. 351–357, 2014.

2. E. B. Rozenbaum, D. A. Glazov, V. M. Shabaev, K. E. Sosnova, and D. A. Telnov, "Dual-kinetic-balance approach to the dirac equation for axially symmetric systems: Application to static and time-dependent fields," *Phys. Rev. A*, vol. 89, p. 012514, Jan 2014.

3. A. A. Kotov, D. A. Glazov, V. M. Shabaev, and G. Plunien, "One-electron energy spectra of heavy highly charged quasimolecules: Finite-basis-set approach," *Atoms*, vol. 9, no. 3, 2021.

4. E. Fermi and E. Teller, "The capture of negative mesotrons in matter," *Physical Review*, vol. 72, no. 5, p. 399, 1947.

Nonlinear scattering of classical and non-classical signals on single superconducting artificial atom

Dmitriev A.Yu.[1,2,*], Vasenin A.V.[1,3], Gunin S.A.[1,3], Remizov S.V.[4], Sabirov T.[1], Elistratov A.A.[4], Pogosov W.V.[4,1] and Astafiev O.V.[3,1]

[1]*Moscow Institute of Physics and Technology, Insitutskij per., 9, 141701 Dolgoprudny, Moscow Region, Russia*

[2]*Russian Quantum Center, Skolkovo, Moscow 121205, Russia*

[3]*Skolkovo Institute of Science and Technology, Bolshoy Boulevard 30, bld. 1, Moscow, Russia 121205* [4] *Dukhov's institute for automatics, Suschevskaya str. 22, 119017 Moscow, Russia* e-mail: [*]dmitrmipt@gmail.com

Superconducting electrical circuits in quantum regime could be treated as single artificial atoms with arbitrarily engineered and controllable energies and transition rates. We place a single two-level superconducting atom into the coplanar waveguide, and a strong coupling between the circuit and electromagnetic modes of the continumm is easily achieved [1]. We study nonlinear mode mixing (intermodulation) on the single atom [2, 3], and find specific features of nonlinear spectra, which could be attributed to the quantum nature of the scatterer. Finally, we construct and study the cascaded quantum system of two artificial atoms, and observe non-classical features of nonlinear intermodulation within the system.

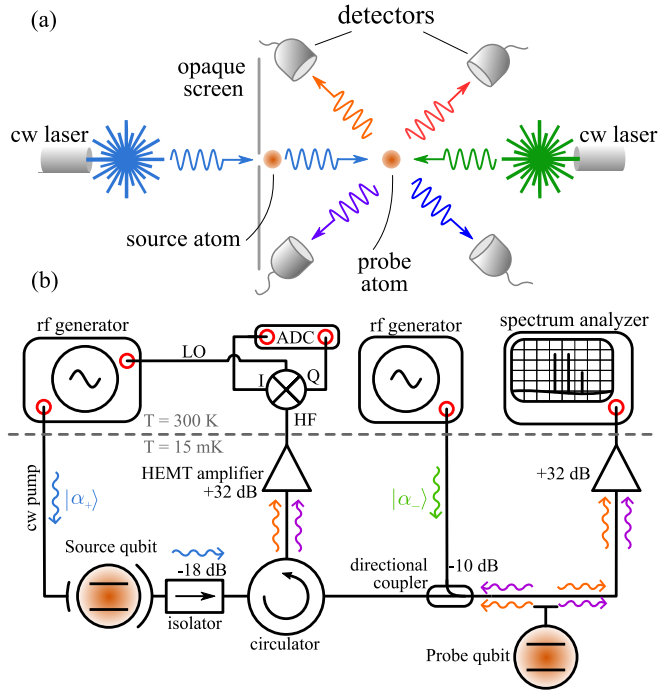

Fig. 1: (a) The optical concept of the experiment. The probe atom scatters two coherent fields: the non-classical one cominng from the source excited through small aperture in opaque screen, and the classical wave comes from external rf generator. In turn, the field from the probe is carefully detected and analyzed. (b) The simplified sketch of waveguide-QED microwave setup for the same type of experiment with two superconducting transmon qubits in the dilution refrigerator.

References

[1] Astafiev O. *et al.* Resonance fluorescence of a single artificial atom. *Science*, **327**, 840-843 (2010)

[2] Dmitriev A. *et al.* Probing photon statistics of coherent states by continuous wave mixing on a two-level system. *Physical Review A*, **100(1)**, 013808 (2019)

[3] Dmitriev, A. *et al.* Quantum wave mixing and visualisation of coherent and superposed photonic states in a waveguide. *Nature Communications* **8**, 1352 (2017).

Qantum model of optical phase modultion process with multi-frequency radio-field

Dron A.A. [1], Trifanov A.I. [2], Tushavin G.V. [3]

[1,2,3] Saint Petersburg National Research University of Information Technologies, Mechanics and Optics (ITMO University)

[1]dron.aa@phystech.edu, [2] alextrifanov@gmail.com, [3] gleb@tushavin.ru

Abstract

We theoretically study a quantum model of electro-optical light modulation process assuming a finite number of interacting optical modes. Microwave modulation field is considered to have multi-frequency spectrum. We investigate light spectrum evolution both nonoverlaping and overlapping spectrum parts corresponding to various radio-frequency modes. It was shown that under certain conditions the system has an analytical algebraic solution.

Key words: EOPM, Multiphoton processes, Quantum optics.

Introduction

Quantum optics along with solid state and soft condensed matter physics plays a fundamental role in quantum informatics and technologies [1]. Depends on particular applications polarization, space or frequency degree of freedom are used. Linear electro-optical effects underlie the operation of a number of optical devices that make it possible to work with photons in frequency domain. One of such devices is an electro-optical phase modulator [2], the theoretical description of which is the subject of this article. Here we consider a generalization of the model [3] with microwave modulating field to the case of multi-frequency modulating radio-field. To these end we examine existing exactly solvable theoretical model allowing Hamiltonian to be generated by several commuting algebras.

Model

We consider a model which implies the classical microwave field and has in its spectrum a finite discrete set of frequency modes which induces a transition between spectral lines of the optical signal. Consideration is given to the case when all modulating frequencies are multiples of some minimum frequency and satisfy the additional condition of resonance. The resulting algebra of generators of the Hamilton operator in this case is formed by the direct product of the Jordan images of the $su(2)$

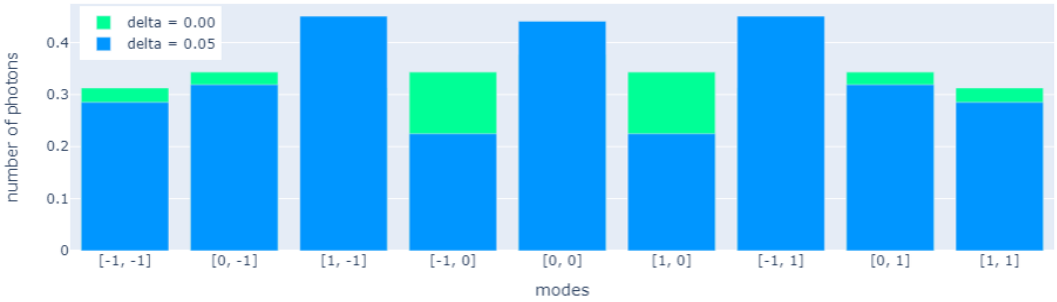

Figure 1: Intensity spectrum

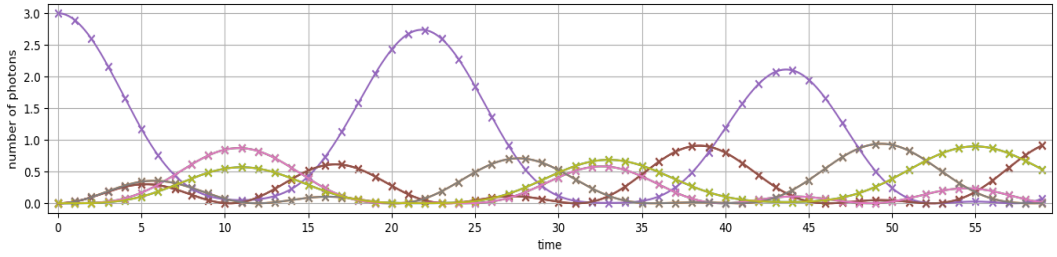

Figure 2: Dynamics of photon distribution by optical modes

Lie algebras. In this paper we consider two practically relevant scenarios. In the first case, the modulating modes are significantly different in frequency and induced parts of the spectrum do not overlap due to interaction. In the second case, spectrum overlap is allowed and the stationary conditions of the Hamiltonian are determined.

Figure 1 shows the intensity spectrum of a modulated optic signal. Two cases are considered: the first one corresponds to the independent evolution of different parts of the spectrum, and the other assumes overlap. Pairs of numbers on the horizontal axis correspond to the indexing of modes for the case of two modeling frequencies. The dynamics of photon distribution by modes in the case of overlapping spectrum components is shown in Figure 2. Each curve corresponds to a particular mode.

One possible direction for further research is to consider the continuous spectrum and spontaneous change of the photon polarization in the process of phase modulation and its transition from one polarization component of the signal to another with preservation of the frequency.

References

1. M. Hayashi, S. Ishizaka, A. Kawachi, G. Kimura, and T. Ogawa, Introduction to Quantum Information Science, Graduate Texts in Physics (Springer, 2015).

2. P. Kolchin, C. Belthangady, S. Du, G. Y. Yin, and S. E. Harris, "Electro-optic modulation of single photons," Phys. Rev. Lett. 101, 103601 (2008).

3. Miroshnichenko GP, Kiselev AD, Trifanov AI, Gleim AV. Algebraic approach to electro-optic modulation of light: exactly solvable multimode quantum model. J Opt Soc Am B 2017; 34(6): 1177-1190. DOI: 10.1364/JOSAB.34.001177.

The International Summer Conference on Theoretical Physics 2024
Faculty of Physics of ITMO University
Abrikosov Center for Theoretical Physics

Anti-PT Symmetry and Exceptional Points in Waveguides with Chiral Media

Jim A. Enriquez[1] and Pedro I. Torres[2]

[1]ITMO University

[2]Universidad Nacional de Colombia

[1]jim.enriquez@metalab.ifmo.ru, [2]pitorres@unal.edu.co

Abstract

We identify a simple and novel approach to implement anti-parity-time (PT) symmetry and exceptional points (EPs) in non-Hermitian systems, which offers a more versatile configuration beyond a spatially arranged optical potential. The introduction of chiral layers, consisting on a purely imaginary chirality parameter into Hamiltonians corresponding to dielectric achiral waveguides, which may be symmetric or asymmetric, give rise to anti-PT symmetric Hamiltonians. Such non-Hermitian Hamiltonians may exhibit EPs where two eigenvalues and eigenvectors of the system coalesce simultaneously and do not require tailored platforms with controlled optical gain and loss. Furthermore, when the waveguide can support higher-order propagation modes, which play the role of eigenstates, it is feasible to generate an EP when a pair of higher-order modes coalesces. Importantly, our waveguide platform is a theoretical proposal that can be exploited for basic research and a broad range of applications.

Key words: Exceptional Points, Anti-parity-time symmetry, chirality parameter, waveguides

Introduction

Non-Hermitian systems as theoretical models of open or dissipative systems exhibit rich novel physical properties and fundamental issues. Non-Hermitian photonic systems supporting anti-PT-symmetric EPs have been demonstrated, among others, using optical waveguides with imaginary couplings and off-the-shelf-component based standard telecommunication single-mode fibre [1].

The configurations mentioned above may have intrinsic difficulties in the experimental stage, especially the most common ones that require complex arrangements with controlled gain-loss interplay. This work introduces a new and simple design concept to obtain anti-PT symmetry and EPs based on the inclusion of chiral layers with a purely imaginary chirality parameter forming waveguides. The coupled-mode theory (CMT) is used to elucidate anti-PT symmetry and EPs in this kind of structures. In

addition, through a model based on a basis vector represented by circularly polarized light, the exact dispersion relations of this kind of structures are displayed to prove phase transitions and EPs.

Main text

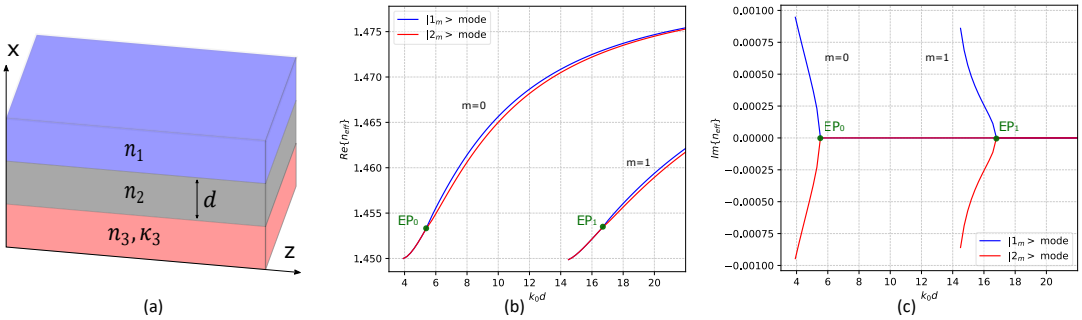

Figure 1: Anti-PT-symmetry breaking and exceptional points in the asymmetric three-layer waveguide with isotropic chiral media. (a) Schematic of the structure, (b) real part of n_{eff}, and (c) imaginary part of n_{eff}.

The waveguide with a chiral medium considered to implement anti-PT symmetry and EPs is described in Fig. 1a. CMT describes the mode hybridization of two uncoupled modes using a two-dimensional matrix representation. A linear superposition of basis vectors, which here represent the well-known TE and TM modes, defines two possible hybrid modes. In this case, a CMT for the treatment of these waveguides has to take into account the constitutive relations of chiral media for waves proportional to $e^{i\omega t}$. This analysis permits to obtain a coupled two-state problem, where the eigenvalues correspond to the propagation constants of the guided modes in the waveguides, which are directly proportional to the effective refractive indices, and the eigenvectors correspond to the coefficients of the TE and TM fields in a linear combination, as follows:

$$\mathbf{\Psi} = [\mathcal{A}\mathbf{\Psi}_{TE}(x) + \mathcal{B}\mathbf{\Psi}_{TM}(x)]e^{-i\lambda z}, \tag{1}$$

in which λ represents the eigenvalues of the system. After applying the CMT, the Hamiltonian and eigenvalues of the system result in:

$$H = \begin{pmatrix} \delta & i\kappa c_{ab} \\ -i\kappa c_{ab}^{*} & -\delta \end{pmatrix} = \begin{pmatrix} p & q \\ r & s \end{pmatrix}, \tag{2}$$

$$\lambda_{1,2} = \frac{\beta_a + \beta_b}{2} \pm \sqrt{\left(\frac{\beta_a - \beta_b}{2}\right)^2 + \kappa^2 |c_{ab}|^2}, \tag{3}$$

where $\delta = \frac{\beta_a - \beta_b}{2}$, β_a and β_b are the propagation constants of TE and TM modes, respectively, c_{ab} is a an overlap integral and κ is the chirality parameter. The hermiticity of the system depends on the chirality parameter. Considering the hermiticity of the Hamiltonian of Eq. (2), and the eigenvalues of Eq. (3), three cases can be identified: (i) the Hamiltonian is Hermitian when the chirality parameter is purely real, it implies real eigenvalues and eigenvectors; (ii) when the chirality parameter is complex, the Hamiltonian becomes non-Hermitian, and the eigenvalues are complex in any case; (iii) when the chirality parameter is purely imaginary, the Hamiltonian is non-Hermitian and anti-PT symmetric since $p = -s^*$ and $q = -r^*$. Isotropic chiral materials to saisfy the conditions mentioned above may be engineered using composite chiral material, i.e., a composite chiral material without losses due to the extinction coefficient can be formed by comprising an active isotropic material and a dissipative chiral material [3],

We describe the hybrid modes of the waveguide in the anti-PT symmetric case as a linear combination of basis vectors represented by right- and left-circularly polarized modes. This approach allows for the exact derivation of the structure's dispersion curves [2], ultimately demonstrating the existence of EPs under these conditions. As an example, the dispersion curves for the propagation modes until second order supported by the three-layer asymmetric waveguide (see Fig. 1a) are illustrated in Figs. 1b and 1c. The following parameters were used to simulate the asymmetric structure: $n_1 = 1.33$, $n_2 = 1.48$, $n_3 = 1.45$, $\kappa_3 = 0.001i$. The existence of higher-order modes in the waveguides permits to obtain EPs as a result of the coalescence of pairs of higher-order modes, which are labeled as $\mathrm{EP_m}$.

In conclusion, this work reveals that anti-PT symmetry and its transition to a broken phase can be performed with a single three-layer waveguide containing chiral media with a purely imaginary chirality parameter and mitigated extinction coefficient. Our findings open opportunities for the compatibility and integration of non-Hermitian systems within standard platforms, different from the previous typical systems to study PT-related physics.

References

1. Arik Bergman, Robert Duggan, Kavita Sharma, Moshe Tur, Avi Zadok, and Andrea Alù. Observation of anti-parity-time-symmetry, phase transitions and exceptional points in an optical fibre. *Nature Communications*, 12(1):1–9, 2021.

2. Jim A. Enriquez and Pedro Torres. Theoretical and computational study of the effects of the complex chirality parameter in planar waveguides. *J. Opt. Soc. Am. B*, 40(4):C86–C95, April 2023.

3. Tom G. Mackay and Akhlesh Lakhtakia. On gain in homogenized composite materials. In *Nanostructured Thin Films IX*, volume 9929 of *Proceedings of SPIE*, page 99290M. SPIE, 2016.

Analytical model of THz generation in p-i-n diode $Al_xGa_{1-x}As/GaAs$

X.Fan[2,*], V. Trukhin [1,2], V. Malevich [3,4]

1Ioffe Institute, 194021 Saint Petersburg, Russia

2 ИТМО University , 197101 Saint Petersburg, Russia

3Belarusian State University of Informatics and Radioe lectronics, Minsk, Belarus

4Stepanov Institute of Physics, Belarusian Academy of Sciences, Minsk, Belarus

*xfan97@gmail.com,

Abstract

This paper presents an analytical model describing the dynamics of photoelectrons excited by femtosecond optical pulses in the i-layer of a p-i-n diode $Al_xGa_{1-x}As/GaAs$. It has been shown that when the reverse bias value is changed, the THz generation mechanism is changed. The waveform of the photocurrent, respectively the THz pulse, (amplitude, duration, peak position) depends significantly on both the reverse bias and the excitation level as well as the optical excitation wavelength. At high internal electric field THz generation in a p-i-n diode is due to acceleration of electrons in the electric field to a velocity much higher than the saturation velocity at times of hundreds of femtoseconds ('velocity overshoot'), followed by a sharp decline associated with the interdomain transition of electrons from the G-valley. At electric fields less than 20kV/cm, the shielding effect has a significant influence on the formation of the photocurrent and, therefore, on the mechanism of THz generation.

Key words: p-i-n diode terahertz radiation, shielding effect, effect «velocity overshoot»

Introduction

The Monte Carlo method is commonly used to study electron transport in semiconductors. In the present work, we have investigated the charge carrier dynamics using an analytical model based on the momentum and energy balance equations with both the parameters τ_p, τ_ϵ, m_ε*, independent of the photoelectron energy and those depending (τ_p - electron momentum relaxation time, τ_ϵ - electron energy relaxation time, m_ε* effective electron mass).

Main text

The investigated medium is an AlxGa1-xAs/GaAs heterostructured p-i-n diode. The optical pulse is absorbed in the i-region of the p-i-n diode. When a p-i-n diode is excited by optical pulses (approximated by a delta function), electrons and holes are born in the i-layer and move in the electric field. Since the effective mass of an electron is much smaller than the effective mass of a hole, in our model we will take into account the dynamics of photoelectrons, considering holes to be stationary. When photoelectrons move in the i-layer, a positive hole charge is generated, which creates an electric field that screens the initial internal field. In this way, the analytical model based on the

momentum and energy balance equations is represented as follows:

$$\frac{dv}{dt} = \frac{q}{m_\varepsilon^*}E - \frac{v}{\tau_p} \quad (1)$$

$$E = E_0 - \frac{qn}{2\varepsilon\varepsilon_0}\int_0^t v dt \quad (2)$$

$$\frac{d\epsilon}{dt} = qEv - \frac{\epsilon - \epsilon_L}{\tau_\epsilon} \quad (3)$$

where q - elementary charge, E - electric field, E_0 - initial electric field strength, v - скорость фотоэлектрона, ε- dielectric constant, ε_0- vacuum dielectric constant, n-electron concentration, ϵ – photoelectron energy, ϵ_L – photoelectron initial energy. In the second equation the second term in the right part is the field produced by the positive charge of holes. The effective mass of the electron and the relaxation times in momentum and energy depend on the electron energy. To first assume them to be energy-independent. Then the solution of equation (1) can be represented in analytical form. From the solution of this equation, it follows that the motion of electrons is both ballistic and drifting. At low electron concentration ($n<10^{15}cm^{-3}$), the shielding is not significant. At high excitation levels, when the condition $\tau_p > (2^{0.5}\omega_p)^{-1}$ is fulfilled, plasma oscillations of electrons occur and the shielding effect is significant (ω_p=плазменная частота). It is worth noting that the time required for photoelectrons to reach the maximum velocity is independent of the applied electric field and is determined by the plasma frequency. Accordingly, the delay of the THz pulse generated by the p-i-n diode will be constant. By considering the dependence of τ_p, τ_ε, m_ε* on the photoelectron energy [1], the photoelectron dynamics changes and the mechanism of THz generation changes. The solutions of equations (1) and (3) were obtained numerically using the "Mathematica" computer program. Fig.1 shows the time dependences of the photocurrent for the initial photoelectron concentration $n=10^{16}cm^{-3}$ and different values of reverse bias of the p-i-n diode.

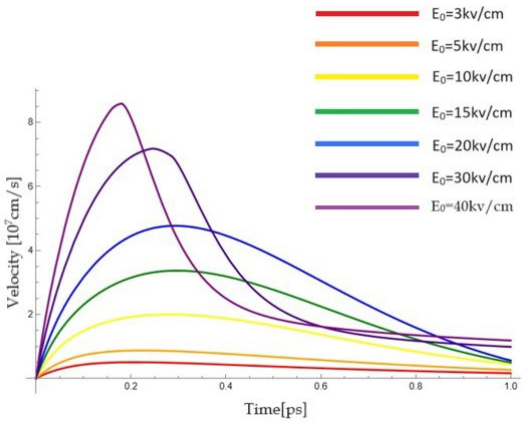

Fig.1 Time dependences of the rate of photoelectrons generated in p-i-n diode

It is clearly seen that the time required for photoelectrons to reach the maximum velocity depends on the applied electric field and the time dependence of the velocity is not monotonic. In addition, the results show that at high internal electric field the photoelectron velocity, respectively, THz generation in heterostructured p-i-n diode AlxGa1-xAs/GaAs, is due to the acceleration of electrons at the ballistic stage in the electric field to a velocity much higher than the saturation velocity at times of hundreds of femtoseconds ("velocity overshoot"), followed by a sharp decline associated with the

interdolin transition of electrons from the G-domain. At electric fields less than 20kV/cm, the shielding effect has a significant influence on the formation of the photocurrent and, consequently, on the mechanism of THz generation. The electron motion occurs in the quasi-ballistic regime. This effect leads to a shift of the maximum of the THz pulse to shorter times when back mixing is reduced, and it begins to prevail at electric fields less than 10 kV.

References

1. B.K. RIDLEY, J. appl. Phys. **48**, 754 (1977)

Laser-induced THz spin correlation dynamics in cubic antiferromagnets

Anatolii E. Fedianin,[1] Alexandra M. Kalashnikova,[1] and Johan H. Mentink[2]

[1] *Ioffe Institute, 194021 St. Petersburg, Russia*
[2] *Radboud University, Institute of Molecules and Materials, Heyendaalseweg 135, 6525 AJ Nijmegen, The Netherlands*

Two-magnon mode is a special type of THz spin excitations in antiferromagnets, usually represented as coupled magnons with opposite wave vectors from the entire magnetic Brillouin zone. Spontaneous Raman scattering (RS) on two-magnon modes was extensively studied since 1960th, both experimentally and theoretically [1–3]. Recent impulsive stimulated Raman scattering (ISRS) experiments demonstrated the excitation of such modes by femtosecond laser pulses [4–6]. This process is linked to laser-induced changes in the exchange interaction [6, 7]. However, when comparing the spectra obtained in two types of experiments, one can detect differences that, in particular, raises a question of whether the contribution from two-magnon modes in a certain part of the Brillouin zone is the same in the case of RS and ISRS [4, 8].

In this work, our goal is to study theoretically the possibility of excitation and detection of ultrafast magnetic dynamics by femtosecond linearly polarized laser pulses, being used in ISRS experiments, and compare it to the case of the RS. For this purpose, we need to introduce the single framework and define the Raman tensor across the Brillouin zone that describes the interaction of two-magnon modes with different wavevectors and light. The use of classical ferromagnetic and antiferromagnetic vectors, in this case, does not allow us to introduce the magnetic dynamics properly, since they do not describe the ground state, which is a complex superposition of wave functions [9], and two-magnon modes [6, 10]. To overcome the limitation of the classical approach, it is necessary to describe the Raman and ISRS spectra within the framework of a unified quantum theoretical approach, in particular, to obtain a Raman tensor that describes the interaction of a certain two-magnon mode with optical radiation.

In this work, we carry out the analysis of RS and ISRS in cubic antiferromagnets within the single framework, in which spin correlations are used as the microscopic parameter describing ultrafast magnetic dynamics [10]. Based on the introduced approach, we obtain the Raman tensor and its dependence on the wavevector. We derived the selection rules for the excitation and detection of spin correlations via ISRS [10], and compare their spectrum with the spontaneous Raman scattering and experimental data [6]. This enables us to reveal, that coherent two -magnon modes driven by femtosecond laser pulses can indeed have different contributions from various parts in Brillouin zone, as compared to the incoherent modes observed in Raman scattering experiments. These findings pave a way to excitation and control of THz spin dynamics with large wavevectors close to the edges of the Brillouin zone, inaccessible by other excitation methods.

This work was supported by RScF grant No. 23-12-00251 (https://rscf.ru/project/23-12-00251/).

[1] R. Loudon, Theory of infra-red and optical spectra of antiferromagnets, Adv. in Phys. **17**, 243 (1968).
[2] P. A. Fleury and R. Loudon, Scattering of Light by One- and Two-Magnon Ecitations, Phys. Rev. **166**, 514 (1968).
[3] R. J. Elliott and M. F. Thorpe, The effects of magnon-magnon interaction on the two-magnon spectra of antiferromagnets, J. Phys. C: Solid State Phys. **2**, 1630 (1969).
[4] J. Zhao, A. V. Bragas, R. Merlin, and D. J. Lockwood, Magnon squeezing in antiferromagnetic MnF_2 and FeF_2, Phys. Rev. B **73**, 184434 (2006).
[5] D. Bossini, S. Dal Conte, G. Cerullo, O. Gomonay, R. V. Pisarev, M. Borovsak, D. Mihailovic, J. Sinova, J. H. Mentink, T. Rasing, and A. V. Kimel, Laser-driven quantum magnonics and terahertz dynamics of the order parameter in antiferromagnets, Phys. Rev. B **100**, 024428 (2019).
[6] F. Formisano, T. Gareev, D. Khusyainov, A. Fedianin, R. Dubrovin, P. Syrnikov, D. Afanasiev, R. Pisarev, A. Kalashnikova, J. Mentink, *et al.*, Coherent THz spin dynamics in antiferromagnets beyond the approximation of the Néel vector, APL Materials **12** (2024).
[7] J. H. Mentink and M. Eckstein, Ultrafast quenching of the exchange interaction in a Mott insulator, Phys. Rev. Letters **113**, 057201 (2014).
[8] D. Bossini, S. Dal Conte, Y. Hashimoto, A. Secchi, R. V. Pisarev, T. Rasing, G. Cerullo, and A. V. Kimel, Macrospin dynamics in antiferromagnets triggered by sub-20 femtosecond injection of nanomagnons, Nat. Comm. **7**, 10645 (2016).
[9] P. Anderson, Limits on the energy of the antiferromagnetic ground state, Phys. Rev. **83**, 1260 (1951).
[10] A. E. Fedianin, A. M. Kalashnikova, and J. H. Mentink, Selection rules for ultrafast laser excitation and detection of spin correlation dynamics in a cubic antiferromagnet, Phys. Rev. B **107**, 144430 (2023).

Unitary equivalence of twisted quantum states

N. Filina[1] and S. Baturin[2]

[1,2] School of Physics and Engineering, ITMO University

[1]nvfilina@bk.ru, [2]s.s.baturin@gmail.com

Abstract

We provide a new angle on the evolution of twisted quantum states in a longitudinal non-stationary (non-homogeneous) magnetic field based on the formalism of Arnold transformations. We construct a unitary operator parameterised by a single function that must satisfy the Ermakov-Pinney equation. Proposed approach provides a convenient tool for the analysis of evolving twisted states.

Key words: Theoretical physics, quantum optics, Landau levels, twisted particles

Introduction

The construction of the theory of motion of twisted charged particles in electromagnetic fields is an important step towards the development of a new megascience-class machine for accelerating and studying such particles. The main applications of such particles can be diagnostics and microscopy of nanomaterials, investigation of metasurfaces with nano-features, analysis of biological molecules, quantum informatics as well as fundamental high-energy physics. [1, 2].

We present a theoretical description of the nonrelativistic motion of twisted electrons along the z axis in a time varying (or equivalently z varying) magnetic field $\mathbf{B}(t)$. The particle is considered as a wave packet localized along the propagation axis, which allows us to write $z = ct$. Therefore we describe our system in 2D. Spin effects are not taken into account.

Results

The transverse part of the Hamiltonian for a massive charge particle in the Landau gauge can be written as follows:

$$\hat{H}_\perp = \frac{p_x^2 + p_y^2}{2m} w(t) + \frac{m\omega^2(t)(x^2 + y^2)}{2w(t)} + \omega(t) L_z, \tag{1}$$

where $\omega(t) = \frac{|e|B(t)}{2m}$ is a time-dependent precession frequency for the non-stationary system and $B(t)$ is the modulus of the magnetic field directed along the z axis. We

include a linear dissipation within the Cardirola-Kanai model by introducing the dissipation factor with $w(t) = \exp\{-\int \gamma(t)dt\}$ [3] into the Hamiltonian. Where $\gamma(t)$ is the classical coefficient of friction.

To find non-stationary wave functions for the system with the Hamiltonian (1) it is convenient to use the formalism of Arnold transformations [4]. We show that under the conditions of cylindrical symmetry, there exists a unique unitary operator $\hat{\mathcal{E}}^{2D}_{1\mapsto 2}$ that establishes equivalence between the two systems with different parameters $w(t)$ and $\omega(t)$ [5]. This transformation has the form:

$$\hat{\mathcal{E}}^{2D}_{1\mapsto 2} = \exp\left\{-i\int\limits_0^{t_2} \omega_2 \hat{L}_{z_2} dt''\right\} \hat{\mathcal{E}}_{1\mapsto 2}(x,y) \exp\left\{i\int\limits_0^{t_1} \omega_1 \hat{L}_{z_1} dt'\right\}, \tag{2}$$

where operator $\hat{\mathcal{E}}_{1\mapsto 2}(x,y)$ is a trivial generalisation of the Ermakov operator [4] to the two-dimensional case without coupling between x and y degrees of freedom in the Hamiltonian. Namely,

$$\hat{\mathcal{E}}_{1\mapsto 2}(x,y) : \begin{cases} x_2 = x_1 b(t_2) \\ y_2 = y_1 b(t_2) \\ \int\limits_0^{t_1} w_1(t')dt' = \int\limits_0^{t_2} \frac{w_2(t'')}{b^2(t'')} dt'' \\ \widetilde{\psi}_2(x_2,y_2,t_2) = \frac{1}{b}\,\widetilde{\psi}_1\left(x_1,y_1,t_1\right) e^{\frac{i}{2}\frac{m}{w_2}\frac{\dot{b}}{b}(x_2^2+y_2^2)}. \end{cases} \tag{3}$$

Above, t_1 and t_2 are moments in system 1 and system 2, respectively, which pass into each other under the equivalence mapping. The function $b(t_2)$ is the parameter of the transformation that satisfies the Ermakov-Pinney equation [6, 7] of the form:

$$\ddot{b} + \dot{f}_2(t_2)\dot{b} + \omega_2^2(t_2) b = \frac{w_2^2(t_2)}{w_1^2(t_1)} \frac{\omega_1^2(t_1)}{b^3}. \tag{4}$$

The function $b(t_2)$ defines the dispersion of the wave packet during the evolution.

Many interesting consequences can be derived from the explicit form of the transformation (2). First we consider the case $w_1 = w_2 = 1$, $\omega_1 = \omega_2 = const$, which corresponds to the mapping of the system onto itself. Under the 2D Ermakov operator, a well-known stationary Landau state transforms into a non-stationary Landau state. Moreover, it turns out that such a simple connection allows a convenient evaluation of matrix elements involving nonstationary states based on the known matrix elements calculated on stationary Landau states. As an example, we show that the average energy of the nonstationary Landau state is always larger than the energy of the Landau state with the same quantum number. We also prove that during evolution in

a symmetric magnetic field a twisted electron remains twisted with the same value of the projection of the orbital angular momentum.

The work is funded by Russian Science Foundation and St. Peterburg Science Foundation, project № 22-22-20062, https://rscf.ru/project/22-22-20062/.

References

1. K. Bliokh, I. Ivanov, G. Guzzinati, L. Clark, R. Van Boxem, A. Béché, R. Juchtmans, M. Alonso, P. Schattschneider, F. Nori, and J. Verbeeck, "Theory and applications of free-electron vortex states," Physics Reports, **690**, pp. 1–70, 2017. — DOI: 10.1016/j.physrep.2017.05.006.

2. Ivanov I. P. Promises and challenges of high-energy vortex states collisions // Progress in Particle and Nuclear Physics. — 2022. — pp. 103987. — DOI: 10.1016/j.ppnp.2022.103987.

3. Caldirola P. Forze non conservative nella meccanica quantistica // Nuovo Cimento. — 1941. — **18**. — pp. 393–400. — DOI: 10.1007/BF02960144.

4. López-Ruiz F. F., Guerrero J. Generalizations of the Ermakov system through the quantum Arnold transformation // Journal of Physics: Conference Series. — 2014. — Oct. — **538**, 1. — pp. 012015. — DOI: 10.1088/1742-6596/538/1/012015.

5. N. V. Filina and S. S. Baturin, "Unitary equivalence of twisted quantum states," Phys. Rev. A, **108**, p. 012219, Jul 2023.

6. Ermakov V. P. Transformation of differential equations // Univ. Izv. Kiev. — 1880. — **20**, 1.

7. Pinney E. The nonlinear differential equation $\ddot{y} + p(x)y + cy^{-3} = 0$ // Proc. Amer. Math. Soc. — 1950. — **1**, 5. — pp. 681–681. — DOI: 10.1090/S0002-9939-1950-0037979-4.

Smith-Purcell radiation from metasurface

D. I. Garaev[1], D. Yu. Sergeeva[2], A. A. Tishchenko[3]

[1,2,3]1National Research Nuclear University "MEPhI", Moscow, Russia

[2,3]Laboratory of Radiation Physics, Belgorod National Research University, Belgorod, Russia

[1]DIGaraev@mephi.ru, [2]DYSergeyeva@mephi.ru, [3]3Tishchenko@mephi.ru

Abstract

We present general theory for Smith-Purcell radiation (SPR) from metasurface, which is a 2D array of subwavelength particles (see Fig. 1). In contrast to traditional gratings, additional dispersion relation appears determining non-zero azimuthal angles of radiation propagation. The pre-wave zone effects are considered, and schemes for its suppression are suggested. We also propose a scheme for beam position monitor.

Key words: Smith-Purcell radiation, metasurface, metamaterial, pre-wave zone, focusing, beam diagnostics

When electron moves near periodical structure (grating) it radiates. First this effect was theoretically predicted by Frank in 1942 [1] and experimentally observed only 11 years later by Smith and Purcell [2], after whom the radiation was named. Smith-Purcell radiation (SPR) stands out among other types of diffraction radiation for its especial spectral-angular distribution: (i) radiation is concentrated in a plane, perpendicular to the grating, and, (ii) what is more important, radiation is quasi-monochromatic. It means that along any direction only radiation of specific frequency is propagating. These features make SPR of huge interest in concern of radiation sources, beam and structure diagnostics.

In the case of two-periodic gratings spatial distribution of SPR changes drastically [3]. Radiation is not concentrated in a single surface, but its peaks appear for non-zero azimuthal angles according to the additional dispersion relation. We provide general theory due to the case of oblique incidence of the electron [4], which reveals significant influence on the spatial distribution. Most of the theories for radiation are valid only for the far zone, where the source of radiation looks like point-like. The paper of Verzilov [5] says that the remoteness of the far zone for diffraction radiation depends on the velocity of the electron, and for ultra-relativistic electrons it may be many meters away from the target. So, the theory of the pre-wave zone is of great interest. Such theory for SPR from a traditional grating was established was established by Karlovets and Potylitsyn [6]. We developed the theory for metasurface [7]. It follows

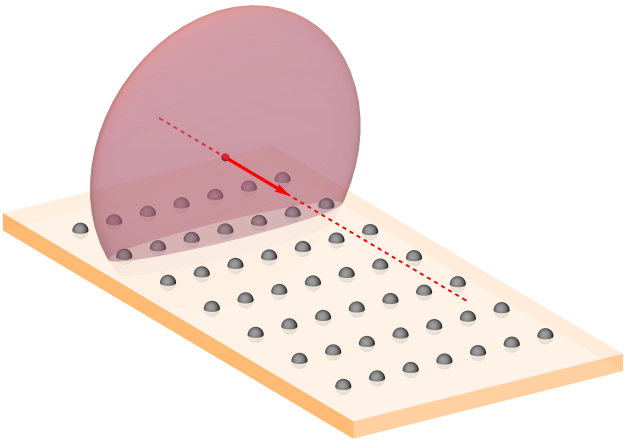

Figure 1: : Scheme of the metasurface and a free electron.

that pre-wave zone effects, associated with defocusing of radiation or, which is the same, with the loose of monochromaticity, may be suppressed by special topology of the metasurface. The general equation for the optimized metasurface is hyperbolas, which transverse in parabolas for ultra-relativistic particles and in lines for the wave zone.

Beam diagnostics based on SPR was developed predominantly for measuring the longitudinal profile [8, 9], while beam position measuring was considered only in a few papers and only for traditional gratings [10]. We propose design of the beam position monitor, based on SPR from metasurface, which promises the ability of measuring both bunch coordinates at once.

The study was partially supported by the Ministry of Science and Higher Education of the Russian Federation, Projects No. FZWG-2020-0032 (2019-1569) and No. FSWU-2023-0075.

References

1. M. Frank, Doppler effect in a refractive medium, Izv. Akad. Nauk USSR. Fizika. **6**, 3, (1942).

2. S. J. Smith and E. M. Purcell, Visible light from localized surface charges moving across a grating, Phys. Rev. **92**, 1069, (1953).

3. D. Yu. Sergeeva, A. A. Tishchenko, and M. N. Strikhanov, Microscopic theory of Smith-Purcell radiation from 2D photonic crystal, Nucl. Instrum. Methods Phys. Res., Sect. B **402**, 206, (2017).

4. D. I. Garaev, D. Yu. Sergeeva, and A. A. Tishchenko, Theory of Smith-Purcell radiation from a 2D array of small noninteracting particles, Phys. Rev. B **103**, 075403, (2021).

5. V. A. Verzilov, Transition radiation in the pre-wave zone, Phys. Lett. A **273**, 135, (2000).

6. D. V. Karlovets and A. P. Potylitsyn, Smith-Purcell radiation in the "pre-wave" zone, JETP Lett. **84**, 489 (2007).

7. D. I. Garaev, D. Yu. Sergeeva, and A. A. Tishchenko, Focusing of Smith-Purcell radiation from a two-dimensional particle array in the prewave zone, Phys. Rev. A **108**, 043515, (2023).

8. I. V. Konoplev, G. Doucas, H. Harrison, A. J. Lancaster, and H. Zhang, Single shot, nondestructive monitor for longitudinal subpicosecond bunch profile measurements with femtosecond resolution, Phys. Rev. STAB **24**, 022801, (2021).

9. V. Blackmore, G. Doucas, C. Perry, and B. Ottewell, First measurements of the longitudinal bunch profile of a 28.5 GeV beam using coherent Smith-Purcell radiation, Phys. Rev. STAB **12**, 032803, (2009).

10. G. Doucas, M. F. Kimmitt, J. H. Brownell, S. R. Trotz, and J. E. Walsh, A new type of high-resolution position sensor for ultra-relativistic beams, NIM A **474**, 10-18, (2001).

Superluminal Cherenkov effect in Compton backscattering

D. V. Gavrilenko [1] and A. A. Tishchenko [2]

[1], 2National Research Nuclear University «MEPhI», Moscow, Russia

[1]Belgorod National Research University, Belgorod, Russia

[1]dvgavrilenko@mephi.ru, [2]tischenko@mephi.ru

Abstract

Inverse Compton scattering is one of the most promising ways to generate bright quasi-monochromatic X-ray radiation from a compact source. In this work, we calculated the coherent luminosity, which allows us to take into account the effects of interference. We also showed the possibility of the appearance of the Cherenkov-like interference maximum, and also determined the parameters at which this direction coincides with the direction of Compton scattering. The proposed scheme opens up the possibility of a drastic increase in radiation intensity.

Key words: Theoretical physics, superluminal Cherenkov effect, Compton backscattering

Introduction

Inverse Compton scattering of a laser beam on relativistic electrons is one of the most promising ways to generate bright quasi-monochromatic X-ray radiation from a compact source. There are various strategies to enhance the photon flux from such sources. Increasing electron and laser beam densities can be of use here; yet, this results in multi-particle scattering and nonlinear effects, which causes a broadening of the spectrum. Alternatively, optimization of the process geometry in terms of individual collision numbers can be effective. In our research [1], we calculated the luminosity of Compton scattering across arbitrary collision and beam tilt angles. The study, however, did not consider coherent effects, which could potentially lead to a quadratic increase in intensity with particle number. Achieving coherence typically involves dividing a large beam into small bunches, each smaller than the wavelength radiation, and spacing them to create interference maxima. Yet, in the X-ray field, where Compton scattering sources are commonly used, and particularly with massive reaction products at colliders, creating suitably sized bunches is technically complicated. Even luminosity, which measures collision perfomance [2], does not inherently consider coherent effects that are essential for radiation enhancing.

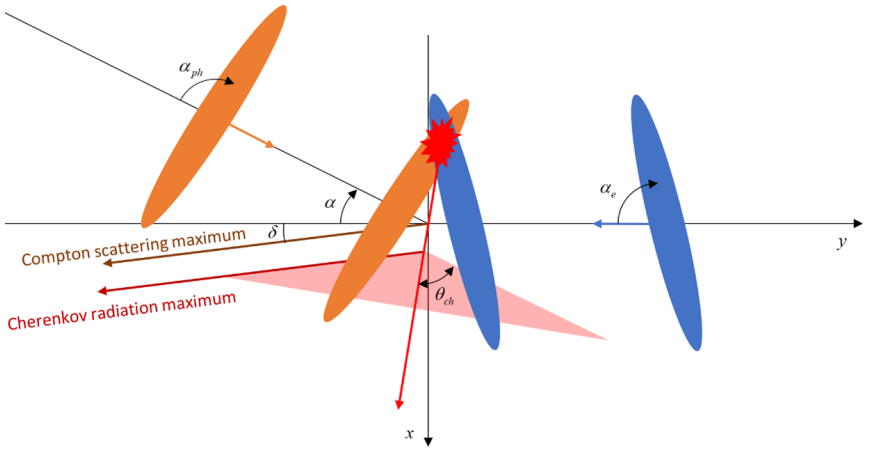

Figure 1: The intersection region of the photon (orange, left) and electron (blue, right) beam moves faster than the speed of light, resulting in a Cherenkov cone. The angles of rotation are chosen such that the maximum of Compton scattering coincides with the radiation cone.

Cherenkov amplification

There are coherent processes with continuous sources as well, for example, Cherenkov radiation. The charge moves along a continuous trajectory with characteristic dimensions not limited by the wavelength of radiation, and the angular distribution depends on frequency only due to the dielectric permittivity dispersion. This is possible because the emitter's velocity exceeds the phase velocity of light in the medium. Similar conditions can be created even in a vacuum. By properly orienting sufficiently elongated beams, it is possible to ensure that the region of their intersection moves faster than the speed of light [3].

Similar phenomena, demonstrating the superluminal Cherenkov effect, have been already explored. Studies shows that under specific conditions, a charge passing over a diffraction grating can induce regions moving faster than light, with Smith-Purcell radiation peaks aligning with the Cherenkov radiation cone [4, 5]. Additionally, in another article [6], researchers investigated a laser-illuminated conductor surface, theoretically revealing that the moving spot could emit surface and free-space waves through the Cherenkov mechanism. Similar investigations were conducted in other studies [7]. In our research, we develop a theory considering coherent effects when two beams collide at arbitrary angles relative to their propagation trajectories, applicable not only to Compton scattering but also to various processes. Using this theory, we calculate coherent luminosity for the cases when both beams are described by Gaussians with arbitrary tilts. We demonstrate that with appropriate beam tilting, a coherent

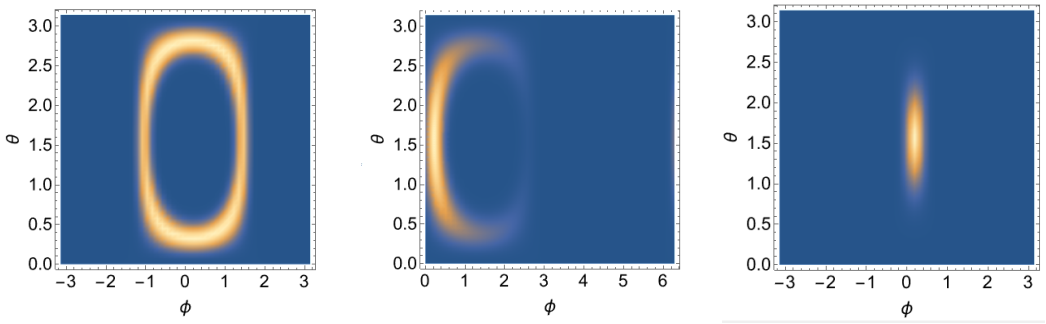

Figure 2: Different forms of coherent maxima during the collision o tilted beams.

maximum in the form of a Cherenkov cone is formed, and we identified parameters where the direction of this maximum coincides with the direction of Compton scattering, see Fig. 1.

References

1. A. P. Potylitsyn, D. V. Gavrilenko, M. N. Strikhanov, and A. A. Tishchenko, Crab crossing in inverse Compton scattering, Phys. Rev. Accel. Beams **26**, 040701 (2023).

2. W. Herr and B. Muratori, Concept of luminosity, in the proceedings of the CERN Accelerator School and DESY Zeuthen: Accelerator Physics, Zeuthen Germany, September 15–26 (2003).

3. V. L. Ginzburg, Theoretical Physics And Astrophysics, Pergamon (1979).

4. D. Yu. Sergeeva, A. A. Tishchenko, and M. N. Strikhanov, Conical diffraction effect in optical and x-ray Smith-Purcell radiation, Phys. Rev. Accel. Beams **18**, 052801 (2015).

5. A. P. Potylitsyn, D. Yu. Sergeeva, M. N. Strikhanov, A. A. Tishchenko, Diffraction radiation from a charge as radiation from a superluminal source in a vacuum. Phys.-Usp. **63**, 303 (2020).

6. M. I. Bakunov, A. V. Maslov, and S. B. Bodrov, Cherenkov radiation of terahertz surface plasmon polaritons from a superluminal optical spot, Phys. Rev. B **72**, 195336 (2005).

7. R. M. Arkhipov, I. Babushkin, M. K. Lebedev et al., Transient Cherenkov radiation from an inhomogeneous string excited by an ultrashort laser pulse at superluminal velocity, Phys. Rev. A **89**, 043811 (2014).

Nonstationary dynamics of a vortex electron in a magnetic lens

The work is dedicated to investigation of the dynamics of a vortex electron in a magnetic lens. The key feature of the work is that it considers a charged particle that enters the magnetic field region from free space crossing the boundary between the two regions. Such a scenario is most appropriate for describing the state of a particle and its dynamics at electron microscopes, inside focusing elements (magnetic lenses) at accelerators and etc. In this work we derive the nonstationary wave function that describes the transfer of the particle from free space to the magnetic field. The nonstationary solution allows one to account for the initial conditions, that is the state of the particle at the boundary. With this nonstationary solution we show that the r.m.s. of an electron oscillates in time, which is in accordance with the well known results, obtained from the Heisenberg equation. However, considerations of the Heisenberg equation do not allow one to derive the the time-averaged value of the r.m.s. radius, which can, however be done with the nonstationary wave function, that we have found. When show, that in general, when the size of the particle, when it crosses the boundary, does not match the size of an electron in a Landau state, the r.m.s. radius oscillates in time around a value typically much greater than the Landau r.m.s.. The behaviour of the r.m.s. of an electron for several experimental scenarios is presented in the following figures.

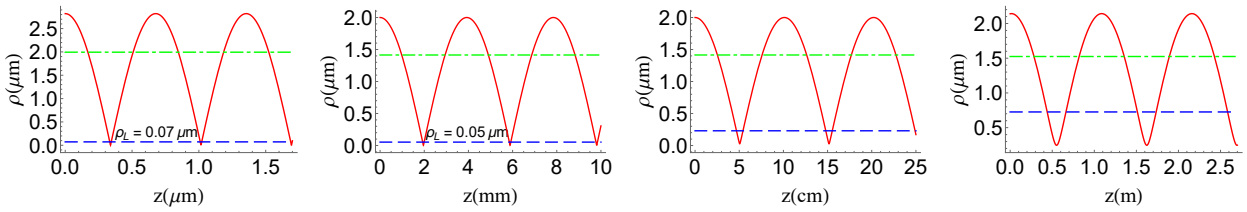

(a) (b) (c) (d)

Figure 1: Oscillations of the r.m.s. radius of the $\mathrm{NSLG_H}$ wave packet in a magnetic field (solid red line), $\rho_{\mathrm{st}} = (1/T_{\mathrm{c}}) \int_0^{T_{\mathrm{c}}} \rho^2(t)dt$ (dot-dashed green line) and ρ_{L}(dashed blue line) (a) SEM, (b) TEM, (c) medical linac, (d) conventional linac.

The International Summer Conference on Theoretical Physics 2024
Faculty of Physics of ITMO University
Abrikosov Center for Theoretical Physics

Bosonization and nonlinearities in exciton-polariton systems within the path integral approach

A. Grudinina[1,2] and N. Voronova[1,2]

[1] National Research Nuclear University MEPhI (Moscow Engineering Physics Institute), 115409 Moscow, Russia

[2] Russian Quantum Center, 121205 Moscow, Russia

grudinina.am@mail.ru

Abstract

In this work, we develop the theory of bosonization in the electron-hole-photon mixture with the exciton pairing channel, based on the equilibrium path integral technique. The approach allows one to track the nonlinearities appearing in the regime of strong coupling with photons, and includes finite temperatures, mixing of the exciton excited states, and the dark exciton contributions to so called polariton saturation self-consistently.

Key words: Theoretical physics

Introduction

Exciton-polaritons, half matter–half light quasiparticles resulting from strong coupling between excitons and photons, are considered as a promising system with high nonlinearities that can be operated even at room temperature. Reports on the scattering rates arising due to various nonlinearities in the system, such as the exciton-exciton Coulomb interaction and the Pauli blocking that leads to the saturation of the exciton oscillator strength, however, are contradictory.

Recent experiments reveal not only a substantial disagreement with those predictions but also contradictory results in comparison to each other. In particular, while some giant exciton saturation constants were recently reported for $1s$-excitons in WS_2 [1], Ref. [2] reports on the numbers two orders of magnitude smaller for the same material. Still, the saturation-related nonlinearity g_{sat} in both works exceeds the exciton-exciton interaction nonlinearity g_{ex} (in Ref. [1] the nonlinearity due to exciton pair interaction is considered overall absent). Similar studies performed in [3] for $MoSe_2$ revealed g_{ex} and g_{sat} to be of the same order, whereas in [4], these constants are smaller by one and two orders of magnitude, respectively.

Main text

In this regard, we develop the theory of bosonization in the electron-hole-photon mixture with the exciton pairing channel, based on the equilibrium path integral technique. This approach has been originally applied for excitons [5] and allows to take into account finite temperatures when considering interactions. In contrast to the standard exciton case, the presence of photons in the polariton system modifies interactions between electrons and holes within the excitons and, consequently, the Bethe-Salpeter equation, leading to the so-called 'flexible' exciton regime (when the Rabi splitting is not negligible compared to the exciton binding energy).

To get insight into the possible explanation of experimentally-observed large saturation nonlinearity in polariton systems based on transition-metal dichalcogenide crystals [1, 2, 3, 4], we restrict ourselves here to the simple limit of 'rigid' (as opposed to flexible) $1s$-exciton state. In this case, our analysis provides important results relevant to understanding the giant nonlinearities observed in TMD-based microcavities. First, we show that finite temperatures result in a sizeable change of the interaction constants so the usual zero-T expressions cannot be used for the estimates in room-temperature studies. Second, we reveal that the exciton-photon conversion is affected by the presence of reservoir particles (such as dark excitons) when considering the spins of particles at $T = 0$. We rigorously derive the terms involving the dark exciton fields in effective action, and the dark-exciton density contributions to the Rabi splitting renormalization and assume that the dark exciton-assisted exciton-photon coupling could be the possible explanation of the experimental observations.

The work of the authors is financially supported by the NRNU MEPhI Program Priority 2030. The work of A.G. is funded by the Foundation for the Advancement of Theoretical Physics and Mathematics "BASIS", under the Grant No. 22–1–5–30–1.

References

1. J. Gu, V. Walther, L. Waldecker, D. Rhodes, A. Raja, J. C. Hone, T. F. Heinz, S. Kéna-Cohen, T. Pohl, and V. M. Menon, Enhanced nonlinear interaction of polaritons via excitonic Rydberg states in monolayer WSe_2, Nat Commun **12**, 2269 (2021)

2. J. Zhao, A. Fieramosca, K. Dini, R. Bao, W. Du, R. Su, Y. Luo, W. Zhao, D. Sanvitto, T. C. H. Liew, and Q. Xiong, Exciton polariton interactions in Van der Waals superlattices at room temperature, Nat. Commun **14**, 1512 (2023)

3. P. Stepanov, A. Vashisht, M. Klaas, N. Lundt, S. Tongay, M. Blei, S. Höfling, T. Volz, A. Minguzzi, J. Renard, C. Schneider, and M. Richard, Exciton-exciton interaction beyond the hydrogenic picture in a $MoSe_2$ monolayer in the strong light-matter coupling regime, Phys. Rev. Lett. **126**, 167401 (2021)

4. L. Zhang, F. Wu, Sh. Hou, Zh. Zhang, Y.-H. Chou, K. Watanabe, T. Taniguchi, S. R. Forrest, and H. Deng, Van der Waals heterostructure polaritons with moiré-induced nonlinearity, Nature **591**, 61–65 (2021)

5. V.S. Babichenko and M.N. Kiselev, Superconductivoty in systems with excitonic instability, Journal of Moscow Phys. Soc. **2**, 311 (1992).

Plasma Grating Electron Density Evolution in Liquid Water

S. Hilal[1], A. Ismagilov[2], A. Tcypkin[3], M. Melnik[4]

[1,2,3,4]Laboratory of Femtosecond and Femtotechnologies, ITMO University, Kadetskaya line., St. Petersburg, 197101, Russia

[1]shireenhilal@itmo.ru [2]ismagilov.azat@itmo.ru, [3]tsypkinan@itmo.ru, [4]mmelnik@itmo.ru

Abstract

A theoretical study on the evolution of free electron density in a plasma grating in liquid water was conducted, yielding insights into its spatio-temporal distribution. This work serves as a preparatory step for an upcoming experimental endeavor.

Key words: Plasma grating, Plasma dynamics, Plasma modulation

Introduction

Laser-induced plasma is an intriguing area of research due to its contributions to various applications such as material processing, spectroscopy, laser-driven particle acceleration and many others [1]. Also, it works as a radiation source e.g X-ray and THz radiation [1,2]. One of the interesting configurations of plasma is the plasma grating, which is formed through the interplay of intense femtosecond laser pulses, have emerged as pivotal entities in the realm of laser-plasma interactions. These gratings serve as versatile optical elements with applications ranging from beam manipulation to probing intricate laser-plasma dynamics [3]. Liquid jets are excellent media for plasma formation due to their fluidity and ability to avoid permanent damage, high molecular density, and low ionization energy, resulting in unique nonlinear effects [2]. However, studying plasma formation in liquid jets under intense femtosecond conditions remains limited but important.

Main text

In this work, we aim to investigate theoretically the dynamics of plasma in the plasma grating configuration within liquid water. Our present results illustrate the evolution of electron density in the zone of laser pulse interaction. This investigation is beneficial for comprehending the behavior of plasma gratings in liquid water jets, understanding the optical properties of plasma including its refractive index modulation

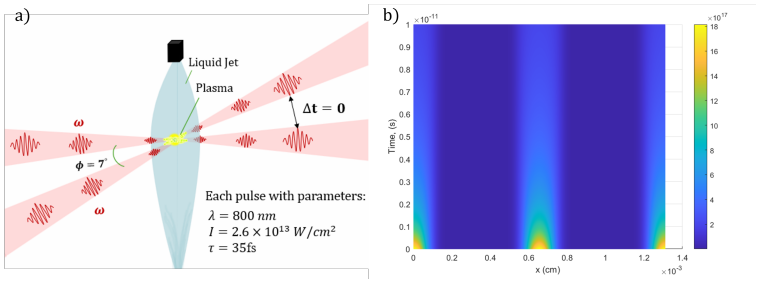

Figure 1: a) Schematic drawing of the plasma grating formation setup in water liquid jet. b) Electron density distribution in the area of the two laser pulses interaction.

and diffraction efficiency, and analyzing the spatial and temporal variations of electron density within the plasma grating. Our theoretical model is based on [3], where researchers investigated the evolution of electron density in plasma gratings in various gases. The novelty of our work lies in applying this model to liquid water. The model considers the maximum electron density resulting from ionization, as well as the decrease in free electron density over time due to ambipolar diffusion and recombination mechanisms. The pump source is a Ti:Sapphire laser with a wavelength of $\lambda = 800nm$, and, a laser density of $I = 2.6 \times 10^{13} W/cm^2$, two identical pulses are interacting simultaneously with each other at a crossing angle of $\phi = 7°$ degrees. Figure 1 depicts the spatial-temporal electron density distribution in the area of two laser pulses interaction. The maximum free electron density reaches $1.8 \times 10^{18} cm^{-3}$ in the central region of the fringes. It is evident that distinct areas with fringe separation $\Lambda = \lambda/[2\sin(\phi/2)] = 6.55 \times 10^{-4} cm$ are observable.

This model serves as a preparatory step, paving the way for our upcoming experimental endeavor. With a solid theoretical foundation in place, we are able to compare and analyze the experimental outcomes effectively.

Funding: This work was supported by the Ministry of Science and Education of the Russian Federation (No.2019-0903).

References

1. Bruggeman, Peter J., et al. "Plasma–liquid interactions: a review and roadmap." Plasma sources science and technology 25.5 (2016): 053002.

2. Ponomareva, Evgenia A., et al. "Varying pre-plasma properties to boost terahertz wave generation in liquids." Communications Physics 4.1 (2021): 4.

3. Durand, Magali, et al. "Dynamics of plasma gratings in atomic and molecular gases." Physical Review E 86.3 (2012): 036405.

A huge hysteresis in a metal-semiconductor-metal structure with a potential application as a memristor

Abolfazl Mahmoodpoor[1], Alexandr Marunchenko[1], and Sergey Makarov[1,2,*]

[1]ITMO University, School of Physics and Engineering, Kronverkskiy pr. 49, 197101, St. Petersburg, Russia
[2]Qingdao Innovation and Development Center, Harbin Engineering University, Qingdao 266000, Shandong, China
[*]corresponding author: Sergey Makarov (s.makarov@metalab.ifmo.ru)

ABSTRACT

In this study, we investigate the phenomenon of hysteresis in a metal-semiconductor-metal system, focusing on the manipulation of majority charge carriers within the bulk semiconductor through high barrier Schottky contacts. Our results demonstrate a significant current offset between forward and backward scans when applying a triangular electrical pulse to the Schottky contact, suggesting the potential for a novel memristor design based on electronic carriers. Moreover, our work lays the groundwork for the advancement of crystalline semiconductor-based memristors. While various semiconductors with tunable doping densities could be viable candidates for such memristors, our analysis using silicon highlights the promising integration of this material with current technology for two-terminal memristor applications. This research that is made on numerical calculation of drift-diffusion model opens up exciting possibilities for the development of new-generation of memristor with a tunable current amplitude by means of doping level.

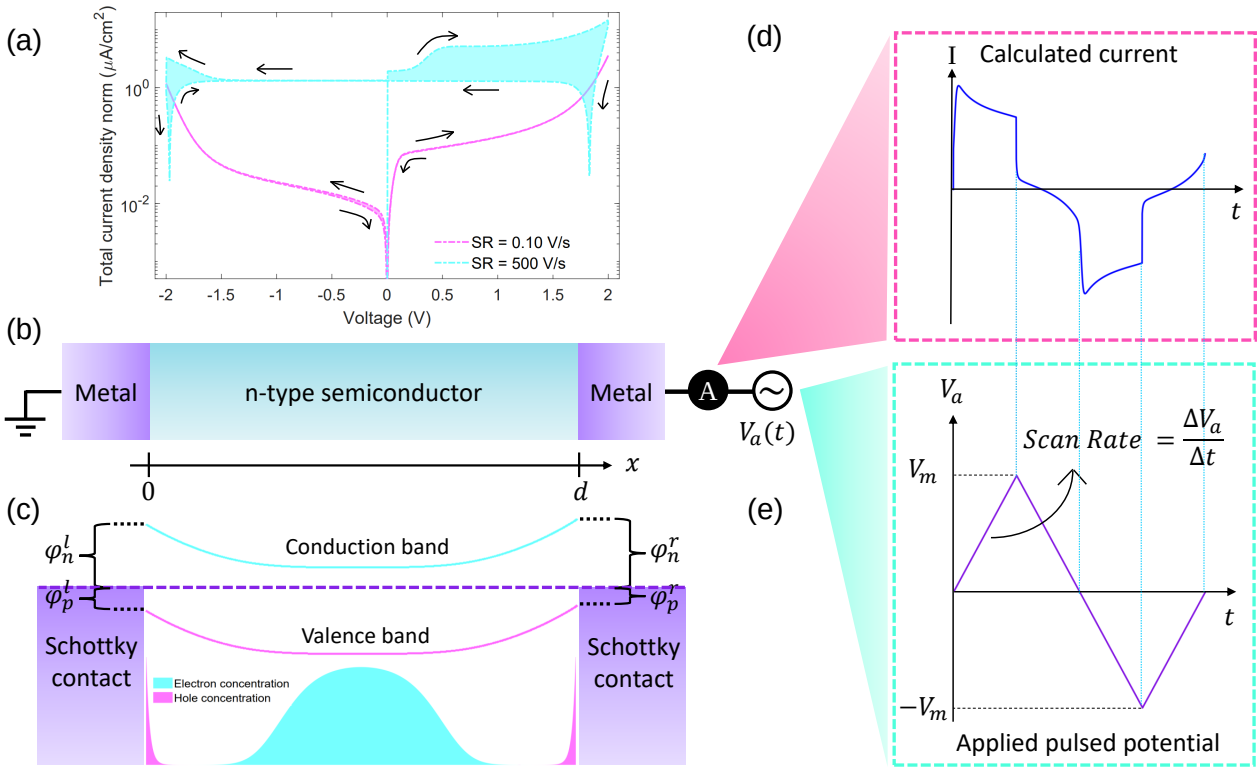

Figure 1. Simulated device. Characteristic JV curve of MSM for two SR of 0.1 V/s and 500 V/s (a), schematic of simulated devise (b), with a applied pulsed voltage (V_a) on the right contact (e) and measuring current from same contact (d), in addition to band bending due to presence of Schottky contacts and charge carrier distribution in non-logarithmic scale (c). (Schottky barrier for electron and hole is presented by $\varphi_{n,p}^{l,r}$ for electron and hole in left and right contact in "(c)" panel.)

Exciton localization on magnetic domain wall in $MoSe_2$-CrI_3 heterostructure

S. Mikkola[1], I. Chestnov[1], I. Iorsh[1,2], V. Shahnazaryan[1,3]

[1]ITMO University, Saint Petersburg 197101, Russia

[2]Queen's University, Kingston, Ontario K7L 3N6, Canada

[3]Abrikosov Center for Theoretical Physics, MIPT, Dolgoprudnyi, Moscow Region 141701, Russia

[3]vanikshahnazaryan@gmail.com

Abstract

The existence of spontaneous magnetization that fingerprints a ground-state ferromagnetic order was recently observed in two-dimensional (2D) van der Waals materials. Despite progress in the fabrication and manipulation of the atom-thick magnets, investigation of nanoscale magnetization properties is still challenging due to the concomitant technical issues. We propose a promising approach for a direct visualization of the domain walls formed in 2D magnetic materials. By interfacing 2D magnet with a transition metal dichalcogenide (TMD) monolayer, the strong proximity effects enable pinning the TMD excitons on the domain wall. The emergent localization stems from the proximity-induced exchange mixing between spin-dark and spin-bright TMD excitons due to the local in-plane magnetization characteristic of the domain wall in the magnetic monolayer.

Key words: exciton, atomic monolayer, magnetization domain wall, localization

Introduction

We consider excitons in $MoSe_2$ monolayer placed on top of a 2D magnet, represented by monolayer CrI_3, see Fig. 1 for the details. As in other Mo-based TMDs, its pristine ground state exciton is spin-bright and optically active, while the spin-dark state lies several meV above, see Fig. 1b. The temperature of heterostructure is set below the Curie temperature which results in spontaneous formation of the long-range magnetic ordering. Due to the large magnetic anisotropy of CrI_3, the spins of chromium ions point out-of-the plane within the regions of homogeneous magnetization. In between two antiparallel domains, the unit magnetization vector $\boldsymbol{M}$ makes a π-rotation and hence acquires an in-plane component. Without loss of generality we focus on the Néel-type DW which implies that spins rotate about the y-axis parallel to the wall,

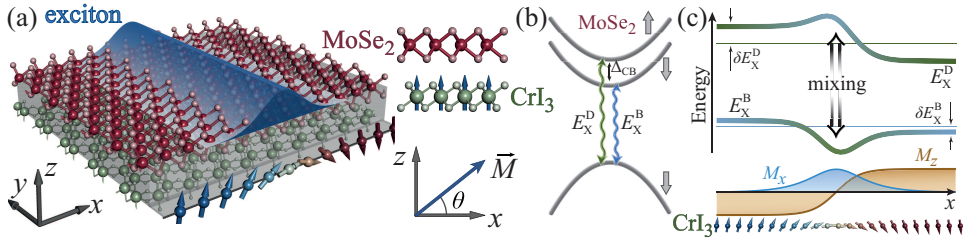

Figure 1: (a) A sketch of the heterostructure. The bottom atom-thick layer of CrI_3 contains magnetic domain wall along y-direction while the top layer of $MoSe_2$ hosting excitons is covered by a bulk hBN (not shown). The blue dome denotes the exciton state confined over the DW region. The color arrows illustrate spin orientation across DW. (b) Schematics of the $MoSe_2$ energy band structure near the K-point which features spin-bright E_X^B and spin-dark E_X^D exciton transitions. (c) A sketch of the dark-bright exciton mixing due to in-plane spin orientation in the bottom layer of CrI_3. The out-of-plane magnetization M_z (the orange curve) leads to the proximity-induced exchange valley-Zeeman splitting, which pulls exciton energy in opposite directions at the complementary sides of the DW. The in-plane magnetization component M_x locally mixes $MoSe_2$ conduction bands with opposite spins resulting in the exciton level repulsion in the DW core region. The hybridized exciton state is localized at the bottom of the resulting potential trap.

see Fig. 1(a). To be specific, we assume that the x-dependence of the spin orientation angle θ reads

$$\theta(x) = \arctan(x/l_{\rm dw}), \tag{1}$$

where $l_{\rm dw}$ stands for the DW width. Due to proximity exchange effects, both normal $M_z = \sin(\theta)$ and in-plane $M_x = \cos(\theta)$ magnetization components affect exciton states in $MoSe_2$. In particular, M_z yields a position-dependent energy shift of both spin-bright E_X^B and spin-dark E_X^D exciton species. However, as $\boldsymbol{M}$ acquires an in-plane component, spin is no longer a good quantum number for the conduction and valence band states, resulting in a local mixing between the dark and bright excitons within the same K valley, similar to the external in-plane magnetic field. This effect is sketched in Fig. 1(c). The corresponding effective Hamiltonian in real space reads:

$$\hat{H}(X) = \begin{pmatrix} -\frac{\hbar^2}{2M_{\rm B}}\frac{{\rm d}^2}{{\rm d}X^2} + E_{\rm X}^{\rm B}(X) & \alpha_e M_x(X) \\ \alpha_e M_x(X) & -\frac{\hbar^2}{2M_{\rm D}}\frac{{\rm d}^2}{{\rm d}X^2} + E_{\rm X}^{\rm D}(X) \end{pmatrix}. \tag{2}$$

Here X, $M_{\rm B[D]}$ are the coordinate and the effective mass of the bright [dark] exciton center-of-mass dynamics. Due to translation invariance along DW, the Y-dependence can be factored out. $E_{\rm X}^{\rm B[D]}(X)$ are the position-dependent resonance energies of

the bright [dark] excitons governed by the local modification of the exciton internal structure in the exchange magnetization field.

Main text

The exchange-induced mixing at the core of the DW enables exciton localization. The localized ground state has a fraction of dark exciton as a direct implication of local mixing. We note that the effective potential acting the lower hybridized exciton state is

$$E_{\mathrm{X}}^{\mathrm{eff}} = \frac{1}{2}\left(E_{\mathrm{X}}^{\mathrm{B}} + E_{\mathrm{X}}^{\mathrm{D}} - \sqrt{(E_{\mathrm{X}}^{\mathrm{B}} - E_{\mathrm{X}}^{\mathrm{D}})^2 + 4\alpha_e^2 M_x^2}\right), \tag{3}$$

which represents an eigenvalue of the potential energy terms in Eq. (2). It features a potential trap at the DW position, which qualitatively explains the effect of exciton localization. This trap originates from the local mixing while its depth is governed by the exchange coupling parameters $\alpha_{e,h}$ as well as the conduction band splitting Δ_{cb}, see Fig. 1(b). The mixing is maximized at the DW center, $X = 0$, where its efficiency is governed by the ratio $\alpha_e/|E_{\mathrm{X}}^{\mathrm{B}} - E_{\mathrm{X}}^{\mathrm{D}}|$.

The emergent asymmetry of the trap shape stems from the different effective g-factors of the bright and dark states. Given by the antiparallel spin configuration, the dark exciton is more sensitive to the out-of-plane magnetization. Therefore, on the one side of the DW the dark-bright energy splitting $\left|E_{\mathrm{X}}^{\mathrm{B}} - E_{\mathrm{X}}^{\mathrm{D}}\right|$ is reduced thus reinforcing mixing effect. On the opposite side exciton states pull apart and quench mixing. Note that the shape of the trap is mirror reflected in the K' valley. Further details can be found in Ref. [1]

References

1. S. Mikkola, I. Chestnov, I. Iorsh, and V. Shahnazaryan, Exciton localization on a magnetic domain wall in MoSe2-CrI3 heterostructures, Phys. Rev. B **108**, L201403 (2023).

Gaussian basis set for vacuum polarization calculation

V.K. Ivanov[1], A.V. Volotka[1], D.A. Glazov[1]

[1]School of Physics and Engineering, ITMO University, 197101 St. Petersburg, Russia

[1]vladislav.ivanov@metalab.ifmo.ru

Abstract

We calculate vacuum polarization effect using the finite basis set method. The Gaussian basis set is used. We calculated induced charge density and Wichmann-Kroll corrections for various κ contributions. Various heavy hydrogen-like ions were considered. We present results for induced charge density as plots, which are in good agreement with results, calculated using other methods.

Key words: Theoretical physics, quantum electrodynamics, vacuum polarization, highly-charged ions

Introduction

In the presence of heavy nucleus, the quantum electrodynamics (QED) approach is necessary. Moreover, since the coupling constant $Z\alpha$ is quite large for such systems, non-perturbative bound-state QED is used [1]. The QED effects are important for g-factor and atomic spectra calculations [2, 3]. One of such effects is the vacuum polarization (VP). Traditionally, this effect has been calculated using the Green function integration, which is a complicated and time-consuming procedure. On the other hand, for self-energy QED diagrams, the finite basis set method is being widely used [4]. For VP calculation, this method was proposed recently [5]. In our work, we follow the proposed approach of using finite basis set method for VP calculation. We use Gaussian basis set, since it shows best results for the VP calculations.

Main results

We found the VP charge density, using expression [1, 5]

$$\rho(\mathbf{x}) = ie\,\mathrm{Tr}\big\{S_F(x,x')\gamma^0\big\}\big|_{x\to x'} = \frac{e}{2}\sum_n \mathrm{sgn}(E_{\kappa,n})\phi_n^\dagger(r)\phi_n(r) \tag{1}$$

where ϕ_n are solutions to the Dirac equation in the external field of the nucleus. In the finite basis set approach, the sum is assumed to be finite, and the wave functions

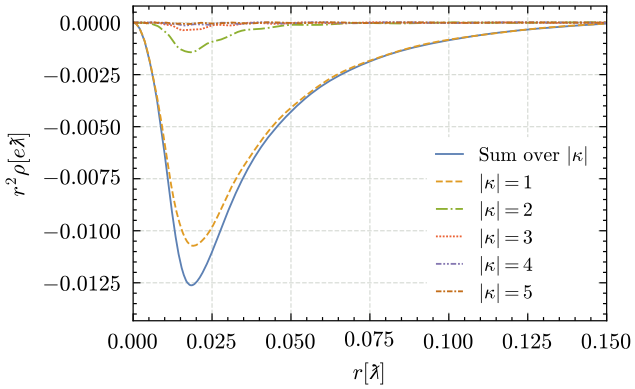

Figure 1: VP density for Uranium with $Z = 92$ and nucleus radius $r_n = 5.751$. Results for $|\kappa| = 1..5$ and sum over these components are shown

are found using variational methods, in which one take a finite sum of known basis functions and find coefficients numerically. In this work, we use Gaussian basis [5]:

$$\pi_i^{\pm}(r) = N r^{|\kappa \pm \frac{1}{2}| + \frac{1}{2}} e^{-\beta_i r^2}, \tag{2}$$

where N is normalization constant and β_i are some coefficients, defining the basis. We performed calculations for hydrogen-like heavy ions, using basis set sizes $n = 30$ and $n = 100$. The divergent Uehling term was subtracted. Using these charge densities, we calculated the Wichmann-Kroll correction for the first few electron orbitals. Results are in good accordance with results, found by other methods. For example, we found for Uranium: ΔE^{WK} =5.0332 eV and 0.8293 eV for $1s_{1/2}$ and $2s_{1/2}$ accordingly.

The studies are supported by the Russian Science Foundation (Grant No. 22-12-00258; https://rscf.ru/en/project/22-12-00258/).

References

1. P. J. Mohr, G. Plunien, and G. Soff, Physics Reports **293**, 227 (1998).

2. A. V. Volotka, D. A. Glazov, G. Plunien, and V. M. Shabaev, Annalen der Physik **525**, 636 (2013).

3. A. N. Artemyev, V. M. Shabaev, and V. A. Yerokhin, Phys. Rev. A **56**, 3529 (1997).

4. V. M. Shabaev, I. I. Tupitsyn, V. A. Yerokhin, G. Plunien, and G. Soff, Phys. Rev. Lett. **93**, 130405 (2004).

5. M. Salman and T. Saue, Phys. Rev. A **108**, 012808 (2023).

Influence of annealing of oxygen vacancies on the defect structure of bulk gallium oxide crystals

Dmitrii A. Kalganov[1], Vladislav A. Spiridonov[1], Dmitrii Iu. Panov[1], Dmitrii A. Bauman[1], Vladimir V. Kaminskii[1], and Alexey E. Romanov[1]

[1]ITMO University

May 6, 2024

The study of the spectrum of bulk's eigen oscillation in the ultrasonic frequency region can provide complete information on the elastic constants even for low-symmetry systems, such as the monoclinic crystal structure of the beta phase of gallium oxide [1]. However, obtaining such information is associated with the necessity to study the complex pattern of steady-state oscillations by laser interferometry and to perform complex calculations [2]. When studying the real structure of bulk crystals of different degrees of structural perfection, the most effective acoustic method remains the study of the resonance of the first longitudinal mode [3].

In this work, bulk crystals $\beta - Ga_2O_3$ obtained by the Stepanov method under different growth conditions were investigated. The degree of crystalline perfection was evaluated from the X-ray diffraction rocking curve for the (8 0 0) peak. The acoustic properties corresponding to the structural features were investigated by the ultrasonic composite oscillator technique. For the investigated samples, a value of the half-width of the rocking curve up to 15" was obtained, corresponding to a high degree of crystallinity. Annealing the samples in the 900°C 2h+2h+2h regime reduced the amplitude of the internal friction peak and the hysteresis area responsible for the interaction of dislocations with oxygen vacancies - Hasiguti relaxation.

References

[1] K. Adachi, H. Ogi, N. Takeuchi, N. Nakamura, H. Watanabe, T. Ito, and Y. Ozaki. Unusual elasticity of monoclinic Ga2O3. *Journal of Applied Physics*, 124(8):085102, 08 2018.

[2] M. Higashiwaki and M. H. Wong. Beta-Gallium Oxide Material and Device Technologies. *Annual Review of Materials Research*, 54, 2024.

[3] Vladimir V. Kaminskii, Dmitrii A. Kalganov, Dmitrii I. Panov, Vladislav A. Spiridonov, Andrey I. Ivanov, Margarita V. Rozaeva, Dmitrii A. Bauman, and Alexey E. Romanov. A study of gallium oxide by using the piezoelectric composite oscillator technique at a frequency of 100 kHz. *Condensed Matter and Interphases*, 25(4):548–556, 2023.

Acustomechanics of particles near an elastic substrate

V. Kleshchenko[1] and M. Petrov[2]

[1,2]Faculty of Physics of ITMO University

[1]v.kleshchenko@metalab.ifmo.ru, [2]m.petrov@metalab.ifmo.ru

Abstract

We investigated the acoustic forces acting on particles located near an elastic substrate. The resonant behavior of the force, caused by the excitation of surface waves in an elastic substrate during the scattering, was examined. Additionally, we studied the effects of binding by surface acoustic waves excited by particles, which promote the formation of stable configurations of scatterers.

Key words: Acoustic forces, scattering, surface acoustic waves, stable configurations

Introduction

Acoustic forces, arising from the exchange of momentum between sound waves and matter during the scattering process, allow for the non-invasive manipulation of mechanical objects. This effect has applications in the field of biophysics, particularly in techniques such as acoustic tweezers which can be used to sort, separate, and pattern[1] biological cells.

In the case of multiple scattering, induced interaction or binding forces between particles can lead to their self-organization into stable configurations[2]. The effects of multiple scattering on two or more particles in various regimes have been investigated, although most studies focused on scattering in free space, which may not accurately reflect practical applications. Some works have been devoted to studying scattering above the substrate, where additional contributions to the acoustic force due to multiple reflections occur. However, the effects of surface wave excitation at the interface with an elastic substrate and its influence on the formation of stable configurations are of particular interest.

Results

We investigated acoustic forces arising from scattering on systems of one and two particles located near an elastic substrate. Using the monopole approximation[3] and Green's functions formalism, we studied contributions to the acoustic forces from

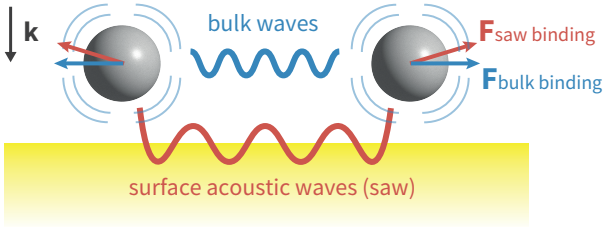

Figure 1: Acoustic forces induced by a normally incident wave on a substrate.

surface waves excited in the substrate. We analytically derived a compact expression for the effective polarizability of spherical scatterers taking into account multiple reflections between the substrate and rescattering between particles. These expressions allowed for a precise analysis of the influence of surface leaky Rayleigh waves on the acoustic force acting on a particle near an elastic substrate. These waves are excited when a plane wave impinges at a certain angle and propagate along the solid interface, radiating into the fluid half-space. They can also be excited even under normal incidence due to rescattering between the object and the substrate, resulting in resonant behavior in the acoustic forces acting on both single and multiple scatterers.

In the case of scattering on two particles under normal incidence of an external field, the acoustic forces acting parallel to the substrate are solely caused by multiple scattering between the particles. This interaction leads to the binding of scatterers along the horizontal axis. Moreover, while the normally incident external field does not directly excite a surface wave, particles positioned close to the substrate can generate surface waves themselves due to multiple reflections. These waves result in additional contributions to acoustic binding forces, creating an extra coupling channel between the particles. This effect is especially evident at large distances between the scatterers, as the surface wave propagates only in two dimensions. This allows the particles to be manipulated at large distances, ensuring a strong binding between them. Finally, stable configurations were identified in both the vertical and horizontal directions by analyzing force components for various particle arrangements.

References

1. Silva G. T. et al.. Particle patterning by ultrasonic standing waves in a rectangular cavity, Phys. Rev. Appl., **11**, 5, (2019).

2. Clair N. S. et al., Dynamics of acoustically bound particles, Phys. Rev. Res., **5**, 1, (2023)

3. Toftul I. D. et al., Acoustic radiation force and torque on small particles as measures of the canonical momentum and spin densities, Phys. Rev. Lett., **123**, 18, (2019).

Magnetic Soft Matter based on polyurethanes filled with microparticles toward Programmable and Multifunctional Miniature Machines

D. S. Konovalov[1] and V. V. Zuevr[2]

[1,2]ITMO University

[1]1dimannorm610@yandex.ru, [2]vvzuev123@gmail.com

Abstract

Miniature machines that are highly controllable have received widespread attention due to their potential applications in smart medicine and micromanipulation, especially those developed based on soft matter. The inherent compliance of soft matter can enhance the adaptability of miniature machines to a complex working environment or the objects being manipulated.: **Konovalov_ISCTP2024.pdf**.

Key words: Polyurethane, synthesized biobased polyurethane, soft machines.

Introduction

In the biomedical field, sensors that meet the long-term needs for full-scale human motion detection, including pressure caused by small activities (e.g., swallowing activity) and a large range of motion (e.g., running), have been a hot research topic. This requires sensors that meet not only high sensitivity and wide operating range but also excellent electrical conductivity, flexible wearability, lightweight, suitable modulus, excellent biocompatibility, and easy processing. The flexible skin sensors have attracted great interest in various practical medical fields, such as artificial skin and human motion health monitoring. The first function of such sensors is to monitor bodily signals and intervene in diseases promptly. The second function is to enhance human adaptability to harsh environments and facilitate the completion of challenging tasks. With the help of conformal human-machine interfaces, wearable machines (such as exoskeletons) can be controlled to perform difficult tasks. Moreover, biodevices can even replace human organs to augment their capacity.

Main text

Polyurethane is an excellent and widely used polymer material. In synthesizing polyurethane, the structure of soft and hard segments in polyurethane could be adjusted, which can obtain better properties than other polymer materials, such as good mechanical properties and biocompatibility. In recent years, due to their excellent

chemical stability, biocompatibility, and low cytotoxicity, polyurethanes have been widely used for biomedical applications. We synthesized a new biobased polyurethane and macro- and nanosized particles with magnetic properties. The polymer composites with different level of magnetic particles loading were prepared and their physical properties were studied. The response of these active soft matter on magnetic fields was studied with goal of comprehensive understanding of its deformation and actuation. Besides, systematic study on on-demand programming of material components and physical properties at the submillimeter, micro-, and even nanoscale levels was provided. Hence, the in-depth research on the material composition, response mechanisms, and programming methods of soft matter to promote the construction of novel and practical soft machines in the future was made.

The International Summer Conference on Theoretical Physics 2024
Faculty of Physics of ITMO University
Abrikosov Center for Theoretical Physics

Toroflux: A counterpart of the Chandrasekhar-Kendall state in noncentrosymmetric superconductors

M. Chernodub[1], J. Garaud[2], A. Korneev[3], A. Molochkov[4]

[1,2]Institut Denis Poisson CNRS/UMR 7013, Université de Tours, France

[3,4]Pacific Quantum Center, Far Eastern Federal University, Russia

[1]maxim.chernodub@idpoisson.fr, [3]korneev.aa@dvfu.ru

Abstract

The broken inversion symmetry of underlying crystals of noncentrosymmetric superconductors gives rise to new nontrivial phenomena. We study noncentrosymmetric superconductor using the Ginzburg-Landau effective model supplemented with a parity-breaking Lifshitz invariant. We show that these superconductors with the O point-group symmetry possess self-knotted configuration of magnetic field, which we term "toroflux". These solutions resemble Chandrasekhar-Kendall states in astrophysical plasma. We demonstrate that a magnetic dipole in the bulk of a noncentrosymmetric superconductor sources finite-energy toroflux solutions.

Key words: broken inversion symmetry, Chandrasekhar-Kendall states, superconductivity

Introduction

Superconductors react differently to an external magnetic field. In ordinary, parity-unbroken superconductors, the magnetic flux is almost totally expelled by the superconducting condensate due to Meissner effect (type I superconductivity). Ordinary type II superconductors also expel weak magnetic fields due to the Meissner effect, while if the magnetic-field background is strong enough, the magnetic flux penetrates thus superconducting medium in the form of a regular lattice or a liquid of Abrikosov vortices. Moreover, quantum or thermal fluctuations can induce unstable closed loops of such quantum vortices. Thus, apart from certain cases demonstrated in multicomponent systems that allow for different topology [1], bulk superconductors do not feature stable, localized configurations of the magnetic field (in three dimensions). Moreover, in a superconductor with a single order parameter, the magnetic flux carried by an Abrikosov vortex is necessarily quantized in units of the elementary magnetic flux.

In spite of these features, we demonstrate the existence of a new class of a compact self-supporting three-dimensional configurations of a knotted magnetic field which

carry, in general, a non-quantized flux [2]. These unusual solutions are supported in the bulk of parity-odd superconductors due to the breaking of the parity reversal symmetry [3].

Such structures are considered as superconducting counterparts of Chandrasekhar-Kendall states - the minimum-energy equilibrium configurations in the magnetohydrodynamics of highly conductive "force-free" plasma. These states appear in various physical systems, such as astrophysical plasma [4] and nuclear fusion plasma. In the latter case, Chandrasekhar-Kendall states are also known as Taylor states, which are magnetic field configurations in a spheromak [5] (a device for confining plasma, which is an analogue of a tokamak).

Main text

The properties of noncentrosymmetric superconductors are studied within the framework of the effective Landau-Ginzburg model, supplemented by the Lifshitz invariant [3], which is responsible for the breaking of inversion symmetry. This term are linear in the magnetic field and in the gradients of the superconducting order parameter: $\propto k_{ij} B_i \mathrm{Im}(\psi^* D_j \psi)$, where $\boldsymbol{D}$ is the gauge derivative of the order parameter ψ, and k_{ij} are coefficients depending on the crystal symmetry.

For the simplest case that corresponds to single component superconductor with chiral octahedral O-symmetry group (for example, PtSbS [6]), Ginzburg-Landau free energy density has following form:

$$\mathcal{F} = \frac{\boldsymbol{B}^2}{8\pi} + k|\boldsymbol{D}\psi|^2 + \frac{\beta}{2}(|\psi|^2 - \psi_0^2)^2 + \gamma \boldsymbol{j} \cdot \boldsymbol{B}\,, \tag{1}$$

where the last term $\gamma \boldsymbol{j} \cdot \boldsymbol{B}$ is a specific form of the Lifshitz invariant, and the prefactor γ controls the degree of inversion-symmetry breaking.

In the London limit we explicitly solve corresponding equations of motion. We also determine the energy and helicity densities for the infinite tower of these states. Next we demonstrate that a ferromagnetic inclusion regularizes the singular behavior of the solution (as common in the London limit), serving, at the same time, as a source for a finite-energy superconducting knotted solution. For one of the solutions the physical fields $\boldsymbol{H}$ and $\boldsymbol{J}$ induced by a magnetic dipole are displayed in the Fig. 1. This figure illustrates that a magnetic dipole impurity induces toroidal, axially symmetric, nested structures. The knotted nature of the toroflux states is rooted in the parity breaking magnetoelectric effect that generates the supercurrent along the magnetic field lines. The supercurrent also produces the magnetic field, thus linking the magnetic field lines of the toroflux.

Such knotted configurations can be experimentally detected using muon spin spectroscopy. The study of the properties of this configuration outside the London limit is planned using lattice field theory methods.

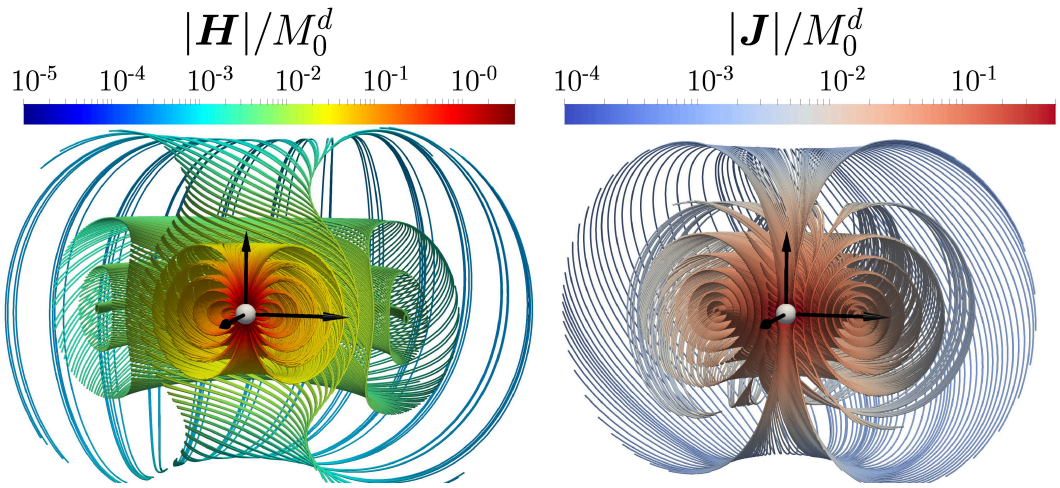

Figure 1: Visualization of a toroflux induced by a magnetic dipole. The left figure shows magnetic field lines **H**, and the right figure shows electric current lines **J**. The sphere in the center shows the position of the magnetized inclusion.

The work was supported by State assignment of the Russian Ministry of Education and Science for project No.FZNS-2024-0002.

References

1. Rybakov F.N., Garaud J., and Babaev E., Stable Hopf-Skyrme topological excitations in the superconducting state, Physical Review B **100**, 094515 (2019).

2. Garaud J., Korneev A., Samoilenka A., Molochkov A., Babaev E. and Chernodub M., Counterpart of the Chandrasekhar-Kendall state in noncentrosymmetric superconductors, Physical Review B **108**, 014504 (2023).

3. Bauer E. and Sigrist M., Non-Centrosymmetric Superconductors: Introduction and Overview. Lecture notes in physics, Springer Berlin, Heidelberg, 2012.

4. Chandrasekhar S. and Kendall P.C., On Force-Free Magnetic Fields, The Astrophysical Journal **126**, 457 (1957).

5. Rosenbluth M.N. and Bussac M.N., MHD stability of Spheromak, Nuclear Fusion **19**, 4, 489 (1979).

6. Mizutani R. et al., Superconductivity in PtSbS with a Noncentrosymmetric Cubic Crystal Structure, Journal of the Physical Society of Japan, **88**, 093709 (2019).

Three-Body Problem and Precision Physics

Vladimir I. Korobov
BLTP, Joint Institute for Nuclear Research, Dubna, Russia

A review of the modern methods in the Coulomb three-body problem will be presented. Variational methods for the nonrelativistic Schroedinger equation, relativistic corrections, and the Nonrelativistic QED will be discussed.

Application of the methods developed to various fields of physics like physics of exotic atoms (antiprotonic/pionic/kaonic helium, μCF), or precision spectroscopy of the hydrogen molecular ions H_2^+ and HD^+. Impact on the fundamental physical constants, precision determination of masses of particles and antiparticles, search for new physics will be given.

Evaluation of higher-order correlation effects in highly charged ions

Y. S. Kozhedub[1], M. Y. Kaygorodov[2], A. V. Malyshev[3], V. M. Shabaev[4], I. I. Tupitsyn[5], A. V. Volotka[6]

[1,2,3,4,5]Department of Physics, St. Petersburg State University, 199034 St. Petersburg, Russia

[3,4]National Research Centre "Kurchatov Institute" B. P. Konstantinov Petersburg Nuclear Physics Institute, 188300 Gatchina, Leningrad district, Russia

[6]School of Physics and Engineering, ITMO University, 197101 St. Petersburg, Russia

[1]y.kozhedub@spbu.ru

Key words: Highly charged ions, high-precision spectroscopy

Abstract

The structure and dynamics properties of highly charged ions (HCIs) up to an extremely high precision are described ab initio by quantum electrodynamics (QED), which is currently considered to be one of the most accurate theories of the fundamental interactions. Compared to neutral atoms or light ions, many physical phenomena are greatly enhanced in HCIs. Relativistic and Breit-interaction effects, QED corrections as well as violations of various selection rules are known to become increasingly important and influential in the structure and radiative properties of HCIs. Since extraordinary precision of QED offers unique scientific opportunities, e.g., in the search for "new" physics, its stringent experimental tests remain to be of high importance. HCI are actively studied experimentally at heavy ion storage rings and small-scale Electron-Beam-Ion-Trap facilities.

High-precision evaluations of the structure and dynamics properties of highly relativistic, tightly bound electrons in HCIs represent one of the most challenging tasks in modern theoretical atomic physics. Achieving the required theoretical accuracy in the case of few-electron HCIs is a very important and complicated problem. The calculation techniques used for high-Z ions are generically different from those used for low-Z ions, because the nuclear-strength parameter αZ (α is the fine-structure constant) is not small. Therefore, it cannot be employed as an expansion parameter, instead, the calculations have to be performed to all orders in αZ. The corresponding method

of calculation for the QED contributions of the first- and second-order diagrams are developing and applying actively, however, the technical complexity of direct calculations of QED corrections grows rapidly with increasing order of perturbation theory and the number of electrons, making them practically impossible on a large scale. In this regard, simple approximate methods for taking these corrections into account are employed [1, 2]. Further improvement of the accuracy of theoretical calculations can be achieved by developing methods that allow us to use the advantages of the exact and approximate approaches. Meanwhile, there are many experimental data whose accuracy exceeds the theoretical one, e.g., for Li-like [3], B-like [4, 5], and F-like [6, 7] ions.

To improve the theoretical predictions obtained by the rigorous QED methods (but only in the lowest orders) the correlation contributions of the higher orders can be taken into account within the lowest relativistic approximation through solution of the Dirac-Coulomb-Breit equation (DCB). The calculations can be performed both for single levels [8, 9], and in the framework of the quasidegenerate perturbation theory to rigorously account for the mixing of close levels of the same symmetry [10, 11].

In such a manner to improve prediction of the QED screening corrections we will employ an approximate approach based on the model QED operator. This can be done by isolating the higher orders of the interelectronic interaction from the QED screening results obtained with the model operator. For this purpose, we will add a small parameter in front of the interelectronic-interaction operator in the calculations with the effective QED operator [1], which will allow us to numerically decompose the QED screening correction by this parameter. Then, separating the contributions of lower orders from the total value, we will find the contribution of higher orders, which will be added to the exact QED values. The accuracy of the results obtained can be estimated from the scatter of the final values, depending on the initial approximation of the perturbation theory on the interelectronic interaction (depending on the initial screening potential).

In the present work we demonstrate merges of the rigorous QED treatment up to the second order of perturbation theory with the higher-order electron-correlation contributions evaluated within the Breit approximation and model QED operator in HCIs. To account for correlation effects in the Breit approximation, the relativistic Dirac-Fock-Sturm configuration interaction method (CI-DFS) in combination with the many-body perturbation theory [12] is utilized.

Acknowledgments

This work was supported by the Russian Science Foundation (Grant No. 22-62-00004).

References

1. V. M. Shabaev, I. I. Tupitsyn, and V. A. Yerokhin, Phys. Rev. A **88**, 012513 (2013).

2. V. V. Flambaum and J. S. M. Ginges, Phys. Rev. A **72**, 052115 (2005).

3. M. Lestinsky *et al.*, Phys. Rev. Lett. **100**, 033001 (2008).

4. S. A. King *et al.*, An Optical Atomic Clock Based on a Highly Charged Ion, Nature **611**, 43 (2022).

5. X. Liu, X. P. Zhou, W. Q. Wen, Q. F. Lu, C. L. Yan, G. Q. Xu, J. Xiao, A. V. Volotka, Y. S. Kozhedub, M. Y. Kaygorodov, Z. K. Huang, W. L. Ma, S. X. Wang, and X. Ma, Phys. Rev. A **104**, 062804 (2021).

6. G. O'Neil, S. Sanders, P. Szypryt, *et al.*, Phys. Rev. A **102**, 032803 (2020).

7. Q. Lu, C. L. Yan, G. Q. Xu, N. Fu, Y. Yang, Y. Zou, A. V. Volotka, J. Xiao, N. Nakamura, and R. Hutton, Phys. Rev. A **102**, 042817 (2020).

8. Y. S. Kozhedub, A. V. Volotka, A. N. Artemyev, D. A. Glazov, G. Plunien, V. M. Shabaev, I. I. Tupitsyn, and Th. Stoehlker, Phys. Rev. A **81**, 042513 (2010).

9. J. Sapirstein and K.-T. Cheng, Phys. Rev. A **83**, 012504 (2011).

10. Y. S. Kozhedub, A. V. Malyshev, D. A. Glazov, et. al, Phys. Rev. A **100**, 062506 (2019).

11. A. V. Malyshev, D. A. Glazov, Y. S. Kozhedub, I. S. Anisimova, M. Y. Kaygorodov, V. M. Shabaev, and I. I. Tupitsyn, Phys. Rev. Lett. **126**, 183001 (2021).

12. I. I. Tupitsyn *et al.*, Phys. Rev. A **68**, 022511 (2003); I. I. Tupitsyn *et al.*, Phys. Rev. A **72**, 062503 (2005)

Simulation of Heat Propagation Processes and Estimation of the Signal-to-Noise Ratio of a Thermoelectric Single Photon Detector

A.A. Kuzanyan, V.R. Nikoghosyan, A.S. Kuzanyan

Institute for Physical Research, Armenian National Academy of Sciences, 0204 Ashtarak, Armenia

astghik@ipr.sci.am

Abstract

This study presents the results of simulating the heat propagation processes occurring in a W/$La_{0.99}Ce_{0.01}B_6$/W multilayer detection pixel of a thermoelectric single-photon detector following the absorption of UV photons. The calculations were performed using a three-dimensional matrix method based on the equation of the heat propagation from a limited volume. Detection pixel designs yielding a signal-to-noise ratio greater than one were identified. The results indicate that the thermoelectric detector is capable of detecting single ultraviolet photons yet exhibiting high count rate.

Key words: Photodetectors, Sensors, Computer simulation, Computational modeling, Sensor phenomena

Introduction

Research in various fields such as spectroscopy, astronomy, quantum computing, biology, security, medicine, and imaging often require the detection of weak radiation, including single photons. While single-photon detectors in the infrared range have been extensively studied, the research on a single-photon detection in the UV region is relatively limited, although some progress has been made. Superconducting nanowire single-photon detectors operating in the UV range with active areas up to 56 μm in diameter, high efficiency (80%), timing resolution as low as 60 ps, and dark count rates of approximately 0.25 cph have been developed [1]. However, there is still significant interest in developing faster detectors with lower noise for various applications.

Thermoelectric single-photon detectors (TSPDs) have emerged as an alternative to superconducting detectors. Studies have shown that TSPDs based on CeB_6 and (La,Ce)B_6 compounds are capable of detecting single photons with high count rates and spectral resolution. In theory, TSPDs compete to superconducting tunnel junctions and transition edge sensors [2]. The detection pixel of a TSPD does not require strict operating conditions or additional power supply and has a simple design, minimizing the heat generation during operation.

Novelty and importance

In this study, we have investigated the feasibility of detecting UV photons using a TSPD detection pixel. The detection pixel comprises a W absorber and heat sink, a $La_{0.99}Ce_{0.01}B_6$ thermoelectric sensor, and an Al_2O_3 dielectric substrate. Through the modeling of the heat propagation processes and evaluating the noise in detection pixels of various geometries at an operating temperature of 1 K, we have determined that for 7.1 eV photons SNR = 1.77 can be achieved. While this value is not particularly high, identified certain trends suggest the

potential for increasing the SNR. It is evident that a higher SNR can be attained when photons with greater energy are detected using the same detection pixel geometry. Overall, our study highlights the possibility of detecting photons with specific energies utilizing the TSPD detection pixel setup. Furthermore, it identifies avenues for improving the SNR by adjusting the detection pixel geometry and the materials used.

Results

Computer simulations were conducted to analyze the heat propagation in th W/(La,Ce)B_6/W detection pixel (below WLW) with surface areas 4 μm²(A4) and 1 μm²(A1), following the absorption of UV photons at operating temperature of 1 K. The absorber thickness (d_1) was varied as 0.1 μm, 0.08 μm, 0.06 μm, and 0.04 μm, while the sensor thickness (d_2) was set to 0.1 μm, 0.05 μm, 0.02 μm, and 0.01 μm.

Simulations show that reducing the surface area of the detection pixel can lead to an increase of the temperature gradient and voltage across the sensor. Figure illustrates the maximum voltage (V_m) values generated on different detection pixel geometries after the absorption of single photons with the energy of 7.1 eV. Notably, detection pixels with a surface area of A1 exhibit significantly higher voltages for all absorber thicknesses considered, but V_m values decrease considerably with increasing absorber thickness.

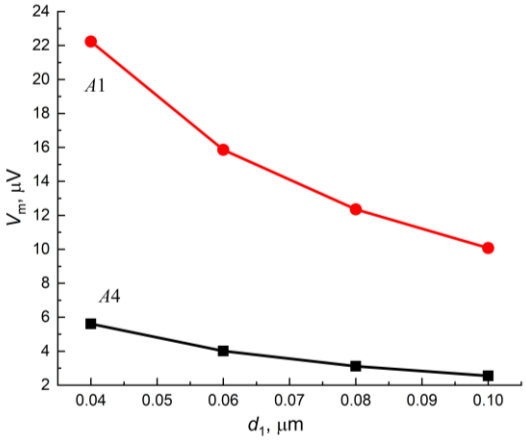

Figure 1: Dependence on the absorber thickness d_1 of maximal voltage arising on detection pixels with surface area 4 and 1 μm², d2 = 0.1 μm²

The decay time (τ) of the temporal dependence of average temperature difference on the sensor boundaries (ΔT_{avs}) increases as the sensor thickness increases, and it is longer for detection pixels with a surface area of A1, as shown in Figure 2.

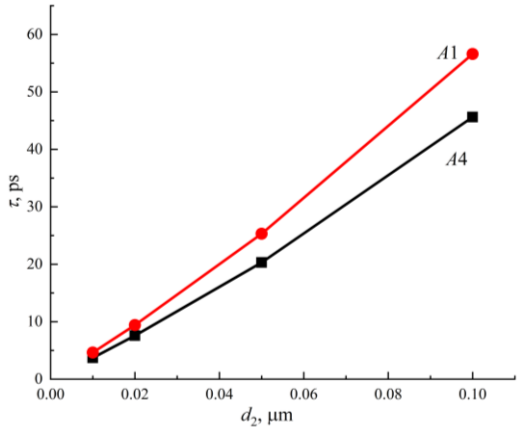

Figure 2: Dependence on the sensor thickness d_2 of the $\Delta T_{avs}(t)$ function decay time, d_1= 0.1μm

The noise of the WLW detection pixel was estimated based on formulas for thermal radiation sensors. The total noise equivalent power NEP of a thermal sensor contains two components: the phonon noise (NEP_P) of the thermal isolation structure and the Johnson noise (NEP_J) of the temperature transducer. For photons with 7.1 eV energy the data of Johnson noise equivalent power, noise power (N), signal power (P), and SNR for A1 is presented in Table 1, SNR for A4 is smaller than 1 for all considered geometries. Phonon noise equivalent power remains the same for all considered detection pixels at a value of 89 fW/Hz$^{1/2}$ due to the constant thickness of the heat sink.

Table 1: The detection pixels Johnson noise, noise power, signal power, and SNR

d1, μm	d2, μm	NEPJ, fW/Hz $^{1/2}$	N, nW	P, nW	SNR
0.10	0.10	737	98.60	2.29	0.023
0.10	0.05	521	105.12	5.73	0.055
0.10	0.02	329	111.17	16.60	0.149
0.10	0.01	233	115.86	34.30	0.296
0.08	0.10	589	84.57	3.04	0.036
0.08	0.01	186	104.71	49.80	0.476
0.06	0.10	443	69.13	4.31	0.062
0.06	0.01	140	93.68	79.60	0.850
0.04	0.10	295	51.84	6.63	0.128
0.04	0.01	93	84.47	149.00	1.770

The work was supported by the Higher Education and Science Committee of RA, in the frames of the research project № 21T-1C088.

1. E. E. Wollman, V. B. Verma, et al, UV supercon-ducting nanowire single-photon detectors with high efficiency, low noise, and 4 K operating tempera-ture, Optics Express **25**(22), 26792, (2017).
2. A. Gulian, K. Wood, et al, Current Developmental Status of thermoelectric (QVD) Detectors Nucl. Instrum. Methods Phys. Res. A **520**, 36 (2004).

Two-photon recombination in the presence of cascade processes

P. Kvasov[1], D. Solovyev[1,2], T. Zalialiutdinov[1,2]

[1]Department of Physics, St. Petersburg State University, Petrodvorets, Oulianovskaya 1, 198504, St. Petersburg, Russia

[2]Petersburg Nuclear Physics Institute named by B.P. Konstantinov of National Research Centre "Kurchatov Institut", St. Petersburg, Gatchina 188300, Russia

st103333@sudent.spbu.ru

Abstract

The work is devoted to the study of two-photon hydrogen recombination in the presence of cascade processes. Within the framework of QED theory and the S-matrix approach, an analytical derivation and a numerical calculation of the radiative corrections to the one-photon recombination cross-section are given. It is shown that the imaginary part of the one-loop bound electron self-energy operator averaged on the wave functions of a continuous spectrum leads to a well-known expression for the cross-section of one-photon recombination. Within this approach, we show that the leading order correction to the free-bound one-photon process can be identified in a similar way by studying the imaginary part of the two-loop self-energy. The results of this study could have significant implications for the theoretical understanding of hydrogen recombination kinetics, and may contribute to ongoing astrophysical research on the primordial hydrogen plasma in the early universe.

Key words: Theoretical Physics, Atomic Physics, Astrophysics

Recently, in the previous work of our scientific group, it was shown that in the presence of cascade processes, there is a fundamental difference between the two-photon level width of the excited atomic state and the corresponding two-photon transition rate [1, 2]. In particular, in [1], using the example of bound $ns/nd - 1s(n \geq 3)$ transitions in hydrogen, it was shown that the two-photon widths of the excited levels, evaluated as the imaginary part of the two-loop bound electron self-energy correction to the energy level, differ from the corresponding two-photon decay rates when one-photon cascade processes are taken into account. The obtained results can be interpreted as radiative corrections to the one-photon width.

In the present work, we continue our study by focusing on free-bound transitions and considering two-photon recombination in a hydrogen atom. Within the framework

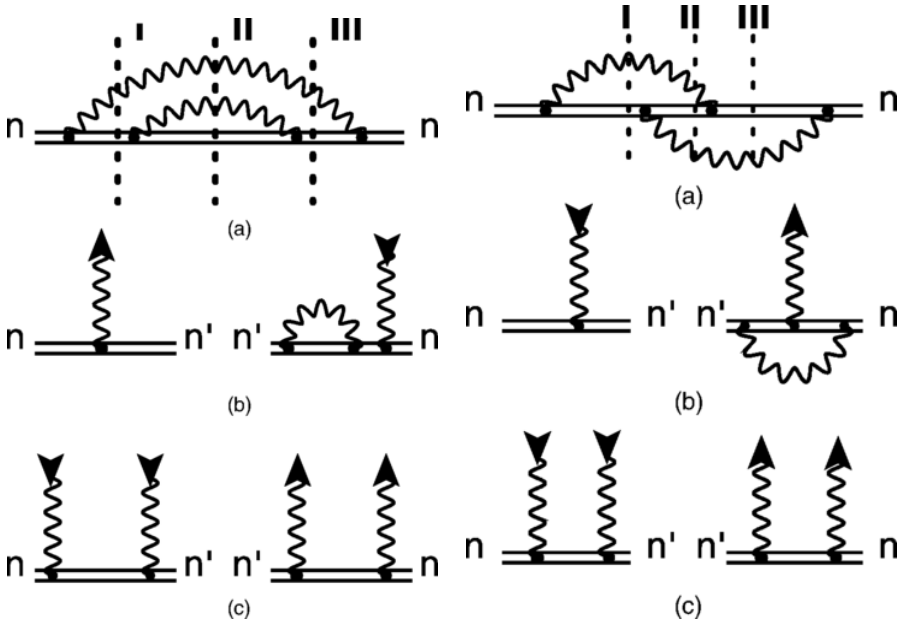

Figure 1: Feynman graphs of irreducible contributions of the two-loop self-energy of a bound electron. The three cuts I, II, II in (a) correspond to the products of amplitudes as depicted for the cut I in (b) and for the cut II in (c). A picture for the cut III is similar to that in (b). These pictures demonstrate that only the cut II corresponds to the contribution to the two-photon width [1, 2].

of QED theory and the S-matrix formalism, an analytical derivation and numerical results of the radiative corrections to the one-photon recombination cross-section is given. Following the work of [4], we consider the imaginary part of the two-loop self-energy operator averaged over the wave functions of the continuous spectrum, see Fig. 1. It is shown that with this approach the resulting expression contains no resonance terms and represents a radiative correction to the one-photon recombination cross section.

References

1. T. Zalialiutdinov, D. Solovyev, L. Labzowsky, and G. Plunien, Phys. Rev. A 89, 052502 (2014)

2. T. Zalialiutdinov, A. Anikin, and D. Solovyev, Phys. Rev. A 102, 032204 (2020)

3. U. D. Jentschura, Phys. Rev. A 69, 052118 (2004)

4. D. Solovyev, T. Zalialiutdinov, A. Anikin, J. Triaskin, and L. Labzowsky Phys. Rev. A 100, 012506 , (2019)

Egor Lazarev

Saint Petersburg University, ITMO University

Gauge invariance of the QED corrections containing self energy for electrons in bound state.

Abstract

This topic is motivated by significantly increased precision of measuring g-factor in the last few years. Therefore, in theoretical physics we have to refine the values of g-factor in order to predict experimental results. The uncertainty depends on QED effects and corrections related to finite nuclear size. The calculation of perturbation theory corrections in different gauge has not only different complexity, but in general, a different result.

QED is constructed as a gauge invariant theory. So, if we change the gauge in the entire system we should receive the same answer. The global idea in this work is to change the gauge locally. Corrections and diagrams could have different divergences and evaluation complexity in different gauge. Accordingly, we can calculate different parts of the diagrams in a different gauge, which allows us to optimize speed, precision and convergence of QED corrections.

To begin with Feynman's and Coulomb's gauges in first and second order QED correction containing self-energy. Examples of considered diagrams are in the figure 1. We will demonstrate the method of changing gauge from Feynman to Coulomb in the self-energy loop and in the other operators the gauge is untouched. As it will be shown, the corrections like self-energy, self-energy with interaction with the external potential and two electron self-energy with one photon exchange contain gauge invariant sets of diagrams where we can apply our local gauge replacement.

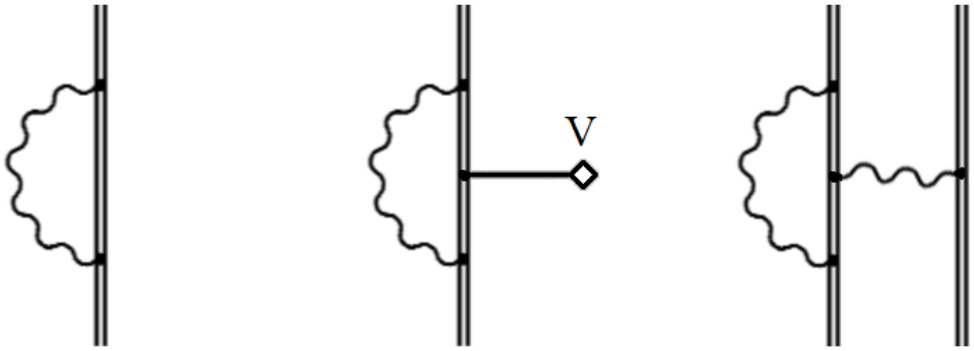

Figure 1: (a) – self-energy, (b) – vertex contribution of perturbed self-energy by an external potential, (c) – two electron self-energy with one photon exchange

After that, possible advantages from partial replacing of Feynman's gauge on Coulomb's are found in example with first-order self-energy. The precision and convergence of a series by the relativistic angular momentum analysis is presented.

The International Summer Conference on Theoretical Physics 2024
Faculty of Physics of ITMO University
Abrikosov Center for Theoretical Physics

Thermal induced energy shifts and level widths within the framework of the QED approach

J. Lopez[1], D. Solovyev [2], T. Zalialiutdnov[3]

[1,2,3] Department of Physics, St. Petersburg State University

[2,3]Petersburg Nuclear Physics Institute named by B.P. Konstantinov

[1] st084172@student.spbu.ru, [2]d.solovyev@spbu.ru

Abstract

A careful derivation of the Stark and Zeeman shifts induced by blackbody radiation (BBR) is given for the hydrogen atom in the framework of quantum electrodynamics (QED). For this purpose, a one-loop self-energy correction for the bound electron is examinated. According to the QED theory, the real part of the corresponding contribution represents the energy shift and the imaginary part constitutes the level width. The finite temperature QED formalism, which includes the substitution of the thermal part of the photon propagator, is used to identify the relevant thermal contributions. Analytical calculations show that thermal one-loop self-energy correction provides the Zeeman shift and magnetic transitions induced by blackbody radiation as next-order corrections with respect to the Stark bias and "ordinary" thermal broadening. The calculation of the latter is relevant for hyperfine transition frequencies used as operating transitions in atomic clocks.

Introduction

A theoretical description of atom interaction with blackbody radiation (BBR) was given by W. Farley and W. H. Wing in [1]. It was shown that the main effects are caused by the off-resonance and resonance components of the BBR. The resonant components of the BBR induce electric-dipole transitions to other atomic energy level, and the off-resonance components induce a dynamic Stark shift. Further discussions and evaluations is carried out for the off-resonant contributions of the BBR. An analitcal derivation of the ac Stark shift within the framework of QED theory at finite temperature was given recently in [2]. In particular, in the leading order, the energy shift was obtained as the real part of the one-loop self-energy correction for the bound electron, and the thermal broadening emerged as the corresponding imaginary part. In the framework of the present study, the thermal Zeeman shift is treated in the framework of QED at finite temperature, which is relevant for atomic clocks operating on hyperfine transitions. The corresponding imaginary part is also calculated. Here we focus on the energy shifts for the hydrogen atom at temperature $T = 300K$,

implying its application to laboratory conditions of spectroscopic experiments. The contribution of the Lamb shift and the hyperfine structure were taken into account for the numerical calculations.

Main text

Within the finite temperature QED approach, we analyse the thermal one-loop self-energy correction for the atomic electron in the one-electron approximation. The BBR induced effects are derived from one-loop self-energy correction within the S-matrix formalism. Utilising the procedure given in [2], the AC Stark shifts and BBR-induced level widths are analysed comparatively with previous results. This provides further rigorous calculations for next-order corrections in the fine structure constant, for the Zeeman shift in particular.

It is well known that the Zeeman shift is smaller than the Stark shift. However, for hyperfine transitions, where the Shark shift approaches zero, the corresponding offset can be significant at the present accuracy of the experiment. In order to obtain the magnetic interactions araised from the BBR, one should evaluate corrections of the next order in the fine structure constant. As a result the angular momentum, $\vec{l}$, and electron spin, $\vec{s}$, operators arise from the thermal one-loop self energy correction in the nonrelativistic limit. The latter represent the thermal Zeeman shift (as the real part) and the BBR-induced broadening of magnetic transitions (as the imaginary part).

For the thermal shifts, arising for specific fields that have no axial symmetry, the effect of the external field appears only in the second order over the field. For atoms with nondegenerate states, this results from the vanishing of the corresponding diagonal dipole matrix element. For isotropic fields (no axial symmetry) there is no distinct direction, so the mean value is zero. Meanwhile, for the Zeeman shift this is not aplicable, since the magnetic interaction is given by the interaction of the operator of angular momentum $\vec{l}$ and the operator of electron spin $\vec{s}$, where this operators comute between each other, that means that the angular momentum and the spin are preserved. Since they are preserved, these operators can be simultaneously reduced to a diagonal form. Therefore, for the Zeeman shift, we evaluate the diagonal matrix elements as the main contribution. The convenience of the proposed approach is the automatic finding of the field quadratic contribution for the one-loop diagram.

The numerical results obtained in the calculation of the thermal Stark shift at temperature of 300 K for various ns states of the hydrogen atom are presented. Our results can be compared with those of [1, 2, 3, 4]. The numerical results obtained for the Zeeman shift are compared with those obtained previously in [5] and [6]

References

1. W. Farley and H. Wing, Accurate calculation of dynamic Stark shifts and depopulation rates of Rydberg energy levels induced by blackbody radiation. Hydrogen, helium, and alkali-metal atoms,Physical Review A. **23**, 2397, (1981).

2. D. Solovyev, L. Labzowsky and G. Plunien, QED derivation of the Stark shift and line broadening induced by blackbody radiation, Physical Review A. **92**, 022508, (2015).

3. D. Jentschura and M. Haas, Reexamining blackbody shifts for hydrogenlike ions, Physical Review A. **78**, 042504, (2008).

4. T. Zalialiutdinov and A. Anikin, and D. Solovyev, Thermally Induced Stark Shifts of Highly Excited States of Hydrogen Atom,Journal of Experimental and Theoretical Physics. **135**, 605, (2022).

5. M. Itano and L. Lewis and D. Wineland, Shift of $^2S_{1/2}$ hyperfine splittings due to blackbody radiation, Physical Review A. **25**, 1233, (1928).

6. J. Han, Y. Zuo, and J. Zhang, Theoretical investigation of the black-body Zeeman shift for microwave atomic clocks,The European Physical Journal D. **73**, 9 (2019).

Investigation of two-photon electron capture by H-like ions

Konstantin N. Lyashchenko[1,2], Oleg Yu. Andreev [1,2], Deyang Yu [3,4]

[1]Petersburg Nuclear Physics Institute, Russia

[2]St. Petersburg State University, Russia

[3]Institute of Modern Physics, Chinese Academy of Sciences, China

[4]University of Chinese Academy of Sciences, China

[1]laywer92@mail.ru

Abstract

We present a study of two-photon electron capture by H-like ions. The energy of the incident electron was chosen to be in the region with the most significant contribution of the dielectronic recombination. We studied the photon emission spectrum. In particular, we calculated the differential over the photon energy cross section including the main resonance groups corresponding to the cascade transitions, and the low-energy photon region, where the infrared divergence required special processing. The calculations were performed within the framework of QED theory.

Key words: Theoretical physics

Introduction

The radiative electron transitions in ions and atoms are the fundamental processes in atomic physics. The one- and two-photon transitions determine the majority of possible radiative transitions. The one-photon transitions are direct transitions which occur without formation of any intermediate state, while the two- and more photon transitions can proceed both through the formation (cascade transitions) and without the formation (noncascade transitions) of intermediate states. In our work we study the two-photon electron transitions during electron capture by H-like ions.

Main text

We study for the first time the photon emission spectrum of the electron capture by H-like ions, without using such common approximations as the single-photon

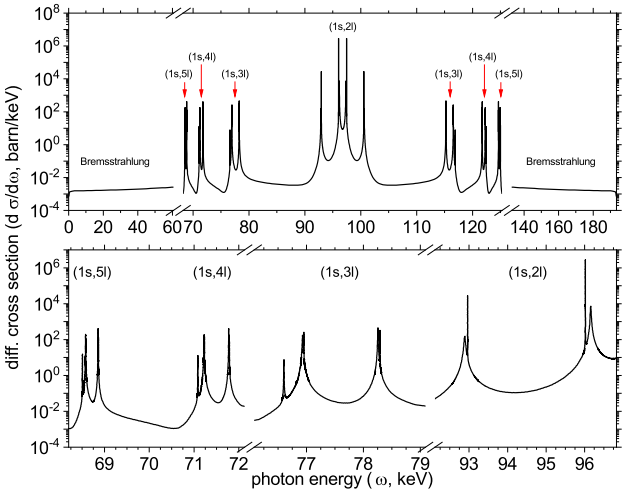

approximation [1] and the resonance approximation. The line-profile approach (LPA) [2] of QED is used for calculations.

It is customary to distinguish two channels in electron capture by ion: radiative recombination (RR) and dielectronic recombination (DR). The RR is a nonresonant channel of electron capture in which the electron is directly captured into a bound state of the ion. In contrast, the DR is a resonant channel in which the electron capture proceeds through the formation of a doubly excited state. The DR can make a significant contribution to the cross section if the energy of the initial state is close to the energy of some of the doubly excited states. Both RR and DR are taken into account in this work.

For illustration, presented figure shows differential cross section of the two-photon electron capture depending on the energy of one of the emitted photons for uranium ion. The energy of the other photon is determined by the energy conservation law. Total photon energy of the both emitted photons is 193.488 keV. The electron kinetic energy is $\varepsilon_k = 63.924\,\text{keV}$, which is close to the DR resonances corresponding to the $(2p_{1/2})^2$, $(2s2p_{1/2})_0$, and $(2s2p_{1/2})_1$ states.

Main results of this work can be found in [3].

References

1. S. Zakowicz, W. Scheid, and N. Grün, J. of Phys. B **37**, 131 (2004).

2. O. Andreev *et al.*, Phys. Rep. **455**, 135, (2008).

3. K. Lyashchenko, O. Andreev, and D. Yu, Phys. Rev. A **109**, 032805, (2024).

Engineering orbital topological states in the optical photonic molecule lattice

M. Mazanov[1], D. Román-Cortés[2], G. Cáceres-Aravena[2,3], C. Cid[2], M. A. Gorlach[1], R. A. Vicencio[2]

[1]School of Physics and Engineering, ITMO University, Saint Petersburg 197101, Russia

[2]Departamento de Física and Millenium Institute for Research in Optics-MIRO, Facultad de Ciencias Físicas y Matemáticas, Universidad de Chile, 8370448 Santiago, Chile

[3]Institute of Physics, University of Rostock, 18051 Rostock, Germany

[1] maxim.mazanov@metalab.ifmo.ru

Abstract

Topological photonics provides strategies to create localized phases of light protected against certain types of disorder and fabrication imperfections. Here, we put forward a concept of photonic molecules made from pairs of closely placed optical waveguides, and create an unconventional topological phase in a one-dimensional lattice comprising such molecules. Both inter-orbital couplings between the molecules and the geometric dimerization mechanism could open the nontrivial bandgap hosting up to a pair of localized edge states at each lattice end. The proposed method could be further applied to two-dimensional lattices to create unconventional topological phases in the optical range.

Key words: Orbital hybridization, topological photonics, femtosecond laser writing

Introduction

Topological photonics provides multiple pathways to shape the flow and localization of light from one to three dimensions as well as synthetic dimensions by utilizing various available degrees of freedom. The engineered topological disorder-robust states range from the analogs of quantum Hall, quantum spin Hall effects and valley Hall states to corner- and hinge-localized states. The large variety of platforms include polaritonic, microring resonator, plasmonic and waveguide lattices, as well as photonic crystals, covering a large spectral range from radiofrequencies to the infrared [1]. However, most designs in optics have been focused on the single-mode waveguide platforms [2], with less flexible profiles of individual waveguides and generally small topological bandgaps.

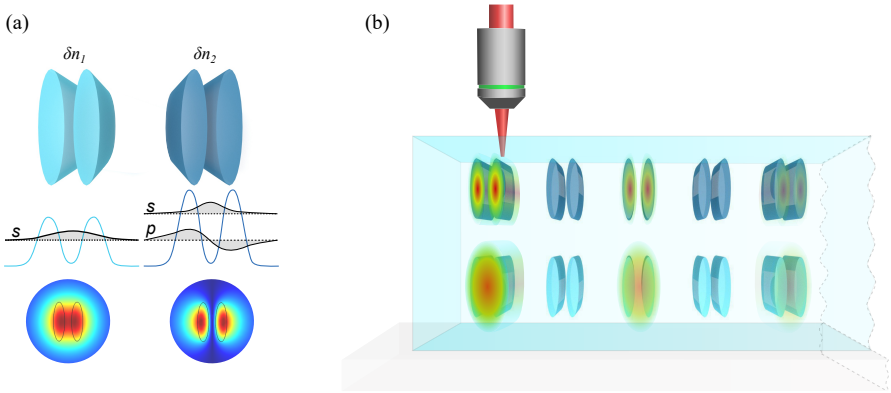

Figure 1: (a) Design of the photonic molecules composed of pair of closely placed waveguides and the corresponding modes (shown below). In a multi-orbital lattice model, the refraction index contrasts $\delta n_{1,2}$ in the two molecules are tuned so that the symmetric s mode in one molecule is degenerate with the anti-symmetric p mode in another one. (b) Design of the photonic molecule array with an edge state intensity profile displayed. The constituent waveguides are fabricated in a glass plate by the femtosecond laser writing technique.

A recent promising strategy involves engineering polarization or orbital degeneracies for individual meta-atoms comprising the lattice or their clusters, creating new pseudospin degrees of freedom. This strategy proved to be fruitful and leading to simpler lattice structures in one [3] and two [4] dimensions. In this work, we put forward a concept of photonic molecules [5] based on pair of optical laser-written waveguides, which opens the way to tuning the relevant orbital degeneracies in optics, see Fig. 1a. The relevant orbital degeneracies in different molecules could be tuned via changing the refractive index contrast by controlling the writing power. Using such molecules with degenerate symmetric and antisymmetric modes, we construct a quazi-one-dimensional lattice hosting up to two edge-localized states in the topological bandgap, see Fig. 1b.

Model and Results

The simple model which highlights the advantages of the photonic molecules is a quasi-one dimensional lattice shown in Fig. 1b with additional Su-Schrieffer-Heeger-like geometric dimerization, which could be described by a tight-binding Hamiltonian

$$\hat{H}(k_x) = \begin{pmatrix} \hat{\beta} & e^{-ik_x}\hat{\kappa}_{1-} + \hat{\kappa}_{2+} \\ e^{ik_x}\hat{\kappa}_{1+} + \hat{\kappa}_{2-} & \hat{\beta} \end{pmatrix}, \tag{1}$$

where $\hat{\beta}$ quantifies detuning of the two modes, and the coupling matrices read $\hat{\kappa}_{i\pm} = \begin{pmatrix} \kappa_{ss,i} & \pm\kappa_{sp,i} \\ \mp\kappa_{sp,i} & -\kappa_{pp,i} \end{pmatrix}$, with positive inter-orbital coupling coefficients $\kappa_{ss,i}$, $\kappa_{sp,i}$ and $\kappa_{pp,i}$ that depend on the vertical and horizontal distances between the molecules, while index $i = 1, 2$ denotes two different horizontal distances between the "rows" of the structure due to the geometric dimerization. As we prove [5], the opening of a complete bandgap in the lattice Bloch spectrum and the resulting topological characteristics depend on the competition between the orbital coupling coefficients and the dimerization, with two distinct topological phases. The first phase also appears in the non-dimerized lattice, is characterized by the conventional Zak phase, and hosts one edge state at each lattice end, according to the previously discovered inter-orbital coupling mechanism [3]. The second, geometrically dimerized phase for the lattice terminated by larger inter-column distances hosts twice as much edge states, and is characterized by the $\mathbb{Z}_3$ invariant. We observe both topological phases in the set of fabricated lattices for different wavelengths and track the topological transitions by carefully analyzing the edge intensity after propagation through the lattice excited at one of its ends, and find reasonable agreement with theoretical predictions [5].

To summarize, in this work we proposed the concept of photonic molecules in the optical range and applied it to construct an unconventional topological phase in a quazi-one-dimensional laser-written waveguide lattice. We hope that, due to the generality of our approach, it will find further applications in two-dimensional topological photonics and acoustics by helping in engineering and tuning the relevant orbital pseudospin degrees of freedom by conventional fabrication techniques.

References

1. T. Ozawa et al., Topological photonics, Rev. Mod. Phys. **91**, 015006, (2019).

2. S. Mukherjee et al., Observation of a Localized Flat-Band State in a Photonic Lieb Lattice, Phys. Rev. Lett. **114**, 245504, (2015).

3. R. S. Savelev, M. A. Gorlach, Topological states in arrays of optical waveguides engineered via mode interference, Phys. Rev. B **102**, 161112, (2020).

4. J. Schulz et al., Photonic quadrupole topological insulator using orbital-induced synthetic flux, Nat. Commun. **13**, 1-6, (2022).

5. M. Mazanov et al., Photonic Molecule Approach to Multiorbital Topology, Nano Lett. **24** (15), 4595-4601, (2024).

Exceptional point in the system of two coupled acoustic resonators

Mark Miroliubov, Mihail Petrov, Andrey Bogdanov

May 2024

In optics Non-Hermitian PT-symmetric systems are well known for there ability to provide Exceptional Point [1], the set of the system parameters, at which two or more eigenstates coalesce. However, PT symmetry requires the gain medium, that disables the transfer of the Exceptional Point formation mechanism into acoustics. In the work we investigate the acoustic system consisted of two resonators with different loss factors. It allows to extract the PT-symmetric part from the resulting Hamiltonian, providing the existence of the Exceptional Point. Tuning the coupling constant between resonators, we have experimentally demonstrated the Rabi splitting in the regime of strong coupling[2], coalescence of resonances near the Exceptional point and the loss-detunning in the weak coupling regime.

References

[1] Mohammad-Ali Miri and Andrea Alu. Exceptional points in optics and photonics. *Science*, 363(6422):eaar7709, 2019.

[2] MA Miroliubov, Anton Kirillovich Samusev, Ivan Dmitrievich Toftul, and Mikhail Igorevich Petrov. Spectral characteristics and time dynamics of tunable acoustic resonators in the strong coupling regime. *JETP Letters*, 113(8):547–553, 2021.

g factor of highly charged ions in ground and excited states: αZ expansion for correlation corrections

A. D. Moshkin[1*], D. A. Glazov[2], A. V. Malyshev[1,3], A. V. Volotka[2], D. V. Zinenko[1]

[1] Department of Physics, Saint-Petersburg State University

[2] School of Physics and Engineering, ITMO University

[3] Petersburg Nuclear Physics Institute named by B. P. Konstantinov of NRC «Kurchatov Institute»

[*]a.d.moshkin@gmail.com

Abstract

We present a study of electron correlation effects on the g factor of lithium-like ions in ground and excited states. Calculations are performed in the first five orders within the Breit approximation using the recursive perturbation theory. The Coulomb potential and various screening potentials are considered as the zeroth-order approximation potential.

Key words: Atomic physics, g factor, correlation effects, highly charged ions.

High-precision measurements of the g factor of highly charged ions provide an unprecedented test of bound-state QED [1, 2]. To date, the experimental accuracy for hydrogen-, lithium-, and boron-like ions has reached values of the order of 10^{-9} – 10^{-11} [3–7]. In particular, the most accurate value of the electron mass was obtained on the basis of these studies [8, 9]. The prospects for the development of theory and experiment with the g factor open the possibilities for independent determination of the nuclear parameters and the fine-structure constant as well as for the search for new physics [10–12].

In our study, the correlation effects on the g factor in ions with the low nuclear charge number Z are investigated for the Coulomb and various screening potentials. In the framework of the QED perturbation theory for bound states, the contribution of the interelectronic interaction $\Delta g_{\rm int}$ can be written as a $1/Z$-parameter expansion:

$$\Delta g_{\rm int} = (\alpha Z)^2 \left[\frac{1}{Z} B_1(\alpha Z) + \frac{1}{Z^2} B_2(\alpha Z) + \dots \right]. \tag{1}$$

The coefficients B_i are expanded in the parameter αZ:

$$B_i(\alpha Z) = b_i^{(0)} + (\alpha Z)^2 b_i^{(2)} + (\alpha Z)^4 b_i^{(4)} + \cdots . \tag{2}$$

We determine the coefficients $b_k^{(i)}$ for lithium-like ions in the Coulomb potential from full numerical calculationsof $\Delta g_{\rm int}$ up to the fifth order. The calculations are based on the dual-kinetic-balance method [13] with a finite basis set composed of B-splines. Corrections due to the interelectronic interaction in the Breit approximation are expanded in powers of αZ for the ground and excited $(1s)^2 2p_{1/2}$ and $(1s)^2 2p_{3/2}$ states. The dependence of the convergence of perturbation series for the energy levels on the choice of the potential in the zeroth-order Hamiltonian was also analyzed. Combining our results with high-precision non-relativistic calculations will improve the accuracy of the theoretical predictions.

References

1. Häffner H. *et al.*, High-Accuracy Measurement of the Magnetic Moment Anomaly of the Electron Bound in Hydrogenlike Carbon, Phys. Rev. Lett. **85**, 5308 (2000).

2. Sturm S. *et al.*, g factor measurements of hydrogenlike $^{20}Si^{13+}$ as a challenge to QED calculations, Phys. Rev. A **87**, 030501 (2013).

3. Sturm S. *et al.*, g Factor of Hydrogenlike $^{20}Si^{13+}$, Phys. Rev. Lett. **107**, 023002 (2011).

4. Köhler F. *et al.*, Isotope dependence of the Zeeman effect in lithium-like calcium, Nat. Commun. **7**, 10246 (2016).

5. Wagner A. *et al.*, g factor of lithiumlike silicon $^{20}Si^{13+}$, Phys. Rev. Lett. **110**, 033003 (2013).

6. Arapoglou I. *et al.*, The g factor of Boronlike Argon $^{40}Ar^{13+}$, Phys. Rev. Lett. **122**, 253001 (2019).

7. Glazov D. A. *et al.*, g Factor of Lithiumlike Silicon: New Challenge to Bound-State QED, Phys. Rev. Lett. **123**, 173001 (2019).

8. Sturm S. *et al.*, High-precision measurement of the atomic mass of the electron, Nature **506**, 467 (2014).

9. Tiesinga E. *et al.*, CODATA recommended values of the fundamental physical constants: 2018, Rev. Mod. Phys. **93**, 025010 (2021).

10. Shabaev V. M. *et al.*, g-Factor of Heavy Ions: A New Access to the Fine Structure Constant, Phys. Rev. Lett. **96**, 253002 (2006).

11. Yerokhin V. A. *et al.*, g Factor of Light Ions for an Improved Determination of the Fine-Structure Constant, Phys. Rev. Lett. **116**, 100801 (2016).

12. Debierre V. *et al.*, Testing standard-model extensions with isotope shifts in few-electron ions, Phys. Rev. A **106**, 062801 (2022).

13. Shabaev V. M. *et al.*, Dual Kinetic Balance Approach to Basis-Set Expansions for the Dirac Equation, Phys. Rev. Lett. **93**, 130405 (2004).

Non-adiabatic polariton condensation in annular optical traps

I. Chestnov[1], E. Cherotchenko[2], A. Nalitov[3,4]

[1]ITMO University

[2]Ioffe Institute

[3]Abrikosov Center for Theoretical Physics, MIPT

[4]University of Wolverhampton

Abstract

In analogy with superfluidity, nonequilibrium polariton condensation can be phenomenologically described in terms of separated condensed and normal fractions. Under the assumption of significantly shorter characteristic timescale, the incoherent part is frequently traced out adiabatically. In this work, we stress the importance of accounting for the time-resolved coupling between the condensed and normal fractions. Even in the case of a significant mismatch in the evolution rates, the coupling with the normal fraction drastically alters the condensate dynamics and leads to a variety of previously overlooked phases in a confined configuration. Focusing on the case of annular optically induced traps for polaritons, we elaborate on the non-adiabatic model of polariton condensation. Using the two-mode approximation, accounting for a couple of quantized polariton vortices with opposite angular momenta, we identify the range of validity for the adiabatic elimination of the incoherent reservoir. Beyond this range, the non-adiabatic interaction with a circularly symmetric trapping reservoir supports multistability, limit cycle dynamics, and formation of a neutral equilibrium standing wave phase featuring spontaneous breaking of the continuous radial symmetry. In the presence of a weak trap asymmetry, the non-adiabaticity prevents formation of giant polariton vortices. We argue that our detailed description gives interpretation to the dominance of the standing wave phase over persistent vortex phase in experimental observations [1].

Key words: Exciton-polariton nonequilibrium condensation

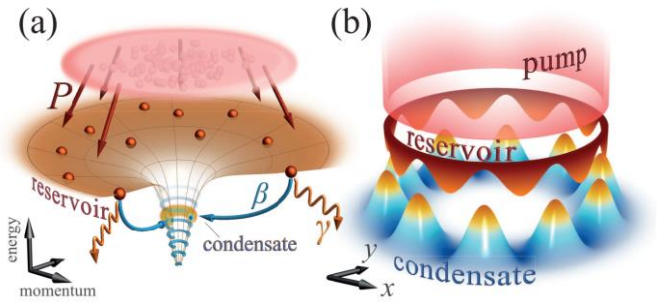

Figure 1: A sketch of nonequilibrium polariton condensation in annular optically induced traps in reciprocal space (a) and in real space (b).

References

1. I. Chestnov, E. Cherotchenko, A. Nalitov, Non-adiabatic polariton condensation in annular optical traps, **arXiv:2311.04102**, (2024).

Various simplified models of inhomogeneous polarization and their influence on effective properties of piezoceramic composites

A.V. Nasedkin

Institute of Mathematics, Mechanics and Computer Science,
Southern Federal University, Rostov on Don, Russia

avnasedkin@sfedu.ru

Abstract

Different polarization models of a piezoceramic composite material are considered, based on the preliminary determination of the polarization field by solving a linear problem of electrostatics, simulating the polarization process of piezoceramics.

Key words: Piezoelectricity, Piezoelectric Composite, Piezoceramics, Inhomogeneous Polarization, Effective Modulus, Anisotropy

Introduction

The effectiveness of using piezoceramic materials in modern technology is determined by their high dielectric constants and coupling electromechanical coefficients. These properties distinguish piezoceramics from most natural piezoelectric substances. In this case, piezoceramics are synthesized as a result of special technological processes, including high-temperature firing and polarization. During the polarization process, the crystallite domains are oriented predominantly by the direction of the applied polarization field, and ultimately, conventional macroscopically continuous piezoceramics can be considered a homogeneous anisotropic material in which the anisotropy properties are related to the direction of the polarization vector. However, composite piezoceramics at the microlevel are inhomogeneously polarized. Therefore, modeling its properties at the micro and macro levels is an important task. Some simplified approaches to solving this problem are discussed in this brief paper.

Modelling of non-uniform polarization and determination of effective properties

Dense piezoceramics is usually considered in the framework of the linear theory of electroelasticity as a homogeneous anisotropic material of the hexagonal system of the 6*mm* class. Its electromechanical modules then have the properties of a transversally isotropic material, for which the Ox_3 axis coincides with the polarization axis, and the position of the Ox_1 and Ox_2 axes in the perpendicular plane is not significant. However, in the case of a composite with a piezoceramic matrix and inclusions of elastic material or pores, the moduli of the effective homogeneous medium may have the properties of materials of other anisotropy classes. This effect can be caused by the presence of preferential orientation of inclusions or pores along certain directions, as well as the anisotropy of representative volumes or periodicity

cells in metamaterials. Besides, in a composite structure, the piezoceramic matrix may already be non-uniformly polarized since the polarization field will be inhomogeneous in the vicinity of inclusions or pores. This will be especially noticeable for piezocomposites with metal inclusions or for porous piezocomposites with metallized pore surfaces [1]. In such cases, when calculating the effective moduli, it is necessary to consider the inhomogeneous polarization of the piezoceramic matrix of the composite.

We first investigate various simplified models for the pre-polarization of piezoceramics in representative volumes of piezocomposites. They are based on a solution using the finite element method to the electrostatic problem of a composite dielectric in a linear formulation under the action of an electric field along the assumed polarization axis. In this problem, it is assumed that the composite consists of an unpolarized piezoceramic matrix, which is treated as an isotropic material, and inclusions or pores. In this problem, it is proposed that the composite consists of a non-polarized piezoceramic matrix, which is considered as an isotropic material, and inclusions or pores. As a result of solving a problem that simulates the polarization process, the electric induction field and the electric field are found, and from them the polarization field is determined, which turns out to be inhomogeneous both in direction and in magnitude. Further, in a representative volume element of the composite, its matrix is considered as polarized piezoceramics with inhomogeneous electromechanical properties.

Various polarization models are discussed, which differ in the methods of determining the moduli of inhomogeneously polarized piezoceramics based on the found directions and values of the polarization vector; by moduli of non-polarized ceramics; and by moduli of uniformly polarized piezoceramics in local coordinate systems related to the direction of the polarization vector [2]. At the same time, in the development of the models from [2], modified models are also considered using moduli of uniformly polarized piezoceramics from various forms of constitutive relations of piezoelectric media, as well as “superpolarization” models with a limitation on the value of the polarization field intensity coefficient.

Next, we study the problems of homogenization of piezocomposites with a nonuniformly polarized piezoceramic matrix, the moduli of which are calculated using previously proposed models. The results of calculations of the effective properties of various piezocomposites are presented and their dependencies on polarization models are analyzed.

This research was supported by the Russian Science Foundation, grant number No. 22-11-00302.

References

1. A. Nasedkin, M.E. Nassar, Numerical investigation of the effect of partial metallization at the pore surface on the effective properties of a porous piezoceramic composite, J. Adv. Dielectr., **11**, 2160009, (2021).

2. A.V. Nasedkin, A.A. Nasedkina, Y.V. Tolmacheva, Computer homogenization of porous piezoceramics of different ferrohardness with random porous structure and inhomogeneous polarization field, Computational Continuum Mechanics, **16**, 476, (2023).

Bound states in the continuum in a chain of ceramic discs with structural disorder

R. Nazarov[1], D. Khanabiev[1], E. Chernysheva[1], E. Maslova[1],

A. Bogdanov[1,2], Z. Kondratenko[1]

[1]ITMO University, School of Physics and Engineering, Lomonosova st. 9, 197101, Saint-Petersburg, Russia

[2]Harbin Engineering University, Qingdao Innovation and Development Center, Sansha road 1777, 266000, Qingdao, Shandong, China

[1]nazarov@metalab.ifmo.ru

Abstract

Being a resonance state with infinite lifetime, bound states in the continuum (BIC) became a curios phenomena for the studying in acoustics, hydrodynamics and optics. Due to the physical limitations in a real structures, BICs become radiative and transform into *quasi*-BICs. Thus, the study of their robustness in a real systems is important task. In this work we experimentally investigate the influence of the structural disorder on the BIC's Q factor. Our results are important from the practical point of view, since the in a real structures defects plays a decisive role.

Key words: Bound states in the continuum, structural disorder, chain of ceramic disks

Introduction

Bound states in the continuum (BIC) can be described as non-radiating resonant states whose energy embedded to the continuum spectrum of propagating waves in the surrounding space [1]. Owing to several constraints imposed by real structures, including finite size, material losses, and the presence of structural defects during fabrication, these states manifest themselves as *quasi*-BICs with a finite lifetime [1]. Therefore, the investigation of BICs' robustness against such limitations in real systems is an urgent task.

Results and Discussion

In this study, we investigate the impact of structural disorder on the Q factor of a *quasi*-BIC (q-BIC) mode with zero orbital angular momentum. Here we consider the

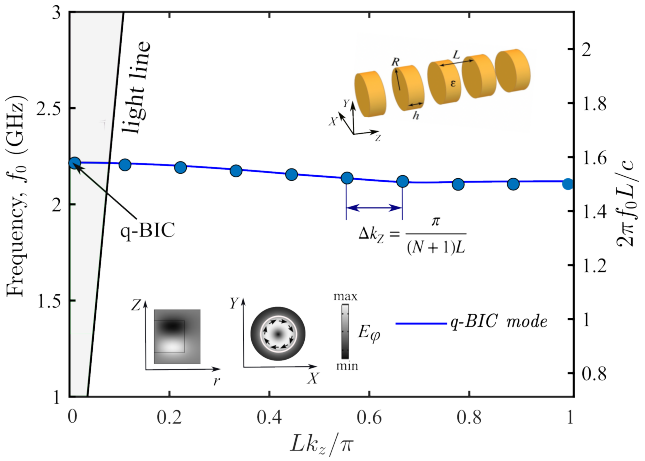

Figure 1: Band diagram and geometry of the disk chain with a period L =34 mm, radius R =15 mm and height h =20 mm.The permittivity of the disk and the loss tangent are $\varepsilon = 44$ and $\tan\delta = 10^{-4}$, respectively. Insets show the field distribution of q-BIC mode. The points in the dispersion curve indicate the zone quantization, where N is the number of disks.

periodic chain of ceramic disks with period L =34 mm, radius R =15 mm and h =20 mm. The ceramic's permittivity and its dielectric loss tangent are equal to $\varepsilon = 44$ and $\tan\delta = 10^{-4}$, respectively. Figure 1 shows the band diagram and mode distribution, which were obtained by COMSOL Multiphysics. Next, we solve eigenvalue problem for finite chain of disks with the presence of the structural disorder. The structural disorder was induced by the parameter σ and by the random change of the disks center coordinates. The random coordinates were uniformly generated in Matlab.

To sum up, we found that the total quality factor of *quasi*-BICs decreases as $Q \propto \sigma^{-1}$, which differs from the quadratic law obtained in [2]. Our results are important for the experimental implementation of BIC in real photonic structures, where structural defects plays a decisive role.

References

1. Kirill Leonidovich Koshelev, Zarina Fail'evna Sadrieva, Alexey Aleksandrovich Shcherbakov, Yurii Semenovich Kivshar, and Andrey A Bogdanov. Bound states in the continuum in photonic structures. *Phys.-Usp*, 93:528–553, 2023.

2. Ekaterina E Maslova, Mikhail V Rybin, Andrey A Bogdanov, and Zarina F Sadrieva. Bound states in the continuum in periodic structures with structural disorder. *Nanophotonics*, 10(17):4313–4321, 2021.

The pilot application of the CCSD (Coupled Cluster Singles and Doubles) method for calculating the structural parameters of perovskites using the Compound-tunable Embedding Potential method

I. Odud[1,2], Yu. Lomachuk[1], D. Maltsev[1], V. Shakhova[1], A. Oleynichenko[1], N. Mosyagin[1], L. Skripnikov[1,2], A. Titov[1,2]

[1]Petersburg Nuclear Physics Institute named by B. P. Konstantinov of NRC «Kurchatov Institute», Gatchina, Russia
[2] Saint Petersburg State University, Russia

Perovskites have proved themselves to be materials with unusual physical and chemical properties. For instance, $BaTiO_3$ perovskite has a high permittivity, and many microelectronics have already been developed based on it. A little over ten years ago, solar panels started to be developed based on perovskite materials. These panels have a much higher efficiency than traditional silicon panels and their production cost is much lower. However, the lifespan of these batteries is still not long enough.

One of the important applications of $BaTiO_3$ in this work was the use of spectroscopic experiments based on $Ba_{0.5}Eu_{0.5}TiO_3$ crystals to measure the electric dipole moment (EDM) of electrons [1]. To process the results of these experiments, it is necessary to have fairly accurate information about the electronic structure near the core of the heavy core being studied. Therefore, theoretical studies of the various properties of perovskites, including optical properties, are a very urgent task in the search for new and effective technological solutions based on them.

The most accurate way to reproduce the electronic structure of a specific area of a crystal is through quantum chemical calculations using the technology of the CTEP [2].

In this work, the geometry of the BaTiO3 crystal was calculated using the DFT-PBE0 method. Minimal clusters $(TiO_6)^{8-}$@CTEP and $(BaO_{12})^{22-}$CTEP were constructed with high precision fragment reproduction. The relaxation of the cluster geometry was calculated using DLPNO-CCSD

Funding The work is supported by the Russian Science Foundation grant no. 20-13-00225.

References

[1] Eckel S., Sushkov A. O., & Lamoreaux S. K. (2012). Limit on the electron electric dipole moment using paramagnetic ferroelectric Eu 0.5 Ba 0.5 TiO 3. Physical Review Letters, 109(19), 193003.
[2] Shakhova V. M., Maltsev D. A., Lomachuk Yu. V., Mosyagin N. S., Skripnikov L. V., & Titov A. V. (2022). Compound-tunable embedding potential method: analysis of pseudopotentials for Yb in YbF_2, YbF_3, $YbCl_2$ and $YbCl_3$ crystals. Physical Chemistry Chemical Physics, 24(32), 19333-19345.

The International Summer Conference on Theoretical Physics 2024
Faculty of Physics of ITMO University
Abrikosov Center for Theoretical Physics

Novel regimes of exciton-polaritons synchronization in a presence of coherent pumping in ring geometry

A. Osipov[1], S. Koniakhin[2], O. Utesov[3], A. Yulin[4]

[1,4]Department of Physics and Engineering, ITMO University, St. Petersburg 197101, Russia

[1,2,3]Center for Theoretical Physics of Complex Systems, Institute for Basic Science (IBS), Daejeon 34126, Korea

[1]aleksey.osipov@metalab.ifmo.ru

Abstract

We theoretically predicted novel solitonic regimes of synchronization for ring-shaped exciton-polariton condensate with coherent pumping. In particular, we observed moving kinks profiles in the relative phase of condensate with respect to coherent pump when initial condensate and resonant pumping have different topological charges(phase winding numbers). The number of kinks is equal to difference in topological charges, the velocity is proportional to the resonant pump detuning with respect to condensate frequency. We derived effective Sin-Gordon like model to describe observed effects in condensate phase. Finally, we studied kinks pinning on potential perturbations and kinks dynamics in multikink regime.

Key words: Exciton-polaritons synchronization, ring-shaped condensates, Sin-Gordon equation

Introduction

Synchronization of exciton-polaritons condensates is actively studying nowadays. Recently, polaritonic XY simulators [1] were proposed as perspective polaritonic devices. This simulators are based on synchronization properties of condensates spots tending to have 0 or π phase differences depending on the inter-spots distances [2]. Several ways to control this synchronization was proposed [3, 4]. In [4] the synchronization of condensates with coherent pumping and, therefore, with each other were predicted.

In the ring geometry, formation of polaritonic quantum vortices were demonstrated [5, 6, 7]. In this case condensate have nontrivial phase winding l with condensate phase growing linearly with azimutal coordinate $\phi_c(\theta) = l\theta$. In [6] authors theoretically demonstrated efficient control of condensate vorticity with usage of coherent pumping.

In our work we predicted new synchronization regimes with coherent pumping when initial condensate and resonant pumping have different topological charges. In

this case, relative phase of the condensate with respect to pump looks like kinks. For example, if condensate's initial vorticity is $l_C = 1$ with linear phase growing from 0 to 2π along the ring and coherent pump vorticity is $l_f = 0$ corresponding to homogeneous pumping, condensate phase become almost constant everywhere, except small region where it steeply changes on 2π. The phase profile along the ring looks like 2π kink. This example is illustrated on Fig 1.

We derived effective Sin-Gordon model for condensate phase along the ring to explain observed effects. Finally, we studied kink dynamics, kinks pinning on potential perturbation and kinks dynamics in multikink regime.

Main text

We started from effective 1D Gross-Pitaevskii equation describing condensate's dynamics along the ring.

$$\partial_t \psi = \left((1 - |\psi|^2) + i\delta - i\alpha|\psi|^2 + iJ\partial_{\theta\theta}\right)\psi - ife^{il_f\theta}, \tag{1}$$

where δ - resonant pump detuning, α - ratio between polariton-polariton interaction and nonlinear saturation. With substitution $\tilde{\psi} = \psi e^{il_f\theta}$ we obtain equations were we have topological charge only in initial condensate $\psi_0 = e^{i\Delta l\theta}$, where $\Delta l = l_c - l_f$ - difference in topological charges. For the big ring radius($J << 1$), small coherent pumping strength and small detuning with respect to condensate blueshift $\tilde{\delta} = \delta - \alpha << 1$, using perturbation theory we derived effective equation for condensate phase.

$$\partial_t \phi = \tilde{\delta} + \boldsymbol{\alpha(J\partial_{\theta\theta}\phi + f\sin(\phi))} - J(\partial_\theta\phi)^2 - f\cos(\phi) \tag{2}$$

The highlighted part corresponds to Sin-Gordon equation. For realistic values of $\alpha \sim 3$ [8], Sin-Gordon equation could be used to effectively describe obsereved kinks in condensate phase. In further, we used textbook kink solution of Sin-Gordon equation and developed perturbation theory to describe kink velocity $v = \frac{2\pi m^2 J - \pi\tilde{\delta}}{4m}$, where $m^2 = \frac{f}{J}$. Finally, we simulated and described dynamics of one and two kinks in a presence of potential disorder.

References

1. N. G. Berloff, M. Silva, K. Kalinin, A. Askitopoulos, J. D. Töpfer, P. Cilibrizzi, W. Langbein, and P. G. Lagoudakis, Realizing the classical XY hamiltonian in polariton simulators, Nature materials **16**, 1120 (2017).

2. H. Ohadi, R. Gregory, T. Freegarde, Y. Rubo, A. Kavokin, N. Berloff, and P. Lagoudakis, Nontrivial phase coupling in polariton multiplets, Physical Review X **6**, 031032 (2016).

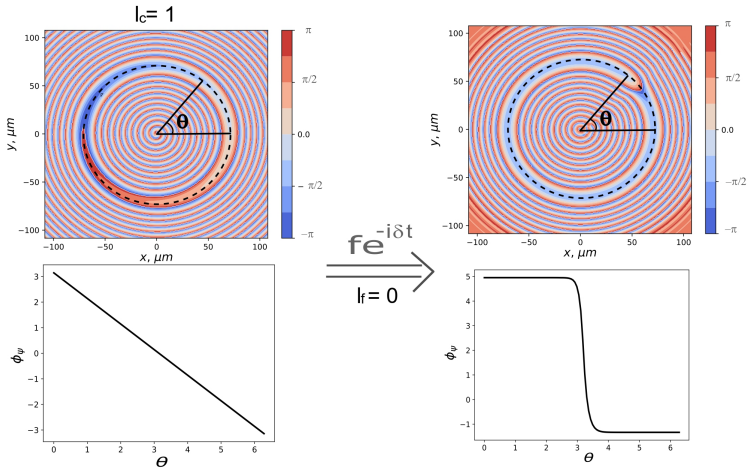

Figure 1: Illustration of transformation of nonresonatly pumped ring-shaped condensate with vorticity $l_c = 1$ to kink in a presence of homogeneous coherent pumping($l_f = 0$). The result was obtained by simulation of 2D Gross-Pitaevskii equation for condensate coupled with excitonic reservoir.

3. S. Alyatkin, J. D. Töpfer, A. Askitopoulos, H. Sigurdsson, and P. G. Lagoudakis, Optical control of couplings in polariton condensate lattices, Phys. Rev. Lett. **124**, 207402 (2020).

4. I. Chestnov, A. Kavokin, and A. Yulin, The optical control of phase locking of polariton condensates, New Journal of Physics **21**, 113009 (2019).

5. A. Dreismann, P. Cristofolini, R. Balili, G. Christmann, F. Pinsker, N. G. Berloff, Z. Hatzopoulos, P. G. Savvidis, and J. J. Baumberg, Coupled counterrotating polariton condensates in optically defined annular potentials, Proceedings of the National Academy of Sciences **111**, 8770 (2014).

6. H. Sigurdsson, O. Egorov, X. Ma, I. A. Shelykh, and T. C. H. Liew, Information processing with topologically protected vortex memories in exciton-polariton condensates, Physical Review B **90**, 014504 (2014).

7. X. Ma, B. Berger, M. Aßmann, R. Driben, T. Meier, C. Schneider, S. Höfling, and S. Schumacher, Realization of all-optical vortex switching in exciton-polariton condensates, Nature communications **11**, 897 (2020).

8. G. Christmann, G. Tosi, N. G. Berloff, P. Tsotsis, P. S. Eldridge, Z. Hatzopoulos, P. G. Savvidis, and J. J. Baumberg, Polariton ring condensates and sunflower ripples in an expanding quantum liquid, Phys. Rev. B **85**, 235303 (2012).

Generation of vortex electrons by atomic ionization

I.I. Pavlov[1], A. D. Chaikovskaia[1], D.V. Karlovets[1]

[1]School of Physics and Engineering, ITMO University, 197101 St. Petersburg, Russia

[1]ilya.pavlov@metalab.ifmo.ru

Abstract

We explore the process of orbital angular momentum (OAM) transfer from a light beam to an electron in an atomic ionization process. It is shown that regardless of the detection scheme the electron represents a wave packet with a size solely determined by the energy of the photon rather than by the transverse coherence of the light beam. The emitted electron also possesses a definite projection of OAM when a single atom is located on the propagation axis of the photon. Shifting the position of the atom yields a finite dispersion of the electron OAM. We also study a more experimentally feasible scenario — ionization of a localized finite-sized atomic target — and address the issue of coherent versus incoherent description of the atomic ensemble.

Key words: Vortex states, angular momentum, photoionization

Introduction

Photoemission of vortex electrons is a first step towards generating high energy electrons beams with OAM. Relativistic electron beams with OAM can become a unique research tool not only in atomic and molecular physics, in the diagnostics of nanomaterials and surfaces, where the orbital momentum allows one to obtain new information about a sample, but also in nuclear physics, spin and hadron physics, where such electrons can be used to analyze the proton spin, study nuclear forces at low energies, instead of the spin-polarized beams, etc [1, 2].

We consider processes with Bessel and Laguerre-Gaussian incoming vortex photons [3] and for the target cathode there are two toy-model options: single (hydrogen) atom in $1s$ state and a finite target consisting of uniformly spread single atoms [4, 5]. The evolved state formalism consists in deriving the wave function of final state the system flows to by itself through possible interactions. This state is defined independently of the postselection protocol chosen for the final states but takes into account full information on the starting conditions.

This study is related to the experimental project of vortex electron generation run by an ITMO-JINR team that is conducted at the accelerator LINAC-200 in Dubna.

Main text

Initial bound state of the electron $|i\rangle$ and the evolved (preselected) state $|\mathrm{ev}\rangle$ are connected via the S-matrix $\hat{S}$. Using the plane waves as a complete set of the free electron states we obtain the expression [6]

$$|\mathrm{ev}\rangle = \hat{S}\,|i\rangle = \int \frac{\mathrm{d}^3 p_f}{(2\pi)^3}\,|\boldsymbol{p}_f\rangle\, S_{fi}(\boldsymbol{p}_f), \tag{1}$$

where $S_{fi}(\boldsymbol{p}) = \langle \boldsymbol{p}|\,\hat{S}\,|i\rangle$ is the transition matrix element. Projecting (1) onto a state with a definite momentum $|\boldsymbol{p}\rangle$ yields the final state wave function in the momentum representation, which is simply the S-matrix element:

$$\psi_{\mathrm{ev}}(\boldsymbol{p}) \equiv \langle \boldsymbol{p}|\mathrm{ev}\rangle = \int \frac{\mathrm{d}^3 p_f}{(2\pi)^3}\,\langle \boldsymbol{p}|\boldsymbol{p}_f\rangle\, S_{fi}(\boldsymbol{p}_f) = \int \mathrm{d}^3 p_f \delta(\boldsymbol{p}-\boldsymbol{p}_f) S_{fi}(\boldsymbol{p}_f) = S_{fi}(\boldsymbol{p}). \tag{2}$$

We show that the state of the emitted electron is *twisted* in the sense that

$$\hat{\ell}_z \psi_{\mathrm{ev}}(\boldsymbol{p}) \equiv -i\frac{\partial}{\partial \varphi_p}\psi_{\mathrm{ev}}(\boldsymbol{p}) = \ell \psi_{\mathrm{ev}}(\boldsymbol{p}). \tag{3}$$

Having derived the wave function of the outgoing electron in momentum representation, we evaluate its Fourier transform and investigate the probability density in coordinate space. As seen from the Fig. 1, the photoelectron represents a wave packet localized around the position of the atom both in transverse and longitudinal directions. In case of Bessel beam with zero OAM the maximum of the probability density lies on the z-axis while for nonzero values of ℓ the wave packet has a well-known "doughnut shape" inherent to vortex states. It can also be seen that the radius of the first ring grows with the increase of ℓ.

It is noteworthy that the *transverse coherence length* (width) of the photoelectron wave packet does not depend on the transverse coherence of the incident light. This feature can be easily explained by analytical expressions for the wave function. Thus, it is the photon energy ω and not its transverse momentum κ that determines the width of the photoelectron wave packet. The width of the electron packet, which is many orders of magnitude less than the Bessel beam radius, decreases with the increase of the photon energy. For $\omega \sim 20|\varepsilon_i|$ with ε_i being the ionization energy the localization becomes comparable to the Bohr radius a, which is the initial localization distance in the atom.

The work is supported by the Russian Science Foundation (Grant No. 23-62-10026).

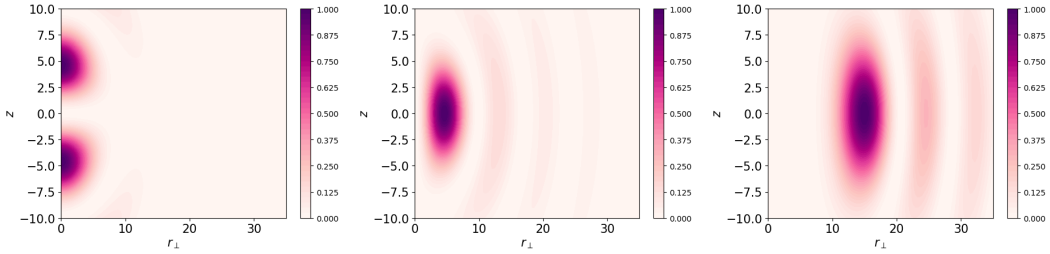

(a) (b) (c)

Figure 1: Normalized probability density $|\psi_{\text{ev}}(r_\perp, z, \varphi = 0)|^2$ of the evolved state. Due to the azimuthal symmetry of the problem there is no dependence on φ. The incident photon represents Bessel beam with $\omega = 1.2|\varepsilon_i|$, opening angle $\theta_k = \arctan(\kappa/k_z) = 1°$. Length is measured in Bohr radii a. (a) $\ell = 0$; (b) $\ell = 1$; (c) $\ell = 5$.

References

1. K. Y. Bliokh, I. P. Ivanov, G. Guzzinati, L. Clark, R. Van Boxem, A. Béché, R. Juchtmans, M. A. Alonso, P. Schattschneider, F. Nori, *et al.*, "Theory and applications of free-electron vortex states," *Physics Reports*, vol. 690, pp. 1–70, 2017.

2. I. P. Ivanov, "Promises and challenges of high-energy vortex states collisions," *Progress in Particle and Nuclear Physics*, vol. 127, p. 103987, 2022.

3. D. L. Andrews and M. Babiker, *The angular momentum of light*. Cambridge University Press, 2012.

4. O. Matula, A. G. Hayrapetyan, V. G. Serbo, A. Surzhykov, and S. Fritzsche, "Atomic ionization of hydrogen-like ions by twisted photons: angular distribution of emitted electrons," *Journal of Physics B: Atomic, Molecular and Optical Physics*, vol. 46, no. 20, p. 205002, 2013.

5. A. Surzhykov, D. Seipt, and S. Fritzsche, "Probing the energy flow in bessel light beams using atomic photoionization," *Physical Review A*, vol. 94, no. 3, p. 033420, 2016.

6. D. V. Karlovets, S. S. Baturin, G. Geloni, G. K. Sizykh, and V. G. Serbo, "Shifting physics of vortex particles to higher energies via quantum entanglement," *The European Physical Journal C*, vol. 83, no. 5, p. 372, 2023.

Angular momentum transfer in the interaction of intense circularly polarized laser pulses with dense structured targets

E. Gelfer[1], E. Peganov[2], S. Popruzhenko[2,3]

[1]ELI-Beamlines, Za Radnici 835, 25241, Dolni Brezany, Czech Republic

[2]National Research Nuclear University Moscow Engineering Physics Institute, Kashirskoe shosse 31, 115409, Moscow, Russia

[3]Prokhorov General Physics Institute of the Russian Academy of Sciences, Vavilova str. 38, 119991, Moscow, Russia

[1]egelfer@gmail.com , [2]egorpeganov.mephi@gmail.com,
[3]sergey.popruzhenko@gmail.com

Abstract

In a near future, multi-beam sources of laser light of intensities $\sim 10^{23}\mathrm{W/cm}^2$ may be built and put in operation. This promises the opportunity of creation of circularly polarised extremely intense femtosecond laser pulses for studies of laser-plasma interactions in the highly nonlinear regime. In particular, such pulses can be used to transfer angular momentum to structured overdense plasma targets, which leads to the generation of strong quasi-static magnetic fields. We consider the interaction of circularly polarized pulses with a plasma slab having a through cylindrical hole. A simulation performed by the PIC-code SMILEI, demonstrates that the magnetic field amplitude can be as high as several Giga-Gauss. A complex electron dynamics induced by the angular momentum absorption near the target edge was observed and shown to be the source of the magnetic field excitation.

Key words: Laser-plasma interaction, angular momentum transfer, strong magnetic fields, PIC simulation

Electromagnetic fields carry angular momentum (AM), which can be separated into the spin and the orbital parts [1]. Typically, the orbital part of circularly polarized (CP) beams is small compared to the spin angular momentum and increases with tightening the pulse focusing. Irreversible AM transfer from electromagnetic field to media opens a way to the excitation of strong electronic currents, which generate high quasi-static magnetic fields.

Several considerably different mechanisms of AM deposition can be identified in the strong-field highly nonlinear regime of interaction. For intensities $10^{24}\mathrm{W/cm}^2$ and higher the Inverse Faraday Effect (IFE) induced by the radiation reaction force was

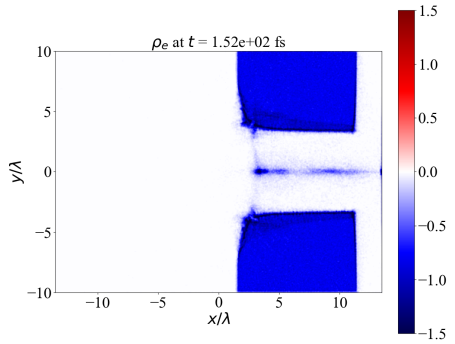

(a) Normalised charge electron density $\rho_e/(|e|n_0)$, with $n_0 = 1.55 \times 10^{23}\text{cm}^{-3}$ being the initial target density.

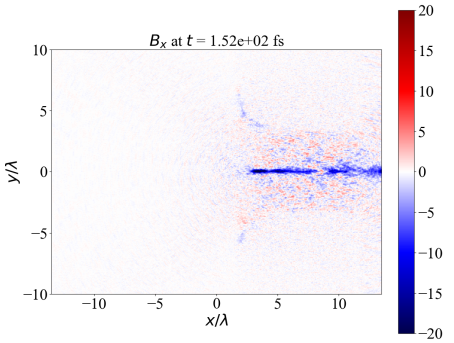

(b) Magnetic field strength component B_x along the laser propagation direction shown in units $B_0 = mc\omega/e = 1.34 \times 10^8$ Gauss.

Figure 1: Distributions in the electron density (a) and the longitudinal magnetic field (b) at a time instant $t \approx 150$fs after the beginning of the interaction.

theoretically shown to be the main mechanism of the AM absorption and magnetic field generation [2]. The peak intensity of a few times of 10^{23}W/cm^2, which can potentially be reached with the modern multi-petawatt sources [3, 4] is insufficient to demonstrate the IFE induced by radiation friction. However, a strong magnetic field can still be excited in the interaction of CP pulses with dense plasma targets having a structured surface.

In this work, we examine a possible mechanism of the AM transfer at intensities $\simeq 10^{23}\text{W/cm}^2$. We consider a laser beam consisting of two linearly polarized (LP) pulses propagating at a small angle (about 10°), and having orthogonal polarizations with a $\pi/2$ phase delay so that in the focal volume the resulting field polarization is close to CP [5]. The wavelength $\lambda = 800$nm corresponds to a Ti:Sapphire laser. The beam interacts with a plasma slab of 10λ thickness and a cylindrical hole of $d = 6\lambda$ diameter. The cylinder is co-axial with the beam axis.

Results of our particle-in-cell simulations made with the help of SMILEI code [6] show a quasi-static longitudinal magnetic field of Giga-Gauss strength at a laser intensity not exceeding 10^{23}W/cm^2 (Fig. 1). The electromagnetic field calculated numerically with the code is close to a quasi-Gaussian beam of 3.8λ waist, peak dimensionless amplitude $a_0 = eE_0/mc\omega = 100$, and a Gaussian time envelope with the FWHM parameter $6.9\lambda/c$. Here e and m are the elementary charge and mass correspondingly, E_0 is the laser field amplitude and c is the speed of light. The laser carrier frequency $\omega = 2\pi c/\lambda$. The initial electron density in the slab is 90 times the critical density for such laser wavelength. These parameters correspond to the case of each LP beam having energy ≈ 100 J and peak power ≈ 20 PW.

Results of our simulations show that for dense targets with a cylindrical hole, a CP

laser pulse with a lateral width comparable to the hole diameter can interact with a plasma in a regime of efficient AM transfer and magnetic field excitation. The excited quasi-static field is concentrated near the target and beam axes. The underlying physical mechanism is a strong lateral inhomogeneity of the plasma, which makes possible the generation of intense cylindrical currents in the rare plasma filling the initially empty cylindrical volume. The magnetic field appears suprizingly high and comparable to that generated through IFE and radiation reaction [2] at intensities more than one order of magnitude higher.

Our results propose a highly promising prospect of structured plasma targets for the laser-induced generation of extreme magnetic fields and for AM transfer from light to matter.

References

1. Jackson J., Classical Electrodynamics Wiley&Sons (1962)

2. Liseykina T.V., Popruzhenko S.V., Macchi A. *New Journal of Physics* **18** 072001 (2016); *NewJournal of Physics* **21** 033009 (2019); *European Physics Journal Plus* **136** 170 (2021).

3. Papadopoulos D.N. et al. *High Power Laser Sci. Eng.* **4** e34 (2016).

4. Yoon J.W. et al. *Optica* **8** 630 (2021).

5. Liseikina T.V., Peganov E.E., Popruzhenko S.V. *Kvantovaya Elektronika* **53** 2 165 (2023)

6. Derouillat J. et al. *Computer Physics Communications* **222** 351 (2018).

Search for $\mathcal{T}$,$\mathcal{P}$-violating axionlike-particle-mediated interactions in the BaF molecule

S. D. Prosnyak[1] and L. V. Skripnikov[2]

[1,2]NRC "Kurchatov Institute" – PNPI, Gatchina, Russia

[1,2]Saint Petersburg State University, Saint Petersburg, Russia

[1]prosnyak.sergey@yandex.ru, [2]leonidos239@gmail.com

Abstract

In the presented study we consider the $\mathcal{T}$,$\mathcal{P}$-violating axionlike-particle-mediated electron-nuclear and electron-electron interactions in the barium monofluoride molecule. In the case of electron-nuclear interaction, the calculations were performed with taking into account the finite size of the nucleus. Using the calculated molecular parameters of the considered interactions, we established constraints on the products of interaction coupling constants corresponding to expected sensitivity of the future experiment with the BaF molecule [A. Boeschoten et al., arXiv:2303.06402 (2023)]. The obtained constraints were compared with current limitations established with hafnium monofluoride molecular cation.

Key words: Theoretical physics, axionlike particles

Introduction

One of the most perspective experiments to search for new physics beyond the standard model are experiments with molecules of heavy atoms, aimed at searching for the effects of spatial parity ($\mathcal{P}$) and time reversal ($\mathcal{T}$) symmetries violation in fundamental interactions. Such effects, for example, include the existence of electron electric dipole moment (eEDM). At the moment, non-zero eEDM has not been detected, but new more accurate experiments are planned. For example, in Ref. [1], an experiment on the barium monofluoride (BaF) molecule was proposed. It is expected that this experiment will establish a constraint at the level of $|d_{\rm e}| < 5.0 \times 10^{-30}\ e \cdot {\rm cm}$. Although this constraint is slightly less stringent than the already obtained $|d_{\rm e}| < 4.1 \times 10^{-30}$ $e \cdot {\rm cm}$ in the experiment [2] with the hafnium monofluoride (HfF^+) molecular cation, performing the experiment on different systems is important for physics not only for the independent verification of the results. Different systems on which the experiment is performed have different sensitivity to different sources of $\mathcal{T}$,$\mathcal{P}$-violation, and thus they can be distinguished. One such possible source is the exchange of virtual axion-like particles (ALPs) between a nucleus and electrons, as well, as between two electrons of the system under consideration. Axions and ALPs are interesting for physics from

several points of view. First of all, these particles are one of the candidates for the role of dark matter. In addition, they appear in the solution of the Pechei-Queen strong $\mathcal{CP}$ problem and various compactifications of string theory. Many experiments are devoted to the search of axions and ALPs, in which constraints on their properties have been established.

Main text

In Ref. [4] we investigated the $\mathcal{T}$,$\mathcal{P}$-violating ALP-mediated electron-nuclear and electron-electron interactions in the BaF molecule. In consideration of $\mathcal{T}$,$\mathcal{P}$-violating ALP-mediated electron-nuclear interaction we performed calculations with taking into account the finite nucleus size effects in the potential of this interaction. In previous theoretical studies with molecular systems, for example in Ref. [3], this effect was not taken into account, and the finite size of the nucleus was taken into account only in the calculation of the electronic wave function. To carry out the calculations with the effect mentioned above, we modified the program code from Ref. [3] designed for calculations with $\mathcal{T}$,$\mathcal{P}$-violating ALP-mediated electron-electron interaction. Using this code, we have calculated the molecular parameter $W_{\rm ax}^{(eN)}(m_a)$, characterizing the $\mathcal{T}$,$\mathcal{P}$-violating ALP-mediated electron-nuclear interaction. In addition, in Ref. [4] we calculated the molecular parameter $W_{\rm ax}^{(ee)}(m_a)$, characterizing the $\mathcal{T}$,$\mathcal{P}$-violating ALP-mediated electron-electron interaction in the BaF molecule. These calculations have been performed for a wide range of ALP masses m_a. Using the calculated values of molecular parameters $W_{\rm ax}^{(eN)}(m_a)$ and $W_{\rm ax}^{(ee)}(m_a)$, we obtained the constraints on $|\bar{g}_N^s g_e^p|$ and $|g_e^s g_e^p|$ products of interaction coupling constants, corresponding to expected sensitivity to eEDM $|d_{\rm e}| < 4.1 \times 10^{-30}\ e \cdot$ cm of the experiment [1].

It is interesting to consider the limiting cases of light and heavy ALPs and compare the expected and current limitations on the products of coupling constants. In the case of light ALPs, the expected constraints on the products $|\bar{g}_N^s g_e^p|$ and $|g_e^s g_e^p|$ about 50% and 40%, respectively, are better than those obtained in Ref. [3] from the experiment [2] on the HfF^+ molecular cation. In the case of heavy ALPs, the constraint on $|\bar{g}_N^s g_e^p|/m_a^2$ is almost twice as weak and the constraint on $|g_e^s g_e^p|/m_a^2$ is about 5% better compared to the HfF^+ molecular cation [3]. It should be noted that this comparisons are based on the present constraint on the energy shift due to the $\mathcal{T}$,$\mathcal{P}$ symmetry violating interaction in HfF^+ [2] corresponding to $|d_{\rm e}| < 4.1 \times 10^{-30}\ e \cdot$cm, and the expected sensitivity of the experiment on BaF [1] corresponding to $|d_{\rm e}| < 5.0 \times 10^{-30}\ e \cdot$ cm. Taking into account the very close constraints on eEDM, the above numbers correspond to the relative sensitivities of HfF^+ and BaF molecular systems to different $\mathcal{T}$,$\mathcal{P}$symmetry violation effects. As noted above, the difference in sensitivity is important for establishing more reliable constraints on the various sources of $\mathcal{T}$,$\mathcal{P}$ symmetry violation effects.

The research was supported by the Foundation for the Advancement of Theoretical Physics and Mathematics "BASIS" Grant according to Projects No. 21-1-2-47-1.

References

1. A. Boeschoten, et al., Novel spin-precession method for sensitive EDM searches, ArXiv:2303.06402 (2023).

2. T. S. Roussy, et al., An improved bound on the electron's electric dipole moment, Science **381**, 46 (2023).

3. S. D. Prosnyak, D. E. Maison, L. V. Skripnikov, Updated Constraints on T, P-Violating Axionlike-Particle-Mediated Electron–Electron and Electron–Nucleus Interactions from HfF+ Experiment, Symmetry **15(5)**, 1043 (2023).

4. S. D. Prosnyak, L. V. Skripnikov, Axion-mediated electron-nucleus and electron-electron interactions in the barium monofluoride molecule, Phys. Rev. A **109**, 042821 (2024).

The International Summer Conference on Theoretical Physics 2024
Faculty of Physics of ITMO University
Abrikosov Center for Theoretical Physics

Crystalline topological insulators via accidental mode degeneracies

K. Rodionenko[1], M. Mazanov[1], M. Gorlach[1]

[1,2,3]School of Physics and Engineering, ITMO University, Saint Petersburg 197101, Russia

[1]k.rodionenko@metalab.ifmo.ru

Abstract

Geometric symmetries of the lattice is a well-known way to craft crystalline topological insulators providing the topological states. We investigate an alternative approach to create those systems by designing the internal symmetries of the Hamiltonian via accidental mode degeneracies. We construct a honeycomb lattice with a single two-mode waveguide in each unit cell, calculate the relevant topological invariants, and reveal edge and corner states.

Key words: Topological effects in photonic systems, crystalline topological insulators

Introduction

Photonic topological insulators are an active direction of research in different fields since their inception. To date, most of fabrication-friendly topological systems scalable towards optical wavelengths rely on the specific crystalline lattice geometries and therefore are called crystalline topological insulators [4]. An important example of such a system is the breathing honeycomb lattice [2]. As first predicted in Ref. [2], C_6-preserving deformation of the honeycomb lattice opens a complete photonic band gap in the dispersion.

Here we present a less intuitive but fruitful approach to make the lattice simpler and subject to flexible tuning. We achieve similar topological properties by tailoring the degeneracy of different orbital modes. In this work we develop an analytical tight-binding description, calculate the relevant topological invariants and corroborate this description by the full-wave numerical simulations.

Theoretical and numerical analysis

We consider a triangular periodic lattice (Fig. 1) consisting of evanescently coupled waveguides supporting two accidentally degenerate pairs of dipolar (p_x, p_y) and quadrupolar $(d_{xy}, d_{x^2-y^2})$ modes. To describe the system we use a tight-binding

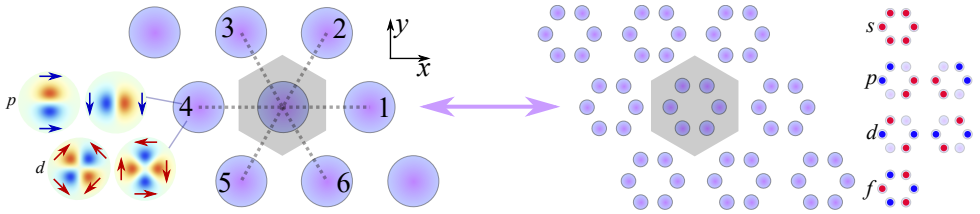

Figure 1: [Fig. 1 from [1]] Design of the triangular periodic lattice with nearly degenerate $p_\pm$ and $d_\pm$ orbital modes (left) and the tight-binding model of a topological insulator based on the breathing honeycomb lattice showing the modes of an isolated six-site unit cell (right) [2]. C_6-symmetric unit cell is highlighted in gray. Color encodes the phase of the eigenmode electric field.

model. Bloch Hamiltonian $\hat{H}$ in the basis of circularly polarized modes $p_\pm = p_x \pm ip_y$, $d_\pm = d_{xy} \pm id_{x^2-y^2}$ ordered as $(p_+, p_-, d_+, d_-)^T$ can be written as:

$$\hat{H} = \sum_{j=0}^{6} \hat{\varkappa}_j \exp\left(ik_x \cos\frac{2\pi j}{3} + ik_y \sin\frac{2\pi j}{3} \right) + \delta\hat{\beta}\,, \tag{1}$$

where $\delta\hat{\beta} = \delta\beta \cdot \hat{\sigma}_z \otimes \hat{I}$ ($\hat{\sigma}_z$ being the third Pauli matrix) captures the difference between the propagation constants of p and d modes. The coupling matrices can be constructing by calculating the overlap integrals of the respective modes [3].

Due to C_6 lattice symmetry, all possible couplings in the lattice are captured by 6 independent real-valued and positive coupling parameters a-f:

$$\hat{\varkappa}(\gamma) = \begin{pmatrix} -a & b\gamma^{-1} & c\gamma^2 & d \\ b\gamma & -a & d & c\gamma^{-2} \\ c\gamma & -d & e & f\gamma^{-2} \\ -d & c\gamma^{-1} & f\gamma^2 & e \end{pmatrix}, \tag{2}$$

with $\hat{\varkappa}_1 = \hat{\varkappa}^T(e^{i\pi})$, $\hat{\varkappa}_2 = \hat{\varkappa}(e^{i\pi/3})$, $\hat{\varkappa}_3 = \hat{\varkappa}_2^T$, $\hat{\varkappa}_4 = \hat{\varkappa}_1^\dagger$, $\hat{\varkappa}_5 = \hat{\varkappa}_2^\dagger$, $\hat{\varkappa}_6 = \hat{\varkappa}_3^\dagger$.

We explore the situation when all six coupling parameters are equal to each other, i.e. $a = b = c = d = f = e = \alpha$. In such a setting, α signifies the strength of the interorbital coupling, while $\delta\beta$ measures the detuning between the propagation constants of p and d modes, respectively. Depending on the ratio between those parameters, we recover different band structures. The spectrum has non-trivial origin in the large range of detunings $-6\alpha < \delta\beta < -2\alpha$. In this case p and d modes experience a significant mixing [Fig. 2(a)]. To examine the topological properties we calculate the indicators for symmetry operators C_2 and C_3 at M, K, and Γ points yielding a non-trivial index $\chi^{(6)} = (2, 0)$ in the topological phase. Topological indices are computed for the C_6 symmetry case. [4]

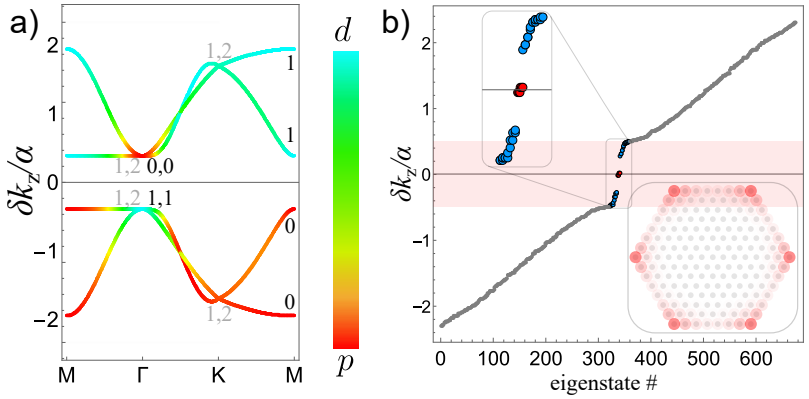

Figure 2: (Fig. 2–3 from [1]) (a) Calculated spectra of propagation constants for $\delta\beta = -4\alpha$. Blue and red colors indicate d and p modes, respectively. The indicators for symmetry operators C_2 and C_3 (numbers p from symmetry operator eigenvalues $\Pi^{(2,3)} = e^{2\pi i(p-1)/N}$ for $N = 2, 3$ [4]) at M, K and Γ points are shown near high symmetry points. (b) Spectra for a finite hexagonal meta-structure. The topological gap is highlighted by light red. Tight-binding calculation are performed for $\delta\beta = -4\alpha$. Inset shows the profile of a corner mode.

Nonzero topological invariants predict the emergence of edge and corner states in a finite structure with open boundary conditions. We compute the spectrum of propagation constants within our tight-binding model [Fig. 2(b)]. We observe six degenerate corner states, one at each obtuse angle of the lattice. To support the tight-binding results, we calculate the spectrum of the finite structure in COMSOL Multiphysics software package exploiting hexagonal waveguides with fine-tuned accidental p-d mode degeneracy and get the same results [1].

To summarize, our work shows the potential of orbital degrees of freedom for tailoring topological phases in two-dimensional lattices. Compared to the original realization Wu and Hu model based on the breathing honeycomb lattice, our proposal utilizes simpler lattice geometry, requires 6 times less meta-atoms and opens an easy access to continuously tune the topological properties by sweeping the operating wavelength, which governs the detuning between the propagation constants of p and d orbital modes.

References

1. Konstantin Rodionenko, Maxim Mazanov, and Maxim A. Gorlach, “Crafting crystalline topological insulators via accidental mode degeneracies”, Phys. Rev. B **109**, 155135 (2024).

2. Long-Hua Wu and Xiao Hu, "Scheme for Achieving a Topological Photonic Crystal by Using Dielectric Material," Physical Review Letters **114**, 223901 (2015).

3. Roman S. Savelev and Maxim A. Gorlach, "Topological states in arrays of optical waveguides engineered via mode interference," Physical Review B **102**, 161112 (2020).

4. Wladimir A. Benalcazar, Tianhe Li, and Taylor L. Hughes, "Quantization of fractional corner charge in Cn-symmetric higher-order topological crystalline insulators," Phys. Rev. B **99**, 245151 (2019).

Exploration of coupling in spherical voids

Evgeny Ryabkov[1,2,*] and Denis G. Baranov[1]

[1]Center for Photonics and 2D Materials, Moscow Institute of Physics and Technology, Dolgoprudny 141700, Russia

[2]Skolkovo Institute of Science and Technology, Bolshoy Boulevard 30, bld. 1, Moscow 121205, Russia

[*]ryabkov.e@phystech.edu

Abstract

The behavior of dielectric systems under the influence of electromagnetic radiation, including their bound states, is one of the fundamental subjects of interest in photonics [1]. An example of a traditional system for study is spherical nanoparticles, for which no fundamental questions were believed to remain unanswered [2,3,4]. However, a structure such as vacuum voids in dielectric materials did not attract researchers' attention until recently [5]. Spherical voids described by Mie theory [6] demonstrate the typical resonant properties of dielectric cavities, and they depend on the materials in which they are formed. In the present work, we theoretically investigate these dependencies and the corresponding coupling occurrence. Starting off with spherical voids in nondispersive dielectrics, we demonstrate the possibility of forming hybrid states - polaritons - in the presence of slight dispersion in the voids. Next, we examine voids in Lorentz materials and characterize the resonant increase of quality factor in the corresponding systems depending on the environmental parameters. The results will open new prospects for material design and control of electromagnetic radiation in nanostructures.

Introduction

The challenge of raising the level of interaction between light and various dielectric nanostructures currently attracts lots of photonics community's attention. Among multiple relevant problems, the scattering of light by spherical particles (Mie scattering) was of high interest due to their role in fabrication of optical structures enabling high degree of confinement and tuning. Recently, the study of light interaction with such nanoparticles has turned mainly practical rather than fundamental due to apparent lack of unanalyzed cornerstones. However, the idea of confining light in voids of higher-index materials has arisen, which promises less requirements for creating high-Q resonances, easier design process, and new applications in wider spectral ranges.
We study spherical voids (Mie voids) in sets of dielectric materials, considering the cases of purely nondispersive materials and the cases with the presence of excitons. We take a closer view to the corresponding quasinormal mode (QNM) analysis with respect to their radial numbers and show theoretical evidence of their weak dependence

on the background parameters. Lorentz background materials feature significant boost in Q-factor near the resonances in the cases of excitons with a low decay rate and the corresponding radial number modes. The central part of our work is the demonstration of polariton formation in the voids with dispersion, which proves that such systems may serve as simpler structures for reaching the desired degrees of coupling.

Main text

We focus on 3 particular systems consisting of spherical voids in dielectric materials: empty voids in nondispersive dielectrics Fig.1(a), voids with excitons in nondispersive dielectrics Fig.1(b), and empty voids in dispersive dielectrics Fig.1(c). In the classical electromagnetic formalism, the permittivity of dispersive dielectric background can be described by the Lorentz model:

$$\varepsilon(\omega) = \varepsilon_\infty + f\frac{\omega_P^2}{\omega_0^2 - \omega^2 - i\gamma\omega} \tag{1}$$

with ε_∞ being the background permittivity (in the cases of nondispersive background we will use $\varepsilon_{background}$ for avoiding confusion with the dispersive case), ω_P being the plasma frequency, ω_0 and γ - the resonance frequency and linewidth, and f being the oscillator strength.

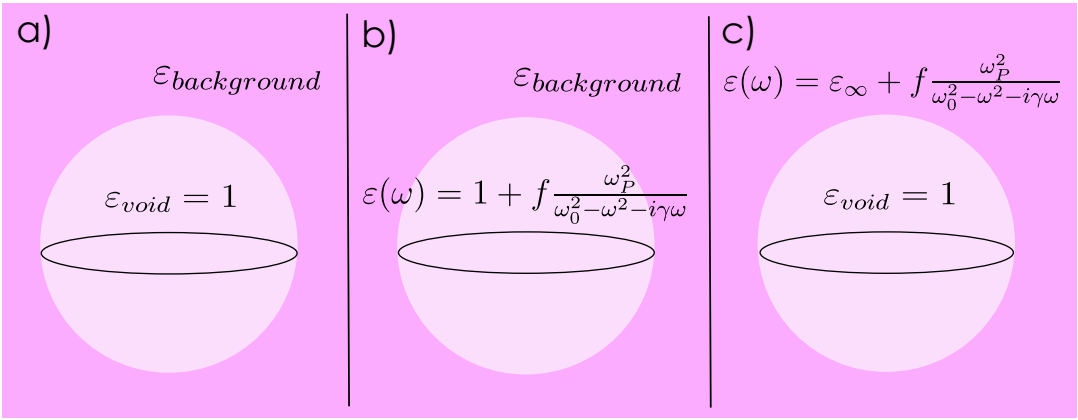

Figure 1: Description of the systems under study. a) empty voids in nondispersive materials; b) voids with excitons described by the Lorentz model in nondispersive materials; c) empty voids in dispersive materials described by the Lorentz model.

We begin our analysis with quantifying the complex eigenfrequencies $(\omega - i\gamma_{cav})$ of the TM and TE quasinormal modes of the spherical voids. They can be found numerically

as the roots of the characteristic equations:

$$n\psi_l(nx)\xi_l'(x) - \xi_l(x)\psi_l'(nx) = 0, \tag{2a}$$

$$n\xi_l(x)\psi_l'(nx) - \psi_l(nx)\xi_l'(x) = 0. \tag{2b}$$

where $x = k_0 r$, $\psi_l(x) = x j_l(x)$ and $\xi_l(x) = x h_l^{(1)}(x)$ are Ricatti-Bessel functions, and $j_l(x)$ and $h_l^{(1)}(x)$ are spherical Bessel and Hankel functions of the first kind, respectively.

We focus on dipolar and quadrupolar modes with a closer look on their differences corresponding to different radial numbers and the hosts' permittivities. All of them can be observed on the complex-frequency plane with further quantifying the quality factor as $Q = \omega/2\gamma_{cav}$, which depends solely on the background permittivity.

Adding excitonic oscillations to the voids enables various types of coupling. We are mainly interested in observation of the coupled photon-exciton modes - polaritonic modes - which are characterized by the presence of anticrossing (or the Rabi splitting, Ω). In the case of resonance ($\omega_{cav} = \omega_0$) for bulk materials [7], $\Omega = \sqrt{4g^2 - (\gamma_{ex} - \gamma_{cav})^2}$, which becomes real-valued when $2g > |\gamma_{ex} - \gamma_{cav}|$ with g being the coupling constant. The same can be assumed and proven for spherical voids with excitonic oscillations, as the light is confined within the voids [5]. Hence, this criterion can be rewritten as:

$$\frac{f}{\varepsilon_\infty}\omega_P^2 > (\gamma_{ex} - \gamma_{cav})^2, \tag{3}$$

which defines the values of the required oscillator strength for observing strong coupling for the given system.

References

1. Bahaa E. A. Saleh, Malvin Carl Teich, Fundamentals of Photonics, Wiley, 1991.
2. Tserkezis, Christos, Stamatopoulou, P. Elli, Wolff, Christian and Mortensen, N. Asger. "Self-hybridisation between interband transitions and Mie modes in dielectric nanoparticles", Nanophotonics, 2024.
3. Fan, X., Zheng, W. & Singh, D. Light scattering and surface plasmons on small spherical particles. Light Sci Appl 3, e179 (2014).
4. Arseniy I. Kuznetsov et al. Optically resonant dielectric nanostructures. Science 354, aag2472 (2016).
5. Hentschel, M., Koshelev, K., Sterl, F. et al., Dielectric Mie voids: confining light in air. Light Sci Appl 12, 3 (2023).
6. Mie, G. Beiträge zur optik trüber medien, speziell kolloidaler metallösungen. Ann. der Phys. 330, 377–445 (1908).
7. Denis G. Baranov, Martin Wersäll, Jorge Cuadra, Tomasz J. Antosiewicz, and Timur Shegai ACS Photonics 2018 5 (1), 24-42.

The International Summer Conference on Theoretical Physics 2024
Faculty of Physics of ITMO University
Abrikosov Center for Theoretical Physics

Variational state preparation with noisy trapped-ion quantum computers

D. Rabinovich[1], Z. Sayapin[2], S. Adhikary[3]

[1,2,3]Skolkovo Institute of Science and Technology

[1,2]Moscow Institute of Physics and Technology

[1]daniil.rabinovich@skoltech.ru, [2]Z.Sayapin@skoltech.ru, [3]s.adhikary@skoltech.ru

Abstract

Noise in quantum devices challenges implementation of quantum algorithms. Our study focuses on noisy trapped ion quantum computers, addressing the errors arising from residual entanglement between electronic and motional levels. We introduce a variational quantum state preparation algorithm for non-ideal ionic quantum computers, achieving in our numerical experiments fidelities in preparing GHZ states with 3-5 qubits up to 0.99. Additionally, we propose optimizing hardware requirements for mixed-state preparation by utilizing ion-specific motional modes as computational resources.

Key words: Variational quantum algorithms, quantum state preparation, trapped-ion quantum computer, Molmer-Sorensen gate

Introduction

In ion quantum computing, ions of some substance are held in a particular configuration in an electromagnetic Paul trap [1, 2]. Usually the ions are arranged in a one-dimensional lattice called an ion chain, which we assume further in our work. A selected pair of electronic levels of each ion are used to encode a qubit whose state is controlled by laser pulses.

At low temperatures, the motion of ions in the trap is quantized in motional modes. These modes are determined by the Coulomb interaction of ions among themselves and their interaction with the trap. The excitation of these modes corresponds to the collective motion of all ions in the chain, and this is used to realize entangling gates between arbitrary qubits. Such gates include the Molmer-Sorensen gate [3, 4].

As the size of ion chains increases, it becomes increasingly difficult to disentangle the electronic and motional degrees of freedom by the end of the execution time of the entangling gate, leading to potential residual entanglement and decreased fidelity of the gate. The presence of such non-idealities is characteristic of modern noisy intermediate scale quantum (NISQ) devices and presents a challenge to the successful implementation of quantum algorithms [5].

Main text

In this work, we have considered noisy ionic quantum computers where the leading source of error is the residual entanglement between electronic and motional levels, which is created by non-ideal Molmer-Sorensen gates. We have developed a variational algorithm for preparing quantum states that accounts for this residual entanglement and yet can successfully prepare a given pure state with high fidelity. We numerically tested this state preparation algorithm by preparing GHZ states with 3, 4, and 5 qubits, achieving fidelity up to 0.99.

The controlled preparation of arbitrary mixed states is a fundamental quantum subroutine [6]. There are two main approaches to its solution. The first approach, called purification, proposes finding such a pure state in a Hilbert space of higher dimensionality that the reduced density matrix over the added subsystem is identical to the target state. This approach has a drawback in that, in the worst case, it requires doubling the number of qubits in the register for its realization. The second approach is related to the representation of the mixed state as a statistical ensemble of pure states and the subsequent preparation of pure states from this ensemble according to their probability distribution. A disadvantage of this approach is the need to prepare a potentially exponentially large set of different states.

We propose a solution to optimize the hardware requirements for mixed-state preparation on ion quantum computers, using platform-specific motional modes as a useful computational resource. We demonstrate that it is possible to prepare mixed states in a register without the use of ancilla qubits, exploiting the entanglement between the electronic and motional subsystems. In numerical experiments, mixed states were prepared for 2 qubits that differed from the target mixed states in terms of the Hilbert-Schmidt distance by no more than 0.01.

References

1. I. Pogorelov et al., Compact ion-trap quantum computing demonstrator, PRX Quantum **2**, 020343, (2021).

2. P. Schindler et al., A quantum information processor with trapped ions, New J. Phys. **15**, 123012, (2013).

3. A. Sørensen, K. Mølmer, Quantum computation with ions in thermal motion, Phys. Rev. Lett. **82**, P. 1971–1974, (1999).

4. A. Sørensen, K. Mølmer, Entanglement and quantum computation with ions in thermal motion, Phys. Rev. A. **62**, 022311, (2000).

5. J. Preskill, Quantum computing in the NISQ era and beyond, Quantum. **2**, 79, (2018).

6. N. Ezzell et al., Quantum mixed state compiling, Quantum Sci. Technol. **8**, 035001, (2023).

The International Summer Conference on Theoretical Physics 2024
Faculty of Physics of ITMO University
Abrikosov Center for Theoretical Physics

Axion-induced hybridization of electric and magnetic multipoles

T. Seidov[1] and M. Gorlach[2]

[1,2]ITMO University

[1]timur.seidov@metalab.ifmo.ru, [2]m.gorlach@metalab.ifmo.ru

Abstract

We explore analytically the electromagnetic fields produced in the static axion surroundings by electric or magnetic multipole. To this end, we solve the problem of a multipole inside time-independent homogeneous axion shell. We find that the fields outside of the shell are presented as a superposition of electric and magnetic multipoles. We identify characteristic features in the response of the structure and show that these features are related to the eigenmodes of the axion shell.

Key words: axion, multipole expansion, mode hybridization, Mie theory, axion electrodynamics

Introduction

Originally, particle named axion was proposed to resolve the strong CP-problem [1], however interesting properties of this particle also made it a prominent candidate for dark matter [2]. Axion is still yet to be observed [3], but axion-like effects are found in many systems in condensed matter physics. This includes multiferroics, magneto-electrics [4], topological insulators [5] and metamaterials [6]. One of the earliest predictions of axion electrodynamics is the Witten effect – emergence of the effective dyon charges from purely electric charges through the interaction with the axion field [7]. This effect has been recently generalized to the case of static dipole moment in presence of oscillating cosmic axion field [8] and proposed to detect cosmic axions.

We further generalized this effect to the situation more suitable for condensed matter realizations [9]. Many of condensed matter systems exhibit vanishing effective axion response at zero frequencies of the incoming signal, while the effective axion field itself is static. We have investigated the response of static spherically symmetric axion media in presence of oscillating dipole. In present work we further investigate the influence of multipole order and change in the geometry on the results found in [9].

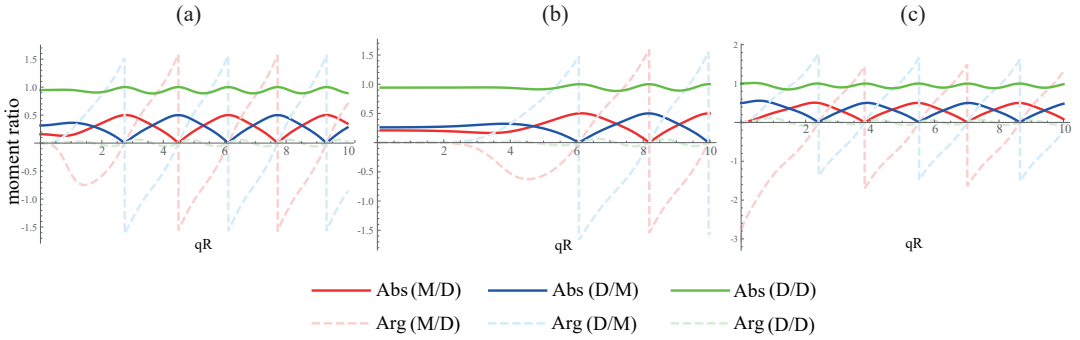

Figure 1: Dependence of the same-order multipole moment ratios with multipole indices l, m on dimensionless wave number: (a) spherical geometry $l = 1, m = 0$; (b) spherical geometry $l = 4, m = 0$; (c) cylindrical geometry $l = 1, m = 0$. In all cases $R = 1, \chi = 0.5$. The nominators of the ratio are the induced moments outside the medium (M for magnetic, D for electric), while the denominator is always the seed moment inside.

Results

We consider a ball and cylinder of radius R with Tellegen parameter χ, inside which there resides an oscillating point multipole. Using multipole expansion techniques, we analytically solve the Maxwell's equations for such system and obtain the fields within and outside the axion medium. We show that due to the boundary conditions, axion medium hybridizes electric and magnetic moments separately for each multipole index combination (l, m). It is demonstrated, that regardless of geometry, type of the seed moment or multipole order, the solutions share characteristical feature of the axion response, namely - nonradiative surface current configurations, known as magnetic and electric anapoles. These states appear at particular frequencies which depend on the particular geometry and multipole indices. However, frequency positions these surface states are always co-located with the maxima of the multipole response of the same type (magnetic response on magnetic seed moment or electric response on electric seed moment). For spherical and cylindrical geometries such frequencies are dictated by zeros of Bessel functions and their derivatives. It is clearly seen from the ratios of induced and seed moments (Fig.1). Moreover, we observe that the same-type multipole ratios are the same in this case, but the different-type (magnetic-electric or electric-magnetic) ratios are in the "antiphase" between each other i.e. the same frequency serves as both zero for M_{out}/D_{in} and maximum for D_{out}/M_{in} and vice versa. By direct calculation it is also seen that the maximum absolute value of different-type ratio is equal to χ itself.

For the purposes of analytical calculations we focus on spherical and cylindrical

geometries. These geometries share significant amount of symmetry, since cylindrical group of symmetries might be viewed as a subgroup of spherical group. Thus, it is yet to prove that the observed behavior can be found in any type of axion shell. However, we believe that our results give a valuable insight and possess a significant generality. They provide theoretical background for experimental research of the systems featuring effective axion fields while also presenting new opportunities for Mie-resonant nanophotonics.

References

1. R. D. Peccei and H. R. Quinn, CP conservation in the presence of pseudoparticles, Phys. Rev. Lett. 38, 1440, (1977).

2. F. Chadha-Day, J. Ellis, and D. J. E. Marsh, Axion dark matter: What is it and why now?, Sci. Adv.8, eabj3618, (2022).

3. K. Choi, S. H. Im, and C. S. Shin, Recent progress in the physics of axions and axion-like particles, Annual Review of Nuclear and Particle Science 71, 225, (2021).

4. D. M. Nenno, C. A. C. Garcia, J. Gooth, C. Felser, and P. Narang, Axion physics in condensed-matter systems, Nature Reviews Physics 2, 682, (2020).

5. G. Rosenberg and M. Franz, Witten effect in a crystalline topological insulator, Phys. Rev. B 82, 035105, (2010).

6. L. Shaposhnikov, M. Mazanov, D. A. Bobylev, F. Wilczek, and M. A. Gorlach, Emergent axion response in multilayered metamaterials,Phys. Rev. B 108, 115101, (2023).

7. E. Witten, Dyons of charge $e\theta/2\pi$, Physics Letters B 86, 283, (1979).

8. C. T. Hill, Axion induced oscillating electric dipole moment of the electron, Phys. Rev. D 93, 025007, (2016).

9. T. Z. Seidov and M. A. Gorlach, Phys. Rev. A 108, 053515, (2023).

Quantum electrodynamics in supercritical field with heavy ions

Vladimir Shabaev[1,2]

[1]St. Petersburg State University
[2]Petersburg Nuclear Physics Institute named by B.P. Konstantinov of National Research Center "Kurchatov Institute"

The current status of QED tests in strong and supercritical Coulomb fields is considered. The main attention is paid to the supercritical regime. It is known that in slow collisions of two bare nuclei with the total charge number exceeding the critical value, $Z_1 + Z_2 > Z_c = 173$, the initially neutral vacuum can spontaneously decay into a charged vacuum and two positrons. The detection of spontaneous emission of positrons would be a direct proof of this fundamental phenomenon. However, the spontaneous emission of positrons is usually masked by the dynamic (induced) emission of positrons, which is caused by a rapidly changing electric field created by colliding nuclei. For many years, it was believed that vacuum decay can only be observed in collisions with nuclear sticking, when the nuclei are bound for a period of time due to nuclear interactions. But to date, there is no evidence that nuclear sticking occurs in such collisions of heavy ions. In our recent papers [1-4] it has been shown that vacuum decay can be observed without any sticking of nuclei. This can be done by measuring the probabilities of the creation of positrons or positron spectra for a given set of nuclear trajectories. The results of this study will be presented in the talk.

This work was carried out with the financial support of the RSF grant No. 22-62-00004.

References

[1] I.A. Maltsev, V.M. Shabaev, R.V. Popov, Y.S. Kozhedub, G. Plunien, X. Ma, Th. Stöhlker, and D.A. Tumakov, Phys. Rev. Lett. 123, 113401 (2019)

[2] R.V. Popov, V.M. Shabaev, D.A. Telnov, I.I. Tupitsyn, I.A. Maltsev, Y.S. Kozhedub, A.I. Bondarev, N.V. Kozin, X. Ma, G. Plunien, T. Stöhlker, D.A. Tumakov, and V.A. Zaytsev, Phys. Rev. D 102, 076005 (2020).

[3] R.V. Popov, V.M. Shabaev, I.A. Maltsev, D.A. Telnov, N.K. Dulaev, and D.A. Tumakov, Phys. Rev. D 107, 116014 (2023).

[4] N.K. Dulaev, D.A. Telnov, V.M. Shabaev, Y.S. Kozhedub, I.A. Maltsev, R.V. Popov, and I.I. Tupitsyn, Phys. Rev. D 109, 036008 (2024).

Zero-Bias Photodetection in 2D Materials via Geometric Design of Contacts

Valentin A. Semkin,[1] Aleksandr V. Shabanov,[1] Dmitry A. Mylnikov,[1] Mikhail A. Kashchenko,[1]
Ivan K. Domaratskiy,[1] Sergey S. Zhukov,[1] and Dmitry A. Svintsov[1]
Center for Photonics and 2D Materials,
[1] Moscow Institute of Physics and Technology, Dolgoprudny
141700, Russia;
Email: semkin.va@phystech.edu

Structural or crystal asymmetry is a necessary condition for the emergence of zero-bias photocurrent in light detectors. Structural asymmetry has been typically achieved via p–n doping, which is a technologically complex process. Here, we propose an alternative approach to achieve zero-bias photocurrent in two-dimensional (2D) material flakes exploiting the geometrical nonequivalence of source and drain contacts. As a prototypical example, we equip a square-shaped flake of PdSe2 with mutually orthogonal metal leads. Upon uniform illumination with linearly polarized light, the device demonstrates nonzero photocurrent which flips its sign upon 90° polarization rotation. The origin of zero-bias photocurrent lies in a polarization-dependent lightning-rod effect. It enhances the electromagnetic field at one contact from the orthogonal pair and selectively activates the internal photoeffect at the respective metal-PdSe2 Schottky junction. The proposed technology of contact engineering is independent of a particular light detection mechanism and can be extended to arbitrary 2D materials.

KEYWORDS: ***zero-bias detector, contact engineering, lightning-rod effect, polarization sensitivity, IR photodetector, 2D materials***

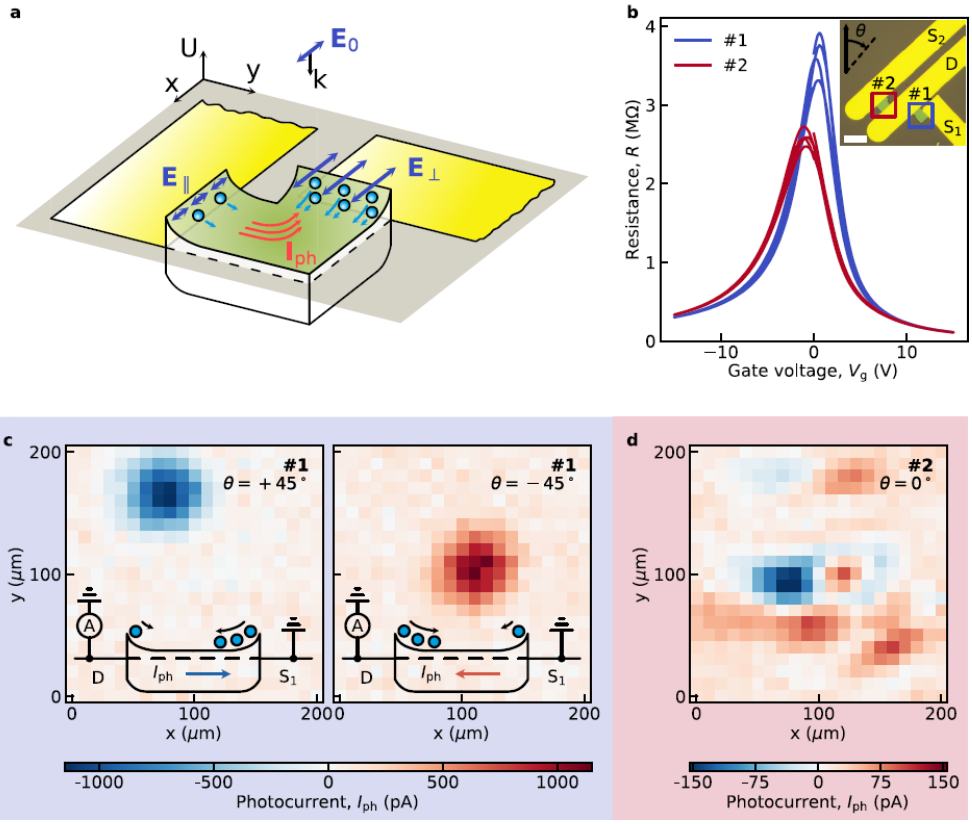

Figure 1. Light detection with asymmetric corner-type and symmetric slit-type detectors. a, Illustration of the operating principle for the corner-type detector: incident linearly polarized field is enhanced by the metal contact orthogonal to the E-field and suppressed by another contact. The Schottky junction at the 'active' contact generates large photocurrent, which cannot be compensated by a small

current at the ‘passive’ junction. b, Gate dependencies of the devices’ resistance. Inset: microphotograph of the devices and the reference direction for polarization angles θ. Scale bar is 10 μm. c,d, Spatial maps of photocurrent recorded at λ0 = 8.6 μm and zero bias voltage. c, Map for corner-type detector #1 at a gate voltage Vg = 20 V and polarization angles θ = +45° (left) and θ = −45° (right). The shift of the photoresponse spot is caused by the polarizer rotation. Insets: band diagrams with device connection scheme and photocurrent directions. d, Map for reference detector #2 at a gate voltage Vg = 10 V and a polarization angle θ = 0°.

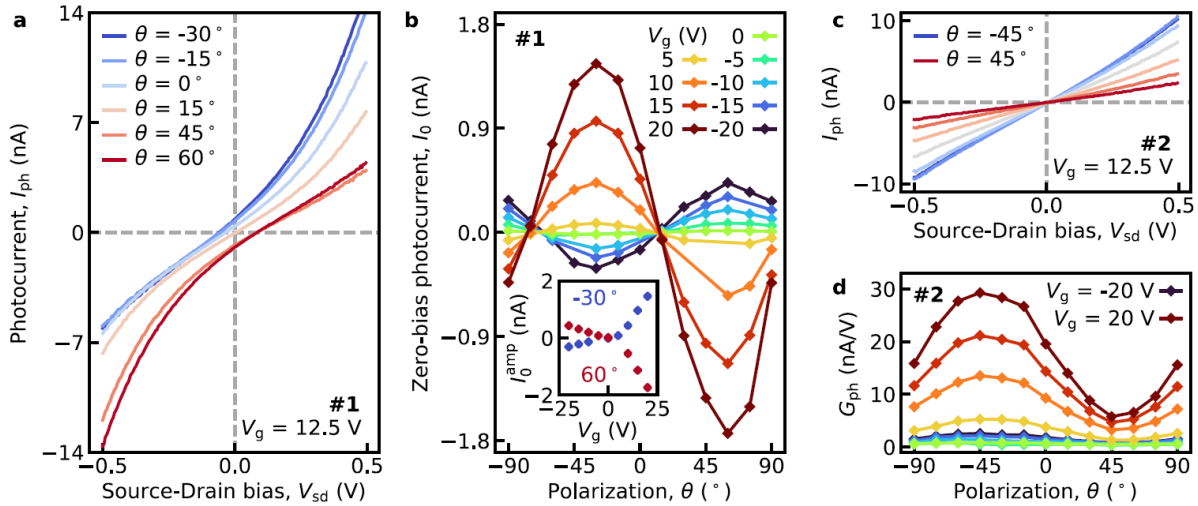

Figure 2. Mid-infrared (8.6 μm) polarization-sensitive photoresponse. a,c, A series of photocurrent Iph dependencies on the bias voltage Vsd at different polarization angles θ for corner-type detector #1 (a) and for reference detector #2 (c). b, Extracted series of zero-bias photocurrents I0 for device #1 vs polarization angle at different gate voltages Vg with step ΔVg = 5 V. Inset: Amplitude of zero-bias photocurrent I0 amp vs Vg at θ = −30° and θ = +60°. d, Extracted series of photoconductivity Gph vs polarization angle for device #2 at different Vg taken with step ΔVg = 5 V. See Figure S6 for I0(θ, Vg) series for #2 and Gph(θ, Vg) series for #1.

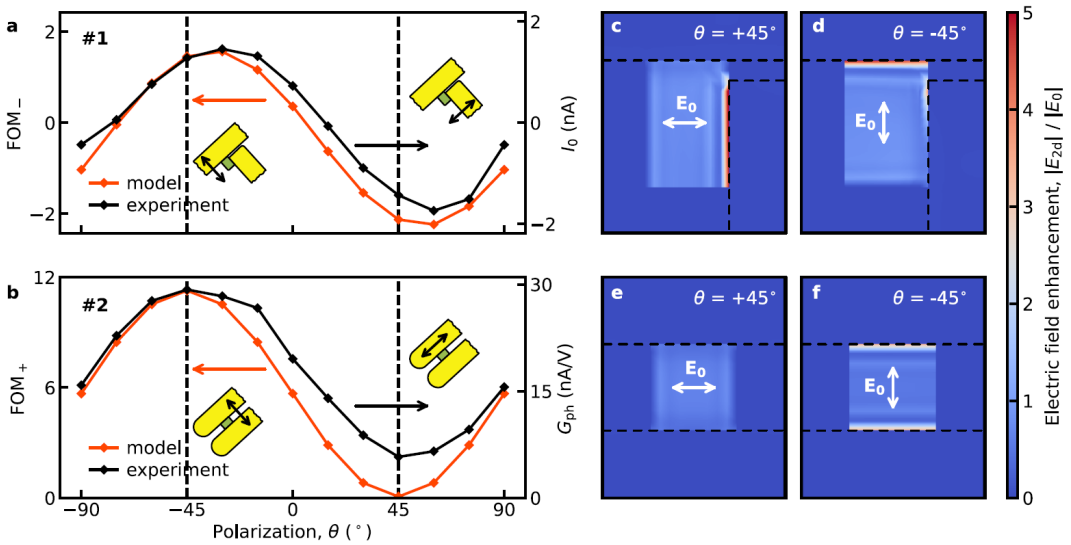

Figure 3. Simulation of contact-engineered detectors. a, Comparison of the measured zero-bias photocurrent I0(θ) with the simulation of the normalized difference of average local intensities at source and drain FOM− for device #1. b, Comparison of the measured photoconductivity Gph(θ) with the simulation of normalized sum of average local intensities at source and drain FOM+ for the device #2. Both experimental curves in a and b were measured at gate voltage Vg = 20 V. Insets: polarization of the incident light at θ = ± 45° is shown by the black arrows relative to the device schematics. c−f, Simulated local electric field in the 2D material plane normalized by the incident field, | E2D/E0| for the corner- type (c and d) and reference slit- type (e and f) detectors. Polarization of the incident light E0 is shown with the white arrow.

The International Summer Conference on Theoretical Physics 2024
Faculty of Physics of ITMO University
Abrikosov Center for Theoretical Physics

Smith-Purcell radiation from a 1D flat fractal photonic crystal

P. G. Shapovalov[1] and A. A. Tishchenko[2]

[1,2]National Research Nuclear University «MEPhI», Moscow, Russia

[1,2]Laboratory of Radiation Physics, Belgorod State University, Belgorod, Russia

[1]PGShapovalov@mephi.ru, [2]Tishchenko@mephi.ru

Abstract

The paper proposes an analytical solution to the problem of diffraction radiation from a charged particle on a fractal photonic crystal. This radiation is similar to Smith-Purcell radiation, and due to the complex interference pattern of different diffraction peaks, the resulting spectral and angular intensity distribution also exhibits fractal behavior. The topics of scaling, quantum limits in the spectrum, and the fractal nature of the emitted radiation are discussed.

Key words: Radiation of charged particles, Smith-Purcell radiation, diffraction grating, fractals, photonic crystals

Introduction

This paper considers the radiation that occurs when a relativistic charged particle moves along a flat one-dimensional fractal lattice. A fractal lattice is a diffraction grating in which each screen is replaced by a number of similar screens, i.e. subgrating, see Fig. 1 (Left). The screens in the sub gratings are also replaced by similar subgratings, this procedure being repeated the required number of times. In this work, the iterative process ends when the period of the sub grating becomes less than the wavelength. When a particle's field scatters on the inhomogeneities of the grating, a complex pattern of interference between secondary waves arises similar to Smith–Purcell radiation. Since such a diffraction grating has a certain symmetry and the particle "feels" the inhomogeneity of wavelength, it is correct to call it a fractal photonic crystal.

Fractality in the radiation spectrum

The radiation filed was calculated in the approximation of scalar waves in the Fraunhofer region [1]. It turns out that the spectral and angular distribution (Fig. 1

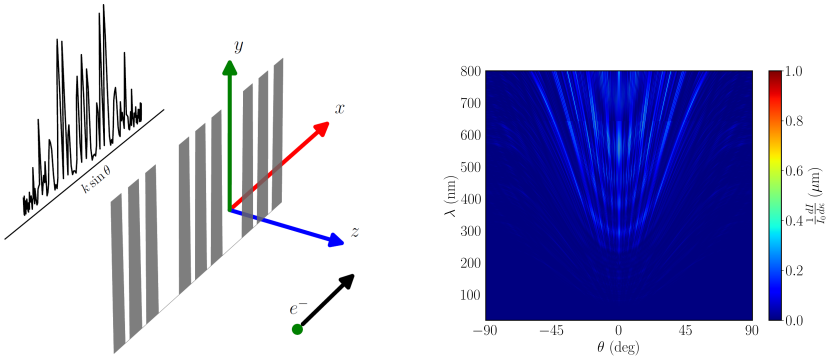

Figure 1: (Left) The electron passes near the fractal lattice and generates Smith-Purcell radiation. (Right) Spectral-angular distribution of Smith-Purcell radiation from a fractal photonic crystal.

(Right)) of the resulting radiation also has a fractal nature. Moreover, if the fractal photonic crystal has a fractal dimension less than 1 and is considered to be a fractal dust ($D < 1$), then the spectrum of radiation has a dimension between 1 and 2, i.e., it is a fractal curve ($1 < D < 2$) [2]. Maxima and minima in the final spectrum of intensity are determined not only by Bragg-Wolf conditions, which are a consequence of periodicity in crystals, but also by dispersion relations for diffraction of a field from a moving particle in a periodic inhomogeneous medium, which allows us to refer to such radiation as Smith-Purcell radiation.

The correlation between the fractal dimension of the grating and the spectrum, as well as the problem of scaling the measurement step, are discussed. The obtained spectra demonstrate the well-known property of fractals, which is self-similar everywhere. This property persists at all scales, seemingly limited only by the uncertainty principle. Analogies with radiation from more complex fractal systems and prospects for experimental verification of the theory are discussed.

The study was partially supported by the Ministry of Science and Higher Education of the Russian Federation, Projects No. FZWG-2020-0032 (2019-1569) and No. FSWU-2023-0075.

References

1. A. P. Potylitsyn, M. I. Ryazanov, M. N. Strikhanov, A. A. Tishchenko, Radiation from relativistic particles, Springer (2011).

2. B. B. Mandelbrot, The fractal geometry of nature, WH freeman New York (1982).

Absorption of the vortex photon by a Dirac electron in strong magnetic field

A.A. Shchepkin [1], D.V. Grosman[2], I.I. Shkarupa[2], D.V. Karlovets[2]

[1] Peter the Great St. Petersburg Polytechnic University, 195251, St. Petersburg, Russia

[2] School of Physics and Engineering, ITMO University, 197101, St. Petersburg, Russia

[1]alexander.shchepkin5@gmail.com, [2]dmitriy.grosman@metalab.ifmo.ru, [4]dmitry.karlovets@metalab.ifmo.ru

Abstract

The work considers the process of absorption of a photon vortex by an electron in uniform magnetic field that can reach the Schwinger value $H_c = 4.4 \cdot 10^{13}$ G. The incident twisted photon density profile was considered as the Bessel wavepacket, and the absorption process was supposed to induce the transition of an electron between the two relativistic Landau states. We claim that the absorption cross section can reach the values $\sigma \sim 10^{-13}$ cm^2, which can be crucial for studying the astrophysical environments with strong magnetic fields and high electron densities, for example, the pulsars accretion columns and the areas near neutron star mergers.

Key words: Vortex photon, vortex electron, strong magnetic fields, Landau states

Introduction

The electron in the magnetic field is one of the oldest problems in quantum mechanics and quantum field theory. The Landau states of charged particles, induced by magnetic field, are common to the quantum theory of synchrotron radiation, which is important in describing astrophysical objects with strong magnetic fields like neutron stars [1]. These states also have significant implications in solid-state physics, particularly in graphene, including quantum Hall effect, in diamagnetism of metals, in plasma, and in the quantum dynamics of charged particles in Penning traps.

In this paper, we study the vortex photon absorption within the first order perturbation theory by an electron in a constant and homogeneous magnetic field $\mathbf{H} = \{0, 0, H\}$, which strength has arbitrary value $H > 0$ up to several Schwinger magnetic field values $H_c = m_e^2 c^3/|e|\hbar$. According to [2], the photon density profile is described by Bessel functions, which possesses an energy ω, momentum projections along the propagation

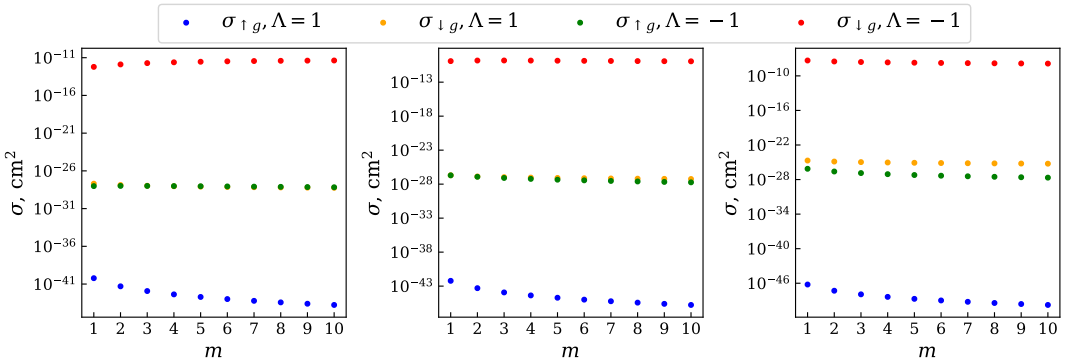

Figure 1: Cross sections of the photon absorption with different m by an electron in the ground Landau state. $s_i = s_f = 0$, $j_i = -1/2$, $\sigma_z = -1/2$, $k_z = 100$ keV, $\kappa = 10$ eV. Left picture is for $H = 0.1 \cdot H_c$, middle - $H = H_c$ and right - $H = 10 \cdot H_c$

direction, k_z, and perpendicular, κ, total angular momentum m and the helicity Λ. Both the initial and final electron states are described with the relativistic Landau ones, which are described by momentum projection p_z along **H**, radial quantum number s, total angular momentum j and spin projection σ_z (see, e.g. [3]).

Results

In Fig 1 it is seen that the cross sections with the spin flip of an electron $(\uparrow, g)$ are lower than without $(\downarrow, g)$, which is in agreement with the Sokolov-Ternov effect, considered in context of vortex photon emission in the same conditions [2, 4]. Here, g stands for ground state ($s = 0$, $j = -1/2$, $\sigma_z = -1/2$). The cross sections can reach the values of $\sigma \sim 10^{-13}$ cm^2 and even more, which ≥ 10 orders greater than Thompson scattering cross section ($\sigma_T \sim 10^{-24}$ cm^2). This makes crucial to account for the possible absorption process studying the astrophysical environments with strong magnetic field.

References

1. T. Maruyama, et al., Phys. Lett. B, **826**, 136779 (2022);
2. I. Pavlov and D. Karlovets, Phys. Rev. D, **109**, 036017 (2024);
3. A. Sokolov and I. Ternov, Relativistic electron, "Nauka", Moscow (1974);
4. K. van Kruining et al., Phys. Rev. D, **100**, 056014 (2019).

The International Summer Conference on Theoretical Physics 2024
Faculty of Physics of ITMO University
Abrikosov Center for Theoretical Physics

Elastic scattering of Laguerre - Gaussian vortex electron wave packets on hydrogen atoms

N. Sheremet[1], A. Chaikovskaia, D. Grosman, D. Karlovets

School of Physics and Engineering, ITMO University

[1]n.sheremet@metalab.ifmo.ru

Abstract

We explore elastic scattering of non-relativistic vortex electrons in the form of standard and elegant Laguerre - Gaussian (LG) wave packets on hydrogen-like targets in the generalized Born approximation and compare these results to the reference with Bessel - Gaussian packets. For scattering on a macroscopic target, the scattering pattern varies as the orbital angular momentum values of the incident wave packets change, which does not happen for the BG packet. Such features can be used to reveal the properties of incident electron wave packets and to distinguish these packets from each other in experimental settings.

Key words: twisted wave packets, elastic scattering, hydrogen atom

1. Introduction

Vortex electrons, i.e. those carrying orbital angular momentum $l = \pm 1, \pm 2, ...$, are actively studied both in theory [1] and in experiments [2]. We consider the twisted states in the form of Laguerre-Gaussian (LG) wave packets which are square-integrable solutions of the Schrödinger equation with a radial quantum number $n = 0, 1, 2, ...$ Specifically, we introduce elegant LG modes, the spatial distribution of which has a noticeable second peak only at rather large values of n, when for a standard LG the number of peaks always equals $n+1$. Twisted beams can be produced experimentally by phase plates, spiral zone plates and diffraction gratings. The main applications of such packets are micromanipulation of particles and electron traps. Recently, theoretical studies of elastic scattering of electron Bessel packets on atoms [3] and molecules [4], and of electron Gaussian packets on atoms [5] were carried out. However, so far, it has not been possible to distinguish different types of twisted electron states in experiment. This work highlights the opportunity to use the experimental scattering data to reveal the wave packet properties for the simplest scenario of scattering on the hydrogen atom.

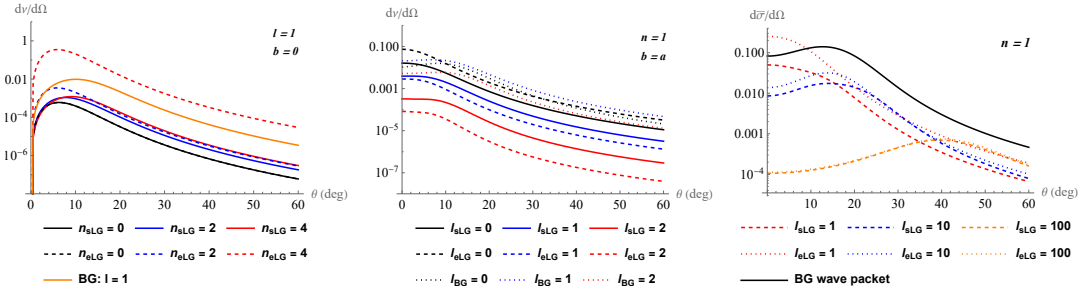

(a) (b) (c)

Figure 1: Scattering of twisted wave packets on a single hydrogen atom for different values of n (a) and l (b); Scattering of twisted wave packets on a macroscopic target for different values of OAM (c).

2. Scattering of LG vortex electrons

We consider the scattering of LG packets by single hydrogen atom. We present the number of events $d\nu(\theta)/d\Omega$ as a function of polar angle θ for different values of the OAM l (Fig. (1, a)), radial quantum number n (Fig. (1, b)) and impact parameter b, which indicates the location of the target with respect to the incident beam. Further, we investigate scattering of wave packets on a macroscopic (infinite-size) atomic target. We show the averaged cross section for different values of OAM l (Fig. (1, c)). We provide an in-depth analysis on the way the particular wave packet properties affect the scattering results, thus leading to the possibility of their distinction in real experiment.

References

1. K. Bliokh, Theory applications of free-electron vortex states, Physics Reports. **690**, 0370, (2017).

2. B. J. McMorran, Electron Vortex Beams with High Quanta of Orbital Angular Momentum, Science. **331**, 192, (2011).

3. D. Karlovets, Scattering of twisted electron wave packets by atoms in the Born approximation, Physical Review A. **95**, 032703, (2017).

4. A. Maiorova, Elastic scattering of twisted electrons by diatomic molecules, Physical Review A. **98**, 042701, (2018).

5. Karlovets D. V. Scattering of wave packets on atoms in the Born approximation, Physical Review A. **92**, 052703, (2015).

Non-Hermitian excitations in nonlinear topological lattice

V. Simonyan[1], D. Smirnova[2], M. Gorlach[3]

[1,3]School of Physics and Engineering, ITMO University, Saint Petersburg 197101, Russia

[2]Research School of Physics, Australian National University, Canberra, ACT 2601, Australia

[1]vlad.simonian@metalab.ifmo.ru

Abstract

Nonlinear and non-Hermitian topological photonics are two new and rapidly developing areas of physics, the interplay between them opens up additional challenging aspects in topological materials physics. These can naturally intertwine to provide enhanced functionality for topoelectric circuits and photonic platforms. Here we demonstrate the subtle interplay between these two areas by investigating the characteristics of small wave perturbations in the background of a self-induced topological edge state in the nonlinear Su-Schreifer-Hieger model. We show that their fundamental physics is described by an effective non-Hermitian Hamiltonian, which includes nonreciprocal couplings and implies an unusual time-dependent localization of the field.

Key words: Topological photonics

Introduction

Discovered initially in condensed matter physics [9, 4], topological effects later spread to other areas of physics, including photonics[7]. The introduction of nonlinear effects into such systems led to the development of a new field - nonlinear topological photonics. The presence of nonlinearity makes it possible to flexibly restructure the topological state of the system by changing the intensity. An example of such a system is nonlinear SSH[2, 3], in which a topological phase transition occurs at intensity growth. Due to the topological properties, a self-induced edge state exists in this system, which is resilient to disorder in the system. Another recent trend is non-hermitian topological photonics[1, 6] also opens up new effects such as the non-Hermitian skin effect. Systems with nonreciprocal couplings are good examples of non-hermitian systems, e.g., the Hatano-Nelson model[5] or non-Hermitian SSH[10]. However, the interplay between these two areas has not yet been explored[8].

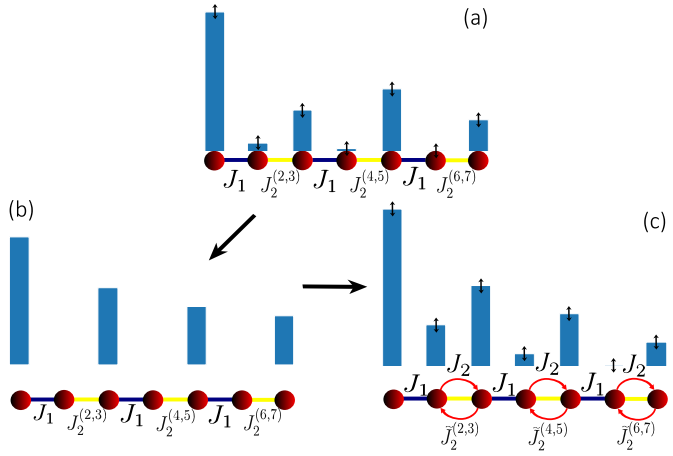

Figure 1: Schematic representation of the relationship between non-Hermitian and nonlinear phenomena. Small perturbation of a nonlinear edge state (a) can be represented as the sum of an undisturbed nonlinear edge state (b) and effectively non-Hermitian excitation in a system where the hopping coefficients from left to right and from right to left are not equal to each other (c).

Main text

Nonlinear SSH is described by the Schrödinger equation in the following form:

$$i\frac{\partial |\Psi\rangle}{\partial t} = \hat{H}(\Psi)\ |\Psi\rangle\ , \tag{1}$$

where

$$\hat{H}(\Psi) = \begin{bmatrix} \omega_0 & J_1 & \ddots & 0 & 0 \\ J_1 & \omega_0 & J_2^{(2,3)} & \ddots & 0 \\ \ddots & J_2^{(3,2)} & \omega_0 & \ddots & \ddots \\ 0 & \ddots & \ddots & \omega_0 & J_1 \\ 0 & 0 & \ddots & J_1 & \omega_0 \end{bmatrix} . \tag{2}$$

After defining the edge mode in it, a small perturbation can be added to it and the behavior of such perturbations can be studied using perturbation theory. The resulting equation for perturbations is a Schrödinger equation with a non-Hermitian

Hamiltonian and can be written as

$$i\frac{\partial}{\partial t}|\phi\rangle = \hat{H}_0|\phi\rangle + 2\hat{A}\cdot \mathrm{Re}\{|\phi\rangle\}. \tag{3}$$

Here $\hat{A}$ is the non-Hermitian matrix where only elements $A_{2n,2n+1}$ are non-zero positive numbers and $\hat{H}_0$ is the linear SSH-type Hamiltonian. Thus, the consideration of perturbations in a nonlinear system [Fig.1(a)] can be reduced to two problems: finding the edge state [Fig.1(b)] and determining the dynamics of perturbations in an effectively non-Hermitian system [Fig.1(c)].

Such a system is quite similar to the non-Hermitian SSH, but due to the phase-dependence of the non-Hermitian part of the Hamiltonian, it does not exhibit sufficiently all the expected effects. The non-Hermitian skin effect is then broken, but a shift of the density of states towards the edge of the chain is observed. In addition, the analysis of the time dependence of the density of states reveals the presence of time-dependent localization of the wave states, which arises due to the nonlinear nature of the non-Hermitian.

References

[1] Emil J. Bergholtz, Jan Carl Budich, and Flore K. Kunst. "Exceptional topology of non-Hermitian systems". In: Reviews of Modern Physics 93.1 (Feb. 2021), p. 015005. ISSN: 1539-0756. DOI: 10.1103/RevModPhys.93.015005.

[2] Yakir Hadad, Alexander B. Khanikaev, and Andrea Alù. "Self-induced topological transitions and edge states supported by nonlinear staggered potentials". In: Physical Review B 93.15 (Apr. 2016), p. 155112. ISSN: 2469-9969. DOI: 10.1103/PhysRevB.93.155112.

[3] Yakir Hadad et al. "Self-induced topological protection in nonlinear circuit arrays". In: Nature Electronics 1.3 (Mar. 2018), pp. 178–182. ISSN: 2520-1131. DOI: https://doi.org/10.1038/s41928-018-0042-z.

[4] M. Z. Hasan and C. L. Kane. "Colloquium: Topological insulators". In: Reviews of Modern Physics 82.4 (Nov. 2010), pp. 3045–3067. ISSN: 1539-0756. DOI: 10.1103/revmodphys.82.3045.

[5] Naomichi Hatano and David R. Nelson. "Vortex pinning and non-Hermitian quantum mechanics". In: Physical Review B 56.14 (Oct. 1997), pp. 8651–8673. ISSN: 1095-3795. DOI: 10.1103/physrevb.56.8651.

[6] Flore K. Kunst et al. "Biorthogonal Bulk-Boundary Correspondence in Non-Hermitian Systems". In: Physical Review Letters 121.2 (July 2018), p. 026808. ISSN: 1079-7114. DOI: 10.1103/PhysRevLett.121.026808.

[7] Tomoki Ozawa et al. "Topological photonics". In: Reviews of Modern Physics 91.1 (Mar. 2019), p. 015006. ISSN: 1539-0756. DOI: 10.1103/RevModPhys.91.015006.

[8] Alexander N. Poddubny. "Interaction-induced analog of a non-Hermitian skin effect in a lattice two-body problem". In: Physical Review B 107.4 (Jan. 2023), p. 045131. ISSN: 2469-9969. DOI: 10.1103/PhysRevB.107.045131.

[9] Di Xiao, Ming-Che Chang, and Qian Niu. "Berry phase effects on electronic properties". In: Reviews of Modern Physics 82.3 (July 2010), pp. 1959–2007. ISSN: 1539-0756. DOI: 10.1103/revmodphys.82.1959.

[10] Shunyu Yao and Zhong Wang. "Edge States and Topological Invariants of Non-Hermitian Systems". In: Physical Review Letters 121.8 (Aug. 2018), p. 086803. ISSN: 1079-7114. DOI: 10.1103/PhysRevLett.121.086803.

Induced emission in the field of a single-photon wave packet

D. V. Grosman, E. O. Lazarev, G. K. Sizykh, and D. V. Karlovets
School of Physics and Engineering, ITMO University, 197101 St. Petersburg, Russia

G. V. Voloshin
Peter the Great St. Petersburg Polytechnic University, 195251 St. Petersburg, Russia

I. INTRODUCTION

Photons with orbital angular momentum (OAM), dubbed vortex photons, are a relatively new subject of study in quantum optic [1] and have found numerous applications in various fields [1, 2] and especially in quantum information [3], where entanglement between photons plays crucial role. One of the easiest ways to obtain two entangled photons is the process of induced emission of an atom in the presence of an incident photon. We study this process when an incoming photon's shape has a complex structure rather than being merely a plane wave. We find the state of the system "atom + field" for an arbitrary time in a Weisskopf-Wigner manner and calculate the observable values comparing the results with the spontaneous emission process. The difference between the perturbation theory approach is underlined.

II. RESULTS

We have found the probabilities to find the system in the initial state $P_{\text{in}}(t)$ and to detect the atom in the excited state $P_{\text{e}}(t)$ at a time t for an incident photon represented by a Gaussian wave packet with dispersion σ in momentum representation:

$$\begin{aligned} P_{\text{in}}(t) &= e^{-\Gamma t}\left(1-\frac{\sqrt{2}\pi}{2}\mathcal{G}\left(\frac{\Gamma}{\sigma}\text{erf}(\sigma t)\right)^2\right), \\ P_{\text{e}}(t) &= e^{-\Gamma t}\left(1-\frac{\sqrt{2}\pi}{2}\mathcal{G}\left(\frac{\Gamma}{\sigma}\text{erf}(\sigma t)\right)^2\right)+\frac{e^{-\Gamma t}}{2}\frac{\sqrt{2}\pi}{2}\mathcal{G}\left(\frac{\Gamma}{\sigma}\left[\text{erf}(\sigma t)-\text{erf}\left(\frac{\sigma t}{\sqrt{2}}\right)\right]\right)^2\left(1-e^{-\frac{\sqrt{2}\Gamma}{2}t}\right), \end{aligned} \tag{1}$$

where $\mathcal{G}=(2\pi)^{3/2}|\gamma^{\boldsymbol{k}_i,s_i}|^2/(\sigma^3\Gamma^2)$ is proportional to the square ratio of the coupling constant to the spontaneous decay rate, describing the interaction of the atom with a Gaussian photon, to the natural width. The difference with the case of a plane-wave incident photon is in the wave packet's volume $V_\sigma=(2\pi)^{3/2}/\sigma^3$ replacing the usual space volume. We have also found the average momentum of the final two-photon state at large times $\langle\hat{\boldsymbol{k}}\rangle=\boldsymbol{k}_i[1+\sqrt{2}\pi\mathcal{G}/2(\Gamma/\sigma)^2]$, which is slightly larger than the average momentum of the incident Gaussian wave packet $\boldsymbol{k}_i$.

We have considered the case of an incident Bessel photon wave packet with the atom being displaced from the quantization axis by an impact parameter $\boldsymbol{b}$. In this scenario the coupling constant is modified as follows:

$$g^{\text{B}*}=-i^l\frac{\sqrt{2\pi\omega_i}}{\kappa}|\boldsymbol{d}|d^1_{l,s_i}(\theta_i)e^{il\varphi_b}J_l(\kappa b), \tag{2}$$

where $l=m+l_e-l_g$. Note that in the limit $b\to 0$ $g^{\text{B}*}\sim\delta_{l,0}$, meaning that when the angular momentum of the photon differs from l_e-l_g, the atom emits radiation spontaneously. On the other hand, when an atom is placed directly on the propagation axis of a vortex photon, the induced emission does not occur when $|m|>1$ and the atom decays spontaneously. However, this effect is due to the dipole approximation, and in higher orders larger values of the incident photon's OAM would contribute to the atom emission.

[1] S. Franke-Arnold, L. Allen, and M. Padgett. Advances in optical angular momentum. *Laser Photonics Rev.*, 2(4):299–313, August 2008.
[2] Carlos Hernández-García, Jorge Vieira, Jose T. Mendonça, Laura Rego, Julio San Román, Luis Plaja, Primoz R. Ribic, David Gauthier, and Antonio Picón. Generation and Applications of Extreme-Ultraviolet Vortices. *Photonics*, 4(2):28, April 2017.
[3] Gabriel Molina-Terriza, Juan P. Torres, and Lluis Torner. Twisted photons. *Nat. Phys.*, 3:305–310, May 2007.

Nuclear magnetization distribution effect in molecules and atoms

L.V. Skripnikov[1,2]

[1]Petersburg Nuclear Physics Institute named by B.P. Konstantinov of National Research Center "Kurchatov Institute" (NRC "Kurchatov Institute" – PNPI), 1 Orlova roscha, Gatchina, 188300 Leningrad region, Russia

[2]Saint Petersburg State University, 7/9 Universitetskaya nab., St. Petersburg, 199034, Russia

[1]skripnikov_lv@pnpi.nrcki.ru

Abstract

We study the finite nuclear magnetization distribution effect in atoms and molecules, which manifests as a contribution to hyperfine splitting. For this a theoretical method is introduced to isolate the nuclear effect from the electronic degrees of freedom. This proposed formalism enables the deduction of nuclear magnetic dipole moment values from hyperfine data for both atoms and molecules. We show that for the case of heavy systems it is enough to introduce just one parameter that characterizes the magnetization distribution.

Key words: magnetic dipole moment of the nucleus; nuclear magnetization distribution

Main text

Theoretical predictions of hyperfine splittings in heavy atoms and molecules hold significant importance across various fundamental physical applications. They serve as crucial tests for the accuracy of calculated characteristics necessary for interpreting experiments aimed at detecting violations of spatial parity (P) or both spatial parity and time-reversal (T) symmetries in fundamental interactions within atoms and molecules, or for making semi-empirical predictions. Hyperfine splittings in the spectra of highly charged ions offer opportunities to test bound-state quantum electrodynamics in strong electric and magnetic fields. Additionally, accurate theoretical predictions are essential for determining the magnetic moments of short-lived isotopes.

In many cases, the largest uncertainty in the theoretically predicted value of the hyperfine splitting arises from the nuclear component of the problem. There are two significant contributions to the hyperfine splitting stemming from the finite size of the nucleus. The first contribution arises from the finite charge distribution within the

nucleus, which can be accurately calculated given the experimental knowledge of this distribution. The second contribution, known as the Bohr–Weisskopf (BW) effect in atoms, arises from the distribution of magnetization within the nucleus.

We propose a model-independent approach to address the BW effect in atoms and molecules [1]. This method is applied to the radium monofluoride molecule ^{225}RaF, demonstrating the possibility of separating the contribution of the BW effect to the hyperfine constant of a heavy atom or molecule into two components: a purely electronic-structure part and a universal parameter dependent on the nucleus. This factorization allows for the extraction of the nuclear magnetization distribution from experimental data on hyperfine structure in an atom or molecule, which can then be used to predict the BW effect in any other compound of the considered atom. Furthermore, this factorization method aids in the analysis of magnetic hyperfine anomalies. Recent experimental verification of this method has been conducted [2].

We also study the hyperfine structure of the Po atom [3]. By employing the factorization method, we achieve substantially improved values for the nuclear magnetic dipole moments of ^{205}Po and ^{207}Po, along with deriving parameters that describe their nuclear magnetization distributions. Additionally, we reassess the electric quadrupole moments of all Po isotopes.

References

1. L.V. Skripnikov, J. Chem. Phys. **153**, 114114 (2020).

2. S.G. Wilkins et al, arXiv:2311.04121 [nucl-ex] (2023).

3. L.V. Skripnikov, A.E. Barzakh, Phys. Rev. C **109**, 024315 (2024).

Edge states in arrays of superconducting resonators and qubits

Solomakhin I.D., Fedorov G.P.
Moscow Institute of Physics and Technology, Dolgoprudny, Russia
e-mail: solomakhin.id@phystech.edu, gleb.fedorov@phystech.edu

Recently, systems in which topological states are observed have been of particular interest [1, 2]. An example of such systems is the Su-Schrieffer-Heeger model (SSH). The main feature of such states is that their existence is conditioned by the presence of symmetries and the topology of the system, rather than by a particular set of parameters. Due to this, such states are robust to disorder of various kinds. This property makes them useful for realization of quantum computations stable to errors.

In this study we consider examples of classical and quantum systems with nontrivial topological properties. Particular attention is paid to the numerical analysis of systems with boundary states whose wave function is concentrated at the boundaries and exponentially damped in the volume. Variants of experimental schemes with tunable coupling [3] based on superconducting transmon-type qubits are proposed.

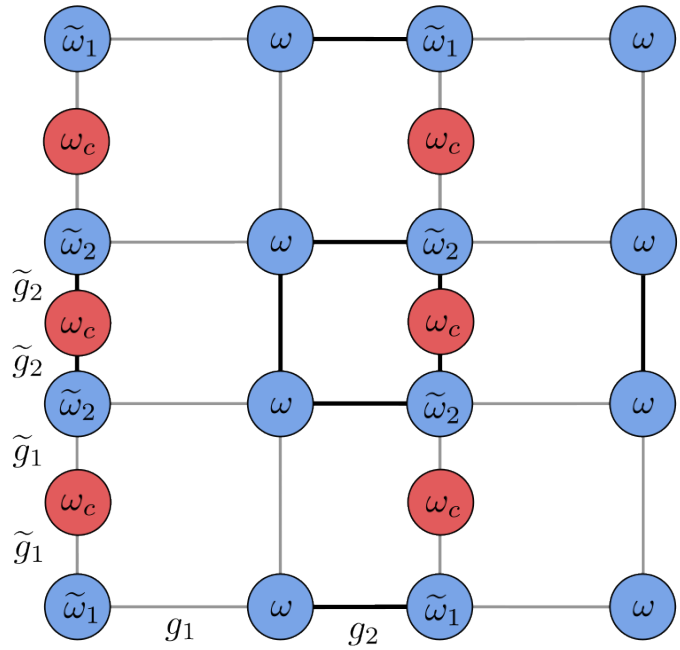

Fig. 1: Array of coupled superconducting qubits, with tuned frequencies and coupling coefficients to observe edge states.

References

[1] Probst, S., Song, F., Bushev, P., Ustinov, A. & Weides, M. Efficient and robust analysis of complex scattering data under noise in microwave resonators. *Review Of Scientific Instruments*. **86**, 024706 (2015,2), https://doi.org/10.1063

[2] Wladimir A. Benalcazar et al., Quantized electric multipole insulators. *Science*. **357**, 61-66 (2017), DOI: 10.1126/science.aah6442

[3] Yan, F., Krantz, P., Sung, Y., Kjaergaard, M., Campbell, D., Orlando, T., Gustavsson, S., & Oliver, W. (2018). Tunable Coupling Scheme for Implementing High-Fidelity Two-Qubit Gates. Phys. Rev. Appl., 10, 054062

Theoretical particularities of photon scattering processes in applications to precision spectroscopic experiments

D. Solovyev[1], T. Zalialiutdnov[2], A. Anikin[3], L. Labzowsky[4]

[1,2,4]Department of Physics, St. Petersburg State University,
Petersburg Nuclear Physics Institute named by B.P. Konstantinov

[3]Department of Physics, St. Petersburg State University,
D.I. Mendeleyev All-Russian Institute for Metrology

[1]d.solovyev@spbu.ru

Abstract

The spectral line profile has become a strictly observable physical quantity in precision spectroscopic experiments. The detection of its asymmetry has become crucial for the accurate determination of transition frequencies and, as a consequence, fundamental physical constants.

Key words: Theoretical atomic physics, photon scattering processes, fundamental physical constants

Introduction

At present, experimental progress ascertained that the spectral line profile can be studied in detail as a precisely measurable quantity. The theory of natural line profile in atomic physics was developed since the pioner works [1] within Quantum Mechanics (QM) and [2] within Quantum Electrodynamics (QED). An extended QED theory of the line profile for many-electron atoms and highly charged ions (HCI) was described in [3, 4]. The development of the line profile theory is closely related to experimental advances in measuring the transition frequency in the hydrogen atom [7]. Such experiments have stimulated interest in theoretical studies of effects beyond the resonance approximation.

Main text

The most important consequences in the line profile theory were found in the form of corrections to the transition frequency arising due to nonresonant (NR) terms in the photon scattering cross section [5, 6]. These corrections expressly demonstrate the breach of the resonance approximation. The largest contribution originates from

the states most close by energy to the resonant one when the differential sross section for the photon scattering is considered. An important step was made in [7], where NR asymmetry was experimentally observed and the distorted line profile theory [6] was used to accurately determine the transition frequency. The effect of line profile asymmetry is shown schematically in Fig. 1.

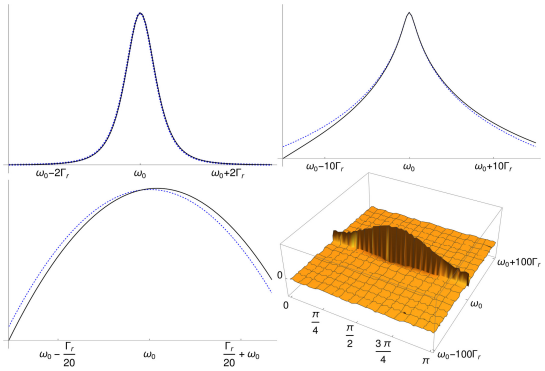

Figure 1: The asymmetry of the line profile due to nonresonant contributions. The left top panel shows the symmetric and asymmetric profiles (indistinguishable to the naked eye); in logarithmic scale in the right top panel. The "line maximum" region is given in logarithmic scale in the left bottom panel. The difference between symmetric and asymmetric profiles is shown in the right bottom panel.

In the present study, the fundamental principles of determining the transition frequency and the role of the line profile asymmetry due to nonresonant terms in the scattering cross section is considered in detail on the example of various processes used in precision experiments.

References

1. V. Weisskopf, and E. Wigner, Berechnung der natürlichen Linienbreite auf Grund der Diracschen Lichttheorie, Zeitschrift für Physik **63** (1), 54 (1930).

2. F. Low, Natural Line Shape, Phys. Rev. **88**, 53 (1952).

3. O. Y. Andreev, L. N. Labzowsky, G. Plunien, and D. A., Solovyev, QED theory of the spectral line profile and its applications to atoms and ions, Physics Reports **455** (4), 135 (2008).

4. T. A. Zalialiutdinov, D. A. Solovyev, L. N. Labzowsky, and G. Plunien, QED theory of multiphoton transitions in atoms and ions, Physics Reports **737**, 1 (2018).

5. L. N. Labzowsky, D. A. Solovyev, G. Plunien, and G. Soff, Asymmetry of the Natural Line Profile for the Hydrogen Atom, Phys. Rev. Lett. **87**, 143003 (2001).

6. U. D. Jentschura, and P. J. Mohr, Nonresonant effects in one- and two-photon transitions, Canadian Journal of Physics **80** (6), 633 (2002).

7. A. Beyer et al, The Rydberg constant and proton size from atomic hydrogen, Science **358** (6359), 79 (2017).

ONE-ELECTRON QUASIMOLECULES IN A SUPERSTRONG MAGNETIC FIELD

D. V. Zinenko [1], E. V. Tryapitsyna [2], D. A. Glazov [2], A. A. Kotov [1], I. A. Maltsev [1], and V. M. Shabaev [1]

(dmitrii.zinenko@gmail.com)

[1]physical Faculty, 7/9 Universitetskaya nab., Saint Petersburg State University, 199034 Saint Petersburg, Russia

[2]physical and Technical Mega-faculty, ITMO University, 49 Kronversky ave., 197101 Saint Petersburg, Russia

Quantum electrodynamics suggests that absolutely new phenomena associated with the instability of the vacuum can occur in very strong magnetic fields [1-3]. In particular, it was shown in some papers [2, 3] that for nuclear charges greater than the critical $Z_{cr} \geq 173$, the ground state of the hydrogen-like ion becomes unstable, which can lead with some probability to vacuum decay and the appearance of a positron. Similar processes can occur in slow collisions of heavy ions whose total charge exceeds the critical one [4,5]. It was shown [6, 7] that a superstrong magnetic field strongly reduces the Z_{cr} , at which the main level dips into the continuum.

In this paper, we consider one-electron diatomic quasimolecules in a magnetic field directed along the molecular axis. The ground state energy is calculated as a function of the internuclear distance D and the magnetic field B, and the critical distance D_{cr} is calculated as a function of the magnetic field. Two types of quasimolecules are considered: lead Pb^{82+} - Pb^{82+} and uranium U^{92+} - U^{92+}. To solve the Dirac equation with a two-center potential, we used the dual kinetic balance method for axially symmetric systems [8, 9]. This method was successfully applied to homonuclear and heteronuclear quasimolecules with one and two electrons [10-13]. Calculations are also performed in the monopole approximation for the two-center potential in order to estimate the effect of an arbitrary direction of the molecular axis.

References:

[1] I. Pomeranchuk, I. and Smorodinsky. J., J. Phys. USSR 9, 97 (1995).

[2] S. Gershtein and Y. B. Zel'dovich, Sov. Phys. JETP 30, 358 (1970).

[3] W. Pieper and W. Greiner, Z. Physik 218, 327 (1969).

[4] I. A. Maltsev, V. M. Shabaev, R. V. Popov, Y. S. Kozhedub, G. Plunien, X. Ma, Th. Stoehlker, and D. A. Tumakov, Phys. Rev. Lett. 123, 113401 (2019).

[5] R. V. Popov, V. M. Shabaev, D. A. Telnov, I. I. Tupitsyn, I. A. Maltsev, Y. S. Kozhedub, A. I. Bondarev, N. V. Kozin, X. Ma, G. Plunien, T. Stoehlker, D. A. Tumakov, and V. A. Zaytsev, Phys. Rev. D 102, 076005 (2020).

[6] V. Oraevskii, A. Rex, and V. Semikoz, Sov. Phys. JETP 45, 428 (1977).

[7] P. Schlueter, G. Soff, K. H. Wietschorke, and W. Greiner, J. Phys. B: At. Mol. Phys. 18, 1685 (1985).

[8] V. M. Shabaev, I. I. Tupitsyn, V. A. Yerokhin, G. Plunien, and G. Soff, Phys. Rev. Lett. 93, 130405 (2004).
[9] E. B. Rozenbaum, D. A. Glazov, V. M. Shabaev, K. E. Sosnova, and D. A. Telnov, Phys. Rev. A 89, 012514 (2014).
[10] A. A. Kotov, D. A. Glazov, A. V. Malyshev, A. V. Vladimirova, V. M. Shabaev, and G. Plunien, X-Ray Spectrometry 49, 110 (2020).
[11] A. A. Kotov, D. A. Glazov, V. M. Shabaev, and G. Plunien, Atoms 9, 44 (2021).
[12] A. A. Kotov, D. A. Glazov, A. V. Malyshev, V. M. Shabaev, and G. Plunien, Atoms 10, 145(2022).
[13] D. Solovyev, A. Anikin, A. Danilov, D. Glazov, and A. Kotov, Phys. Scr. 99, 045401 (2024).

Effect of electron correlations on double ionization of atoms in intense laser fields

D. Tyurin[1] and S. Popruzhenko[1,2]

[1]National Research Nuclear University Moscow Engineering Physics Institute, Kashirskoe shosse 31, 115409, Moscow, Russia

[2]Prokhorov General Physics Institute of the Russian Academy of Sciences, Vavilova str. 38, 119991, Moscow, Russia

[1]Denisturin1999@yandex.ru

Abstract

We consider the influence of the electron-electron interaction on the effect of double tunnel ionization of atoms and negative ions in the field of intense laser radiation. By solving numerically the time-dependent Schrödinger equation for two-electron one- and two-dimensional atomic systems we investigate the impact of a possible channel of two-electron collective tunneling in the case of an ultrashort unipolar laser pulse when the effect of rescattering is eliminated. We show that for one-dimensional two-electron systems the electron-electron repulsion strongly suppresses the collective channel. We also discuss applicability of the single-electron approximation for description of sequential tunnel ionization and show that the electron correlations can suppress the probability of the second electron detachment by several times, compared to the case of independent tunneling of non-interacting electrons.

Key words: Tunneling ionization, strong laser field, correlation effects, collective ionization

The constant interest in the multiple ionization of atoms and ions in strong laser fields is stimulated by the possibility of studying correlation effects in nonlinear non-stationary quantum dynamics. One of such strong-field non-perturbative effects is the rescattering of an electron on the parent ion followed by double ionization. This ionization mechanism is currently described in detail theoretically and examined in experiments [1]. Another possible ionization channel induced by electron-electron interactions – collective tunneling has also been discussed in the literature [2]. It was shown in [3] that if two electrons can tunnel together as a quasi-particle, this should qualitatively change the momentum distribution of doubly charged ions (by a doubly charged ion we mean here an atomic system that lost two electrons relative to its initial state: in the case of initially negatively charged ions, e.g. Br^-, the resulting specie will have the charge $+1$) compared to the case of sequential independent ionization.

In this contribution, using the numerical solution of the time-dependent two-particle Schrödinger equation, we investigate the possibility of the formation of such a two-electron quasi-particle in the field of a strong electromagnetic pulse, which is a unipolar short burst of electric field. Such pulse shape allows to entirely exclude the rescattering channel, which will otherwise dominate the process. This helps to examine alternative correlation mechanisms. Analysis of the Perelomov-Popov-Terentyev formulas [4] for the probability of sequential ionization and their generalization [2] to the case of collective ionization shows that the collective channel could potentially make a significant contribution to the double ionization rate of a negative bromine ion. However, the numerical solution of the time-dependent Schrodinger equation demonstrates that electron-electron repulsion significantly inhibits the formation of a quasi-particle of two electrons, which suppresses the collective ionization channel. This suppression is most significant for one-dimensional systems.

However, electron-electron correlations contribute qualitatively to the double ionization dynamics. The numerically extracted rates do significantly change when the electron-electron correlation is accounted for, making the standard picture of sequential tunneling questionable. Our numerical results demonstrate that in a one-dimensional two-electron system, electronic correlations can considerably reduce the probability of ionization of the second electron compared to the case when tunneling occurs independently.

References

1. Becker W. et al. Theories of photoelectron correlation in laser-driven multiple atomic ionization //Reviews of Modern Physics. – 2012. – Т. 84. – №. 3. – С. 1011.

2. Zon B. A. Many-electron tunneling in atoms //Journal of Experimental and Theoretical Physics. – 1999. – Т. 89. – С. 219-222.

3. Popruzhenko S. V., Lomonosova T. A. On the Possibility to Observe Collective Tunneling in Ionization of Atoms by Intense Laser Fields //JETP Letters. – 2021. – Т. 113. – №. 5. – С. 317-321.

4. Perelomov A. M., Popov V. S., Terentiev M. V. Ionization of atoms in varying electric field //Zhurnal Eksperimental'noi i Teoreticheskoi Fiziki (USSR) For English translation see Sov. Phys.-JETP (Engl. Transl.). – 1966. – Т. 51.

The International Summer Conference on Theoretical Physics 2024
Faculty of Physics of ITMO University
Abrikosov Center for Theoretical Physics

Nonlinear dynamics of optical Wannier-Stark states in a periodic system of interacting resonators

A. Verbitskiy[1] and A. Yulin[2]

School of Physics and Engineering, ITMO University

[1]alexey.verbitskiy@metalab.ifmo.ru, [2]a.yulin@metalab.ifmo.ru

Abstract

In this work, we investigate the behavior of Wannier-Stark states in a dissipative array of coupled optical cavities whose eigenfrequencies depend linearly on the resonator number. It has been shown that laser generation on Wannier-Stark modes can be achieved in the systems with linear gain saturated by the nonlinear losses. We have demonstrated numerically and analytically various stationary solutions including Bloch oscillations. Moreover, it is shown that properly distributed effective linear gain allows to obtain monochromatic lasing in a wide range of pump amplitudes. We have also revealed that the presence of Kerr nonlinearity may result in destabilization of single-frequency generation.

Key words: Optics, Nonlinear waves, Wannier-Stark states, Bloch oscillations

Introduction

Wannier-Stark (WS) states (eigenstates localized in a periodic structure, see [1]) and the effects associated with them have been actively discussed in the scientific literature for more than a decade, see [2]. It is worth noting that the interference of these states may result in the appearance of such an interesting phenomenon as Bloch oscillations (BOs) [3]. The mentioned effects were discovered in solid-state physics, however, are also observed in other physical systems, including optical ones, see, for instance, [4].

From an experimental point of view, the study of optical WS states is more achievable compared to quantum ones. Besides, optical systems make it possible to observe BOs not only in a linear, but also in a nonlinear regime. Namely, stochastic BOs may appear when a one-dimensional array of nonlinear microresonators is excited by a periodic sequence of sufficiently powerful pulses [5].

WS states and BOs are most often observed in conservative systems. However, they may be also utilized in active systems, for example, in microlasers arrays. In order to use WS states as lasing modes in such systems, one can put the resonant frequency as a linear function of the resonator index. The advantage of these active systems is the possibility of frequency tuning by a spatial shift of the pump area. In addition, the working mode may be localized within a sufficiently large number of resonators, which

may result in increasing total generation power. The purpose of this work is to study a laser generation in a one-dimensional array of interacting resonators whose resonant frequencies are the functions of electromagnetic field intensity (Kerr nonlinearity).

Main text

The dynamics of the coupled resonator system may be described by a discrete dissipative nonlinear Schrodinger equation. Then, provided that we work in the tight-binding approximation, the evolution for the complex amplitudes of the resonator modes $U_n(t)$ is assumed to be

$$i\partial_t U_n + \sigma(U_{n+1} + U_{n-1}) + \mu n U_n + \alpha|U_n|^2 U_n + i\gamma_n U_n + i\beta_n |U_n|^2 U_n = 0, \qquad (1)$$

where n enumerates the resonators, σ is the coupling between the neighboring resonators, μ is the steepness of the linear dependency of the resonator eigenfrequencies on their number, α is the nonlinear coefficient, γ and β are the strength of the linear and nonlinear losses, respectively.

Optical or electric pump can make the linear losses negative (thus producing linear gain in the resonator) so that the individual resonator may switch into the lasing regime with the stationary amplitude determined by the balance of the linear gain and nonlinear losses.

In the case of one-cavity pumping we have numerically obtained single- and dual-mode regimes for different kind of nonlinear losses, see Fig. 1. The developed perturbation theory allows to find the amplitude of the stationary solutions in the form of WS states.

For the case when the pump excites several resonator we have still observed the lasing regimes mentioned above provided that the pump is relatively close to the threshold. However, the pump increase results in the emergence of various multi-frequency solutions, some of which were BOs.

In order to expand the range of single-frequency generation based on WS states we have utilized spatially non-uniform losses and pump. This approach made it possible to increase the range of single-mode lasing by two orders of magnitude.

We have also investigated Kerr nonlinearity effect on the stability of monochromatic generation in the form of WS states. It was numerically discovered that when the pump increased some critical value, the destabilization of single-mode regime occurs. Using the perturbation method we found that this dynamics can be explained as a parametric excitation of sideband modes.

Acknowledgments. This work was supported by the Ministry of Science and Higher Education of the Russian Federation, Goszadanie no. 2019-1246.

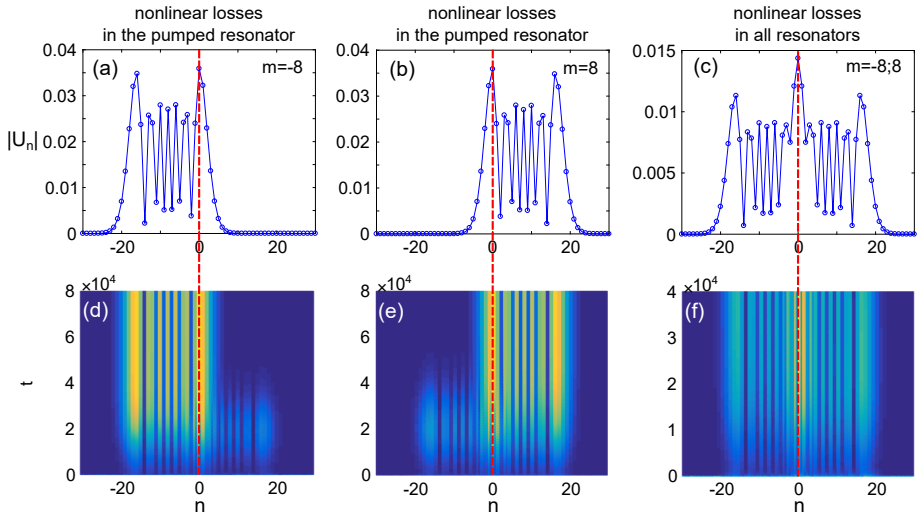

Figure 1: (Color online) Stationary states $|U_n|$ in the form of WS states with (a) $m = -8$, (b) $m = 8$, (c) $m = -8$ and $m = 8$ (time-averaged field); Panels (d), (e) and (f) show the respective evolutions of the field module $|U_n(t)|$. The pump amplitude slightly exceeds the excitation threshold. Nonlinear losses are nonzero only in the excited resonator with $n = 0$, i.e. $\beta_0 = \beta$, for (a), (b), (d), and (e); nonlinear losses are spatially uniform, i.e. $\beta_n = \beta$, for (c) and (f). The blue circles are the resonators, the solid blue lines are guides for eyes, and the dashed red lines are the pump (resonator with $n = 0$). The used parameters are: $\mu = 0.2$, $\gamma = 0.01$, $a = 0.1$, $\beta = 1$.

References

1. G. H. Wannier, Elements of Solid State Theory, Cambridge University Press, London, 190–193, 1959.

2. N. A. Boidi et al., Coexistence of insulating phases in confined fermionic chains with a Wannier-Stark potential, Phys. Rev. B, **109.4**, L041404, (2024).

3. F. Bloch, Uber die Quantenmechanik der Elektronen in Kristallgittern, Z. Phys., **52**, 555, (1929).

4. C. M. de Sterke, J. N. Bright, P. A. Krug et al., Observation of an optical Wannier-Stark ladder, Phys. Rev. E, **57**, 2365, (1998).

5. A. Verbitskiy, A. Yulin, and A. G. Balanov, Chaotic Bloch oscillations in dissipative optical systems driven by a periodic train of coherent pulses, Phys. Rev. A, **107.5**, 053519, (2023).

Subradiant two-photon states in planar atomic lattices

I.A. Volkov[1], **D. K. Kornovan**[1], **A. S. Sheremet**[1],
R. S. Savelev[1] **and M. I. Petrov**[1]

In this work we consider two-photon states in infinite quadratic lattice of similar two-level atoms with out-of-plane polarization of dipolar transition. To obtain dispersion, we apply quasi-infinite lattice method, in which center of mass of two photons can propagate in infinite lattice with no restrictions and relative distance between these photons is restricted to some number of lattice periods. Here we demonstrate different kinds of subradiant two-photon states, consisting of single photon states similar to bound states in continuum (BIC) and band edge (BE) states.

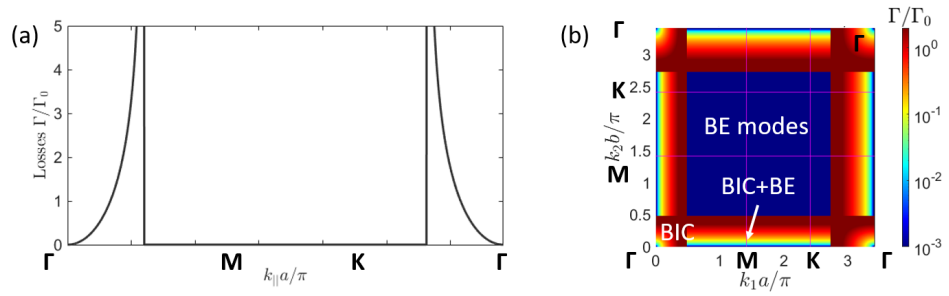

Figure 1: Radiative losses Γ/Γ_0 analytically calculated for quadratic lattice of atoms with out-of-plane transition dipole moments. (a) Single photon dispersion of radiative losses in ΓMKΓ direction. (b) Two-photon dispersion of radiative losses in ΓMKΓ direction. Different dark states are consisting of BIC and band edge single-photon states.

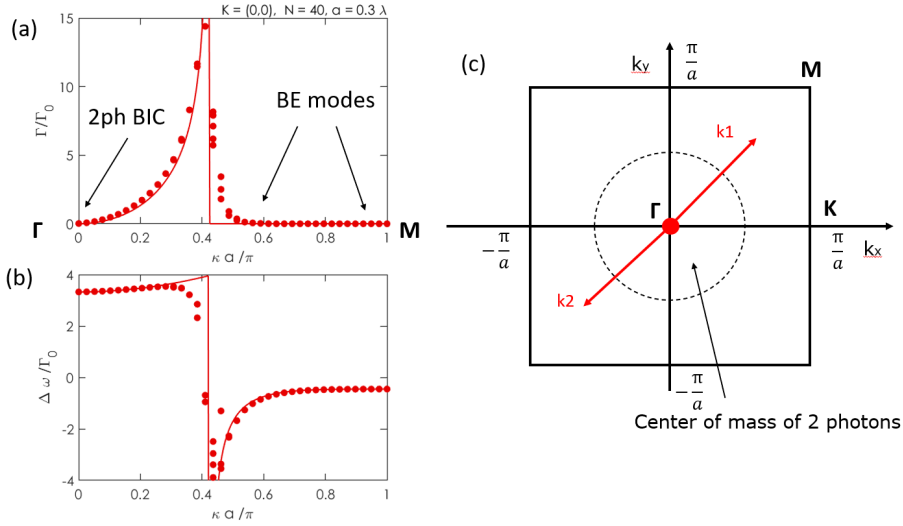

Figure 2: Dispersion features of two-photon states with center of mass photon wavevector $\mathbf{K} = 0$. (a) Dispersion of radiative losses Γ/Γ_0 with respect to $\kappa = k_1 - k_2$, where $k_{1,2}$ is the wavevector of a single-photon state in ΓM direction. (b) Dispersion $\Delta\omega/\Gamma_0$ with respect to κ in ΓM direction.(c) Diagram of two-photon state in the Brillouin zone, consisting of two photons with equal but counter-propagating wavevectors.

The International Summer Conference on Theoretical Physics 2024
Faculty of Physics of ITMO University
Abrikosov Center for Theoretical Physics

Elementary excitations in exciton-polariton systems

Nina Voronova

National Research University MEPhI (Moscow Engineering Physics Institute, 115409 Moscow, Russia

Russian Quantum Center, Skolkovo IC, 121205 Moscow, Russia

nsvoronova@mephi.ru

Abstract

In this talk we address the theoretical approach to description of elementary excitations in diverse exciton-polariton systems, based on the next order beyond zero-temperature mean-field approximation. We develop the self-consistent finite-temperature Hartree–Fock–Bogoliubov description for polaritons, universally addressing the excitation spectrum, momentum-dependent interactions, condensate depletion, and the background population of dark excitons that contribute to the system's chemical potential. We show how this theory can be universally applied to various long-living exciton-polariton systems in thermal equilibrium, as well as to driven-dissipative polariton fluids in dynamical steady-state.

Key words: Exciton-polaritons, Bose condensation, Hartree-Fock-Bogoliubov approximation, elementary excitations

Semiconductor exciton-polaritons, a hybridized superposition of quantum-confined excitons and microcavity or waveguide photons, are interacting bosons with light effective mass in two dimensions. Due to their inherent driven-dissipative nature, they are known to exhibit nonequilibrium Bose condensation (i.e. to form spatially extended, although not infinite, macroscopically coherent fluids) at high critical temperatures. At the same time, in special conditions such as at large positive detunings or in high-finesse materials with extra low losses, polaritons can be brought in thermal equilibrium with the surrounding medium and form a true quantum degenerate Bose-Einstein distribution. In any of these cases, with respect to spectra of low-lying collective excitations polariton systems behave differently from well-known textbook examples such as liquid Helium or cold atom Bose-Enstein condensates (BECs). One peculiarity is the hybridized nature of the particles that results in momentum-dependent mass, interactions, and lifetime. The other specific property of externally-pumped polariton systems is the presence of dark excitons which are created by the pump together with optically active particles. Furthermore, spatial patterning of the material or presence of external fields can make the polariton fluid strongly anisotropic. All of these features can considerably affect the spectrum of elementary excitations of the polariton BEC and hence change its superfluid behaviour.

Here, we discuss the finite-temperature corrections and modifications produced by the momentum-dependent interactions within the Hartree-Fock-Bogoliubov (HFB) theoretical approach applied to a system of exciton-polaritons. The developed theory yields renormalizations of the bare particle spectrum and the particle effective mass, both at $T = 0$ and $T > 0$, resulting in the shifts of the chemical potential and the spectrum of collective excitations of the polariton system, altering the Bogoliubov sound velocity in a non-monotonous manner [1]. This self-consistent HFB approach is applicable to a variety of systems in both thermal and dynamical equilibrium. As such, combined with rate equations for the condensate and excitonic reservoir, it results in an intuitive, analytically solvable model that allows investigating the influence of dark excitons and the bright, thermally distributed polaritonic reservoir on the sound velocity in nonresonantly pumped polariton fluids [2]. On the other hand, when applied to systems with quasi-infinite condensate lifetimes, such as the polariton BEC in the bound-in-the-continuum (BIC) state, it unveils the peculiar features of the Bogoliubov spectrum of excitations for the BIC polariton condensate in an optical waveguide [3]. Curiously, thanks to the dark nature of the BIC state, collective excitations lying directly above the condensate become observable in enhanced detail. Using the HFB thery, we reveal interesting aspects, such as energy-flat parts of the dispersion characterized by two parallel stripes in photoluminescence pattern, pronounced linearization at non-zero momenta in one of the directions, and a strongly anisotropic velocity of sound. Finally, considering exciton-polaritons with a dipole moment in crossed electric and magnetic field, we show that the spectrum of elementary excitations is asymmetric and features pronounced, controllable roton minima [4].

References

1. A. M. Grudinina, I. L. Kurbakov, Yu. E. Lozovik, and N. S. Voronova, Finite-temperature Hartree-Fock-Bogoliubov theory for exciton-polaritons, Phys. Rev. B **104**, 125301 (2021).

2. A. M. Grudinina and N. S. Voronova, Dark and thermal reservoir contributions to polariton sound velocity, Phys. Rev. B **106**, L121301 (2022).

3. A. Grudinina, M. Efthymiou-Tsironi, V. Ardizzone et al., Collective excitations of a bound-in-thecontinuum condensate, Nat. Commun. **14**, 3463 (2023).

4. T. V. Maximov, I. L. Kurbakov, N. S. Voronova, and Yu. E. Lozovik, Tunable Bose-Einstein condensation and rotonlike excitation spectra with dipolar exciton-polaritons in crossed fields, Phys. Rev. B **108**, 195304 (2023).

Finite temperature radiative corrections to the bound electron g-factor, hyperfine structure and atomic clock transitions

T. Zalialiutdinov[1, 2] and D. Solovyev[1, 2]

[1]Department of Physics, St. Petersburg State University, Petrodvorets, Oulianovskaya 1, 198504, St. Petersburg, Russia

[2]Petersburg Nuclear Physics Institute named by B.P. Konstantinov of National Research Centre "Kurchatov Institut", St. Petersburg, Gatchina 188300, Russia

[1]t.zalialiutdinov@spbu.ru, [2]d.solovyev@spbu.ru,

Abstract

The discussion focuses on examining the influence of the blackbody radiation field on the bound electron g-factor of light hydrogen-like ions and the hyperfine splitting in hydrogen, deuterium, and the $^3He^+$ ion within the framework of quantum electrodynamics at finite temperatures for bound states. One-loop thermal corrections are investigated for a broad temperature range, with numerical results presented for various states. The study demonstrates that finite temperature corrections to the bound-electron g-factor for excited states are comparable to current experimental uncertainty, even at room temperatures, and may be discerned within anticipated future measurements. Additionally, we discuss the combination of two-loop radiative corrections, featuring one zero and one finite temperature loop, applied to clock transitions in Sr^+ and Ca^+ ions. The corrections being considered for the transition frequencies are comparable to the dynamic corrections applied to the standard thermal Stark shift.

Key words: Theoretical physics, Finite temperature QED

Introduction

The formation and development of quantum theory for bound states is closely connected with precision spectroscopic experiments performed on the hydrogen atom and a number of hydrogen-like ions. Having their own methodological features, such systems are most accurately theoretically described within the framework of quantum electrodynamics (QED). In the last decades, experimental measurements and theoretical calculations of the hyperfine structure (HFS) and g-factors in simple atomic systems have attracted particular interest. Significant progress in evaluation of QED radiative and nuclear-structure corrections, as well as the improvement of experimental techniques, make it possible to identify the fundamental parameters of the theory (the

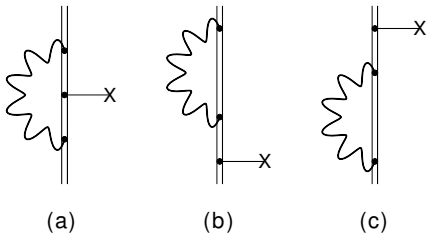

Figure 1: Feynman diagrams describing the TQED contributions to the bound-electron g-factor, HFS and level widths.

electron to proton mass ratio, the Rydberg constant, nuclear parameters, etc.) and to look for manifestations of new physics.

To date, the transition frequencies in various atomic systems are measured with extremely high accuracy and also serve as a tool for building atomic clocks, metrological frequency standards, tests of perturbative quantum electrodynamics and others. In particular, the relative error in measuring the transition frequencies in hydrogen is about $10^{-15} \div 10^{-13}$ [1], the hyperfine interval is determined with an accuracy about 10^{-13} [2], and the g-factor is as accurate as 10^{-12} [3]. Such extraordinary precision stimulates theoretical studies of more subtle effects that are at the level of modern experimental error and less. Along these lines, the influence of the blackbody radiation field (BBR) on these quantities is of particular interest. It is well known that the BBR field leads to a quadratic ac-Stark shift of energy levels and reduces the lifetimes by inducing electron transitions between atomic states. The effects are extremely important in the spectroscopy of Rydberg atoms, the construction of atomic clocks, and the determination of frequency standards. The study of the effect of equilibrium radiation on the characteristics of atomic systems is usually limited to the quantum mechanical approach, in which the root-mean-squared field induced by BBR is considered as a perturbation. In our recent works, bound-state quantum electrodynamics theory at finite temperature (BS-TQED) has been developed to calculate thermal effects in atomic systems.

One-loop radiative corrections to the interaction vertex

Within the framework of the present study we discuss radiative corrections that take into account the finite temperature environment affecting the measurement of the g-factor, the HFS, and the determination of the level widths in simple atomic systems [4, 5, 6, 7]. The lower-order radiative corrections relevant to this study can be depicted using Feynman graphs in Fig. 1. Considering various combinations of the vertex part (attributed to interactions with an external magnetic field or hyperfine interaction) and the loop part (attributed to an "ordinary" or thermal photon), corrections can be evaluated to the g-factor, the HFS as the real part and to the level width as the

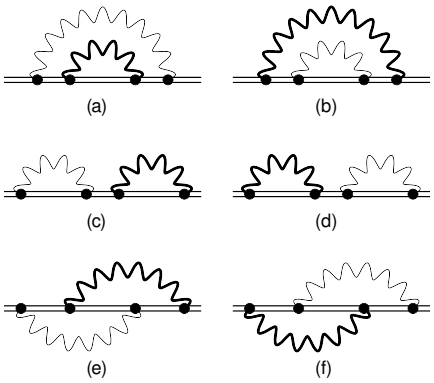

Figure 2: The Feynman graphs representing the combined two-loop self-energy QED corrections to the atomic energy level.

imaginary part of the corresponding contributions.

In particular, the lowest order corrections to the g-factor at different temperatures for the hydrogen and light hydrogen-like ions were described in [4], and within the model potential approach for Rb and Cs atoms in [5]. Thermal radiative corrections to hyperfine structure of light hydrogen-like systems were evaluated in [6]. It is shown that the corrections are at or close to the accuracy level of modern experiments. Further, the discussion of the imaginary part of the contributions corresponding to the graphs in Fig. 1 is considered in detail. The theoretical analysis is devoted to the magnetic interaction given by the vertex part of the diagrams and to two cases: when the loop is attributed to the emission of a photon and its magnitude stimulated by the blackbody radiation. The entire analysis is devoted to the low-lying states of hydrogen and hydrogen-like ions [7].

Combined two-loop radiative corrections

We also investigate combined type of two-loop self-energy corrections, including one zero-vacuum and one loop at finite temperature. By utilizing the method of dimensional regularization, we derived closed analytical expressions for the energy shifts of atomic levels. Our numerical calculations demonstrate that even at room temperature, these corrections can be significant for excited states, reaching the magnitude of the thermal induced Stark contribution [8]. The particular examples are provided for clock transitions in Sr^+ and Ca^+ ions.

Acknowledgments. The work was supported by the Russian Science Foundation under grant No. 22-12-00043.

References

1. P.J. Mohr, D.B. Newell, B.N. Taylor, CODATA recommended values of the fundamental physical constants: 2014, J. Phys. Chem. Ref. Data **45**, 043102 (2016).

2. H. Hellwig et.al., Measurement of the Unperturbed Hydrogen Hyperfine Transition Frequency, IEEE Trans. Instr. Meas., textbf19, 200-209 (1970).

3. G. Werth et.al., Zeeman Spectroscopy in Penning Traps, Adv. At. Mol. Opt. Phys, **67**, 257 (2018).

4. T. Zalialiutdinov, D. Glazov, D. Solovyev, Thermal corrections to the bound-electron g-factor, Phys. Rev. A **105**, 012804 (2022).

5. T. Zalialiutdinov, Y. Kozhedub, D. Solovyev, Can. J. Phys, 101, 11 (2023).

6. T. Zalialiutdinov, D. Glazov, D. Solovyev, Thermal radiative corrections to hyperfine structure of light hydrogenlike systems, Phys. Rev. A **106**, 062808 (2022).

7. D. Solovyev, T. Zalialiutdinov, Radiative corrections to the level width in the presence of magnetic field, Phys. Scr. 98 085406 (2023).

8. T. Zalialiutdinov and D. Solovyev, Phys. Rev. A 108, 042801 (2023).

Relativistic calculation of the g factor of excited states of lithium-like ions

D. V. Zinenko[1], V. A. Agababaev[2], D. A. Glazov[3], A. V. Malyshev[1,4], E. V. Tryapitsyna[3,4], A. V. Volotka[3]

[1]Department of Physics, St. Petersburg State University, St. Petersburg, Russia
[2]St. Petersburg State Electrotechnical University "LETI", St. Petersburg, Russia
[3]School of Physics and Engineering, ITMO University, St. Petersburg, Russia
[4]Petersburg Nuclear Physics Institute named by B. P. Konstantinov of National Research Centre "Kurchatov Institute", Gatchina, Russia

[1]dmitrii.zinenko@gmail.com

Abstract

We present the first relativistic calculations for the g factor of excited states of lithium-like ions over a wide range of nuclear charge numbers $Z = 10 - 92$. The interelectronic interaction contributions are considered in the framework of perturbation theory up to second order. One-loop QED contributions are calculated in all orders of αZ. Nuclear recoil contributions are also taken into account. The quadratic and cubic contributions to the Zeeman effect are considered.

Key words: highly charged ions, quantum electrodynamics, relativistic atomic theory, g factor

The study of the g factor of highly charged ions has recently made significant progress, leading to precise measurements of the electron mass [1] and the potential for independent determination of the fine structure constant α [2, 3]. This progress also allows tests of quantum electrodynamics (QED) beyond the Furry picture [4, 5] and facilitates the determination of magnetic moments and nuclear radii [6, 7]. In particular, the measurement of the g factor of thorium-229 ions helps to determine the lifetime of the isomeric state of this isotope [8].

Many high precision experiments, especially with hydrogen-like ions, have reached accuracies of 10^{-10} [9–12]. Further investigations of lithium- and boron-like ions were stimulated by considering the so-called specific differences, which circumvent the problem of finite nucleus size and significantly improve the accuracy of the comparison between theory and experiment [13, 14].

So far, experiments have focused on the ground states of highly charged ions, with measurements of g factors for excited states limited to lighter systems such as helium and lithium. Recently, however, there have been proposals for experimental approaches

that allow higher precision in the measurement of g factors for excited states. For example, the ALPHATRAP project increased the precision of measuring the g factor of the $2P_{3/2}$ state of boron-like argon by a factor of ten [15], while an experiment using quantum logic technology refined the results to an accuracy of 10^{-6} [16]. These advances open avenues for future measurements of Zeeman splitting in different states of highly charged ions, beyond boron-like ions.

Theoretical calculations of the Zeeman effect for excited states have predominantly been based on the lowest relativistic approximation. The accuracy of such calculations is typically remains around 10^{-4} [17−20], which is insufficient for comparison with high-precision experiments. To solve this problem, our group has performed first relativistic calculations of the g factor of the excited states $(1s)^2 2p_{1/2}$ and $(1s)^2 2p_{3/2}$ of lithium-like ions. The interelectronic interaction correction is considered in the framework of perturbation theory. The first-order $1/Z$ term is obtained in the framework of the strict QED approach, i.e. in all orders of αZ. The second order contribution is calculated in the Breit approximation, taking into account excitations to the negative spectrum. The one-loop QED contributions, self-energy and vacuum polarisation, have been calculated in all orders of αZ. The αZ expansion, which includes the currently known terms, is used to calculate the two-loop corrections. All contributions are calculated using screening potentials in the extended Furry picture to allow partial consideration of higher order contributions. The range of full values obtained in different potentials can be used to estimate unaccounted for contributions, as the exact results should not depend on the initial approximation. We use the core-Hartree potential and the family of x_α-potentials (the Kohn-Sham, Dirac-Hartree and Dirac-Slater potentials, see e.g. [21]).

We have also taken into account the leading contribution of nonlinear Zeeman effects, which are enhanced for closely spaced levels of the same parity, e.g. $2p_{1/2}$ and $2p_{3/2}$ in boron-like ions stirred by an external magnetic field [22, 23]. This effect can be noticeable for excited states, which can be important for the interpretation of experimental data.

For the first time, relativistic calculations have been performed for the excited states of lithium-like ions for $Z = 10 - 92$ with an accuracy of 10^{-6}, providing a valuable tool for verifying future experiments.

The work was supported by the Russian Science Foundation (Grant No. 22-12-00258) and by the Foundation for the Advancement of Theoretical Physics and Mathematics "BASIS".

References

1. S. Sturm *et al.*, Nature **506**, 467 (2014).

2. V. M. Shabaev *et al.*, Phys. Rev. Lett. **96**, 253002 (2006).

3. V.A. Yerokhin *et al.*, Phys. Rev. Lett. **116**, 100801 (2016).

4. V. M. Shabaev *et al.*, Phys. Rev. Lett. **119**, 263001 (2017).

5. A. V. Malyshev *et al.*, JETP Letters **106**, 765 (2017).

6. W. Quint *et al.*, Phys. Rev. A **78**, 032517 (2008).

7. V. A. Yerokhin *et al.*, Phys. Rev. Lett. **107**, 043004 (2011).

8. V.M. Shabaev *et al.*, Phys. Rev. Lett. **128**, 043001 (2022).

9. H. Häffner *et al.*, Phys. Rev. Lett. **85**, 5308 (2000).

10. J. Verdú *et al.*, Phys. Rev. Lett. **92**, 093002 (2004).

11. S. Sturm *et al.*, Phys. Rev. Lett. **107**, 023002 (2011).

12. S. Sturm, *et al.*, Phys. Rev. A **87**, 030501 (2013).

13. V. M. Shabaev *et al.*, Phys. Rev. A **65**, 062104 (2002).

14. A. V. Volotka and G. Plunien, Phys. Rev. Lett. **113**, 023002 (2014).

15. A. Egl *et al.*, Phys. Rev. Lett. **123**, 123001 (2019).

16. P. Micke *et al.*, Nature **578**, 60 (2020).

17. X.-X. Guan and Z.-W. Wang, Phys. Lett. A **244**, 120 (1998).

18. Z.-C. Yan, Phys. Rev. Lett. **86**, 5683 (2001).

19. Z.-C. Yan, J. Phys. B: At. Mol. Opt. Phys. **35**, 1885 (2002).

20. Z.-C. Yan, Phys. Rev. A **66**, 022502 (2002).

21. J. Sapirstein and K. T. Cheng, Phys. Rev. A **66**, 042501 (2002).

22. D. von Lindenfels et al., Phys. Rev. A **87**, 023412 (2013).

23. D. A. Glazov et al., Phys. Scr. **T156**, 014014 (2013).

Theoretical calculations of the hyperfine splitting of the $^2P_{1/2}$ and $^2P_{3/2}$ levels in boron-like Cl^{12+}

D. V. Zinenko[1], D. A. Glazov[2], Y. S. Kozhedub[1], A. V. Volotka[2]

[1]Department of Physics, St. Petersburg State University, St. Petersburg, Russia
[2]School of Physics and Engineering, ITMO University, St. Petersburg, Russia

[1]dmitrii.zinenko@gmail.com

Abstract

We present theoretical calculations of the hyperfine structure constants and the ground state hyperfine splitting energy for $^{35,37}Cl^{12+}$ ions. The interelectronic interaction contributions are considered in the framework of perturbation theory up to second order. One-loop QED contributions are calculated in all orders of αZ. Nuclear recoil contributions are also taken into account. The present theoretical calculations agree with experimental results and provide a possibility to test the bound-state QED effects in five-electron systems.

Key words: highly charged ions, quantum electrodynamics, relativistic atomic theory, hyperfine splitting

Hyperfine splitting, which results from the interaction between the magnetic dipole and electric quadrupole moments of the nucleus and the electromagnetic field of the bound electrons, causes subtle energy level shifts in atoms, providing valuable insights into nuclear and atomic properties. Highly charged ions (HCIs) exhibit enhanced hyperfine effects due to electron-nucleus overlap, making them ideal for exploring fundamental physics. HCIs provide a unique platform for studying strong-field quantum electrodynamics (QED) effects [1, 2] and nuclear structure theories, including the Breit-Rosenthal (BR) effect [3], due to the finite distribution of nuclear charges, and the Bohr-Weisskopf (BW) effect [4], due to the finite distribution of nuclear magnetisation strengths.

For nearly three decades, continuous experimental research has focused on the ground state hyperfine splitting of HCIs. Spectroscopic measurements of hyperfine structures in various HCIs, including H-like ions (e.g. $^{209}Bi^{82+}$ [5]), Li-like ions (e.g. $^{209}Bi^{80+}$ [5]) and Be-like ions (e.g. $^{141}Pr^{55+}$ [6]), have been extensively used due to their significant hyperfine splitting. These studies have contributed to understanding relativity, testing QED effects and exploring nuclear properties. Recently, experiments at GSI revealed a 7σ deviation between experimental and theoretical values of hyperfine splitting in Li-like bismuth [7]. This puzzle was solved [8] and a new value of the

nuclear magnetic moment of bismuth was obtained, restoring the agreement between theory and experiment. This circumstance raised the question of the accuracy of tabulated values of nuclear magnetic moments, which are mainly obtained by nuclear magnetic resonance.

In addition to the influence of the nuclear magnetic moment, inaccuracies in the calculation of the BW effect can lead to precisely measured experimental results that cannot be used as meaningful high-precision QED tests. On the other hand, specific differences in the hyperfine splitting values of HCIs for different charge states in the same nucleus can eliminate the BW effect [9]. Therefore, the study of ions with different charge states is crucial. Furthermore, B-like ions offer smaller relative uncertainties due to the BW effect, allowing easier access to QED effects [9, 10]. Recently, an experiment was carried out at the EBIT laboratory of Fudan University in Shanghai to measure the hyperfine structure of the B-like Cl ion ground $^2P_{1/2}$ and excited $^2P_{3/2}$ states. Therefore, we have performed the corresponding theoretical calculations of the hyperfine structure constants through *ab initio* QED framework.

Our calculations are carried out in the extended Furry picture, which is based on solutions of the Dirac equation with an effective potential. Solving the Dirac equation with this potential and evaluating the hyperfine splitting gives a zero-order result known as the Dirac value. In addition, we use the perturbation theory of bound-state QED. Two main first-order contributions are considered: one-photon exchange and one-loop diagrams, namely self-energy (SE) and vacuum polarisation (VP). The use of the screening potential in the zero-order approximation allows a more efficient account of the interelectronic interaction in the lower-order corrections. Subsequently, the second-order contributions have to be considered. Due to their complexity, the corresponding diagrams are currently beyond the scope of rigorous *ab initio* QED calculations. To solve this problem, we use the Breit approximation and apply the method of configuration interactions in the Dirac-Fock-Sturm orbital basis [11]. As a result, the most accurate values of the hyperfine splitting constants of the B-like $^{35,37}Cl^{12+}$ ions have been obtained for the $(1s)^2(2s)^22p_{1/2}$ and $(1s)^2(2s)^22p_{3/2}$ states.

The theoretical values obtained agree with the experimental data within the error limits, demonstrating the prospects for precision tests of bound-state QED in future measurements in this system.

The work was supported by the Russian Science Foundation (Grant No. 22-12-00258) and by the Foundation for the Advancement of Theoretical Physics and Mathematics "BASIS".

References

1. P. Beiersdorfer *et al.*, Phys. Rev. Lett. **80**, 3022 (1998).

2. M. Lochmann *et al.*, Phys. Rev. A **90**, 030501(R) (2014).

3. J. E. Rosenthal and G. Breit, Phys. Rev. **41**, 459 (1932).

4. A. Bohr and V. F. Weisskopf, Phys. Rev. **77**, 94 (1950).

5. J. Ullmann *et al.*, Nat. Commun. **8**, 15484 (2017).

6. P. Beiersdorfer *et al.*, Phys. Rev. Lett. **112**, 233003 (2014).

7. R. Sanchez *et al.*, J. Phys. B **50**, 085004 (2017)

8. L. V. Skripnikov *et al.*, Phys. Rev. Lett. **120**, 093001 (2018).

9. V. M. Shabaev *et al.*, Phys. Rev. Lett. **86**, 3959 (2001).

10. A. V. Volotka and G. Plunien, Phys. Rev. Lett. **113**, 023002 (2014).

11. I. I. Tupitsyn *et al.*, Phys. Rev. A **72**, 062503 (2005).